STIMULATION OF NEURONS IN THE BRAIN: MECHANISMS AND LIMITATIONS

by

MOHAMMED J ALZAHRANI

A dissertation submitted in partial fulfillment of the
requirements for the degree of

DOCTOR OF PHILOSOPHY IN BIOMEDICAL SCIENCES: MEDICAL PHYSICS

2025

Oakland University
Rochester, Michigan

Doctoral Advisory Committee:

Yang Xia, Ph.D., Chair
Bradley John Roth, Ph.D., Co-Chair
Steffan Puwal, Ph.D.
Eugene Surdutovich, Ph.D.
Alexey Tonyushkin, Ph.D.

To my mother, father, wife and children

ACKNOWLEDGMENTS

I want to express my deep gratitude to my advisor, Dr. Bradley John Roth, for allowing me to be part of his research and for sharing his expertise in implementing methodologies to address the research problems. His insightful feedback always motivated me and helped sharpen my thinking and skills. I would also like to thank Dr. Abdulkadir AlAydarous for his advice on studying in the US; Dr. Xia for his continuous help and support, and Dr. Surdutovich for his encouragement. Additionally, I sincerely thank Dr. Tonyushkin and Dr. Puwal for taking the time to be part of the dissertation committee.

At the end of this journey, I want to express my heartfelt thanks to my wife, Norah; my daughters, Mayar and Bayan; and my son, Ibrahim, for their constant help, care, and inspiration. Lastly, I want to thank my parents, brothers, and sisters.

ABSTRACT

STIMULATION OF NEURONS IN THE BRAIN: MECHANISMS AND LIMITATIONS

by

Mohammed J Alzahrani

Adviser: Yang Xia, Ph.D., and Bradley John Roth, Ph.D.

Scientists have been using electrical stimulation to monitor and treat brain disorders for years. However, the capability to target specific brain regions marked the beginning of brain stimulation. The procedure falls under a larger neuromodulation therapy category, including deep brain stimulation (DBS), transcranial magnetic stimulation (TMS), microcoil recently, and others. These therapies can target specific neurons in the brain, helping to alleviate symptoms associated with movement disorders, epilepsy, depression, and other neurodegenerative disorders. This dissertation aims to discuss different brain stimulation methods and mechanisms.

The study of deep neuron stimulation in the brain involves using the Hodgkin and Huxley model when an external stimulus is applied. In response to a moderate stimulus, the membrane triggers an action potential. However, a high or low stimulus dose not excite an action potential. In other words, weak stimuli do not excite neurons, moderate strength stimuli do, but strong stimuli do not, which means you can excite deeper neurons while not exciting neurons closer to the brain surface.

The electric field produced by a microcoil is too small to cause neural stimulation. The maximum value of the induced electric field due to electromagnetic induction is around 0.026 mV/m. The electric field intensity in the tissue is approximately 4 mV/m due to capacitive coupling with the same current and frequency. Therefore, the electric field produced by capacitive coupling is much larger than that produced by electromagnetic induction.

Considering both large coil (TMS) and microcoil stimulation, the activating function is one source of excitation. The activating function depends on the spatial distribution of the electric field gradient in active membrane analysis and the spatial frequency in spatial-frequency analysis. Both analyses show that a microcoil (tens of microns in size) has a higher threshold than a traditional coil (tens of millimeters in size) when the spatial frequency is large, or the spatial extent of the activating function is small. Consequently, the stimulation threshold for a microcoil is much higher than that of conventional coils.

TABLE OF CONTENTS

TABLE OF CONTENTS—Continued

TABLE OF CONTENTS—Continued

APPENDICES

LIST OF TABLES

LIST OF FIGURES

CHAPTER ONE

INTRODUCTION AND LITERATURE REVIEW

In recent years, neural stimulation has become an important tool to treat many neurological disorders. In some cases, it involves using electrodes to stimulate the nerves and restore their function (Bensmaia and Miller, 2014), like deep brain stimulation for Parkinson's disease (Perlmutter and Mink, 2006), spinal cord injury (Peckham and Knutson, 2005) and cochlear implants for restoring hearing (Zeng et al., 2008). A study by Berger et al. showed that brain-implantable neural prosthetics can restore cognitive functions lost due to damage or disease (Berger et al., 2001).

Dr. Anthony Barker et al. invented transcranial magnetic stimulation, TMS (Barker et al., 1985), which has emerged as a very successful treatment for a variety of neurological disorders, including depression (Rizvi and Khan, 2019). TMS has been investigated for brain stimulation in many studies, helping and improving neurological symptoms (Wyszkowska, Jankowska, and Gas, 2019) such as depression (Yesavage et al., 2018) and Alzheimer's disease (Koch et al., 2018). Furthermore, the evidence-based use of repetitive transcranial magnetic stimulation (rTMS) in several illnesses, including stroke, multiple sclerosis, anxiety, Alzheimer's, epilepsy, panic attacks, and others, have been reviewed by Lefaucheur et al. (2020). Even while TMS therapy is widely utilized, it lacks spatial resolution, which makes it challenging to produce focused stimulation and selectively activate the deeper targeted regions of the brain (Bonmassar et al., 2012; Ridding and Rothwell, 2007; Wagner et al., 2007; Syrek and Bărbulescu, 2017).

The use of implanted microcoils has been proposed for magnetic stimulation as a possible alternative to TMS and scalp electrodes due its higher spatial resolution. Recently, Bonmassar et al. (2012) constructed a 500 μm-radius and 1 mm-high microcoil by winding 21 turns of copper wire, generating an electric field strong enough to excite neurons. Since then, other scientists have constructed several microcoils that require many amps of current and multiple coil turns to excite neurons (Park et al., 2018; Yoshikawa et al., 2022; Lee and Fried, 2015; Sugai et al., 2020; Ye et al., 2023).

This chapter delves into the topic of nerve excitation within the brain, exploring the distinct methods for achieving this. The chapter is divided into four subsections, making it easy to follow along and understand each method in detail. The first method discussed is deep brain stimulation, which involves using an electrode with an external stimulus based on the Hodgkin and Huxley model. The second method is nerve excitation through the electric field generated by a microcoil, and the third method is nerve excitation by capacitive coupling by a current pulse through a microcoil. Finally, we examined the electric field versus the activating function for neural excitation in both TMS and microcoil. The chapter aims to understand and explore different processes involved in nerve excitation within the brain.

1.1 Hodgkin and Huxley Model

The way that the cell membrane generates the action potential is fascinating. First, we know the membrane causes the action potential because we can squeeze out all the axoplasm and replace it with saline, and the nerve still works. In 1962, Baker, Hodgkin, and Shaw conducted such experiments, and they saw no effect on the propagation of the

action potential when they replaced the axoplasm of squid giant nerve fiber with saline "artificial electrolyte solutions" (Baker, Hodgkin, and Shaw, 1962). They demonstrated that the action potential is due to the membrane rather than its axoplasm. So, the action potential is an electrical signal that travels down a neuron's axon and is produced by changes in the cell membrane's electrical potential. At rest, the membrane is negatively charged compared to the outside, and it is maintained via ion channels that enable specific ions to flow through. The sodium-potassium pump helps to maintain the concentration inside and outside the cell membrane, and it requires energy using "adenosine 5' triphosphate" (ATP) to maintain the cell's ion concentration. There is more potassium inside than outside, and more sodium outside than inside. Also, at rest the membrane is primarily permeable to potassium, establishing a resting potential that is negative inside. During the depolarization, the membrane potential reaches a certain threshold, at which point voltage-gated sodium ion channels open, allowing an influx of sodium ions and generating the action potential. The action potential then travels down the axon, allowing the neuron to communicate with other neurons or muscles. At the synaptic connection, the action potential triggers the release of neurotransmitters that communicate with other neurons or with skeletal muscle.

In 1939, Alan Hodgkin and Andrew Huxley experimentally measured the electrical currents passing through the neuron during an action potential in a squid axon (Hodgkin and Huxley, 1939). They used the squid axon because it was large enough (around 0.5 mm in diameter) that they could insert a microelectrode and record the action potential. Ten years later, Hodgkin and Katz showed that the sodium concentration affected nerve excitability. In their experiment, the nerve became more excitable when

they increased the sodium concentration of the extracellular solution, and the nerve became unexcitable when the concentration was reduced (Hodgkin and Katz, 1949). On the other hand, they found that increasing potassium concentration lowers the resting potential, but the action potential is only slightly greater in a potassium-free solution. As a result, the action potential is mainly affected by sodium ions.

In 1952, Hodgkin and Huxley developed a mathematical model describing the cell membrane's electrical behavior (Hodgkin and Huxley, 1952), for which they won the Nobel Prize in Physiology or Medicine in 1963. They published a series of 5 papers that culminated in their 1952 paper (Raman and Ferster, 2021). Their model is based on the voltage-clamp technique, which allows measuring an axon's membrane current for a specified membrane potential (Fig 1.1). This is achieved by inserting a recording electrode into the axon, and a reference electrode into the extracellular fluid. The membrane potential of the axon is the voltage difference between these electrodes.

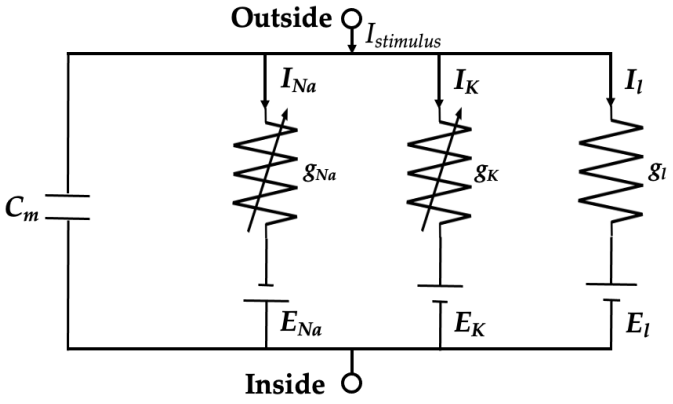

Fig. 1.1: Electrical equivalent circuit for a short segment of squid giant axon for Hodgkin and Huxley model.

During their experiments, they observed voltage-dependent sodium and potassium ion flow through the membrane that we now understand to be happening through selective Na^+ and K^+ ion channels that can open and close using "gates." Sodium and potassium gate dynamics play a crucial role in generating and propagating action potentials. The sodium channel has an activation gate (m) that opens rapidly upon depolarization and an inactivation gate (h) that closes slowly. The potassium channel has only an activation gate (n) that opens slowly. The sodium inactivation gate is responsible for the refractory period. The depolarization is a positive feedback loop: m opens upon depolarization, Na^+ enters with a positive charge, so the membrane potential V_m gets more positive, causing m to open more (Fig 1.2).

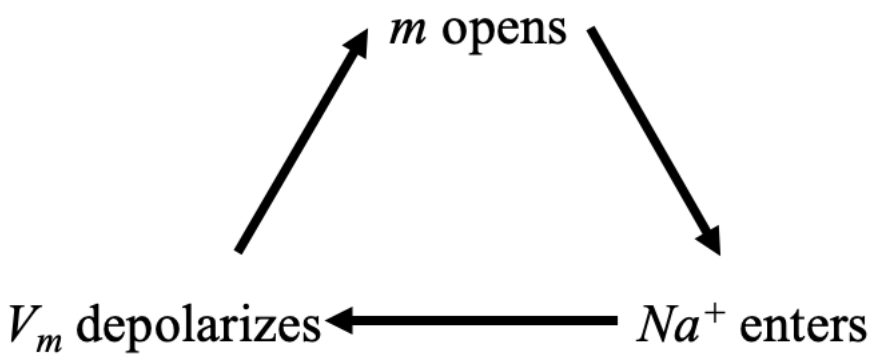

Fig. 1.2: The depolarization feedback loop

During the action potential process (Fig. 1.3), the sodium activation gate opens quickly when the membrane depolarizes, allowing sodium ions to enter the cell and raising the membrane potential. The potential will increase until it reaches the sodium reversal potential, E_{Na}, which is the membrane voltage at which the outward electrical force on a sodium ion is just balanced by diffusion inward. At the same time, the inactivation gate begins to close slowly, which eventually prevents additional sodium

ions from entering the cell. The slow activation of the potassium channel gate is responsible for the efflux of potassium ions out of the cell during an action potential. It is partially closed at rest but opens in response to depolarization of the membrane. When the potassium channel opens, potassium ions rush out of the cell, causing repolarization toward the potassium reversal potential, E_K. The refractory period is primarily caused by the (h) gate being closed even after repolarization. The closing of h and opening of n lead to restoring rest (repolarization). The discussion of the mathematical model in detail is in Chapter 2.

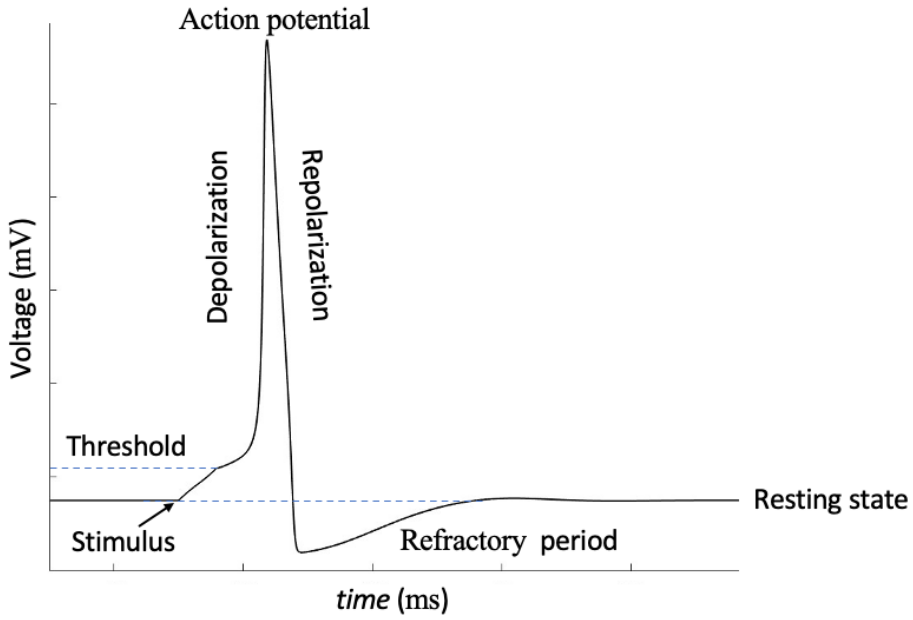

Fig. 1.3: An action potential after applying a threshold stimulus current.

Applying an external pulse of current by the electrode can change the membrane potential and excite the neuron depending on the pulse shape, strength, and duration. A pulse with a duration of 2.9 ms has a stimulus threshold of 3μA/cm^2 (Fig. 1.4a). The membrane current excitation threshold decreased to 2.3 μA/cm^2 when the pulse duration

increased (Fig. 1.4b). With a pulse duration of 21.6 ms, applying a stimulus of 6 μA/cm^2 leads to two action potentials (Fig. 1.4c), and 7 μA/cm^2 leads to three action potentials (Fig. 1.4d). Recent work by Fang, Duan, and Wang (2021) shows that increasing the pulse's strength generates multiple action potentials. Of course, without an external current pulse the membrane stays at rest.

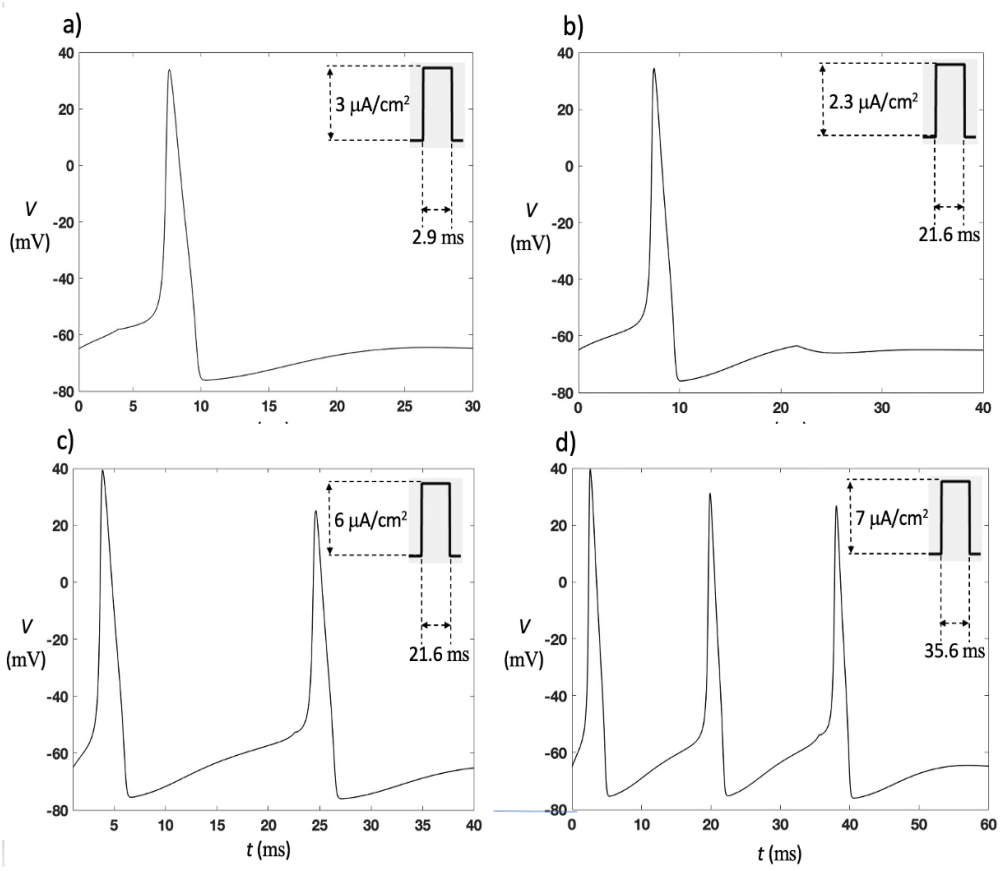

Fig. 1.4: The membrane response to different stimulus strengths and durations: a) short duration 2.9 ms, with a pulse of 3 μA/cm^2, b) long duration 21.6 ms with a pulse of 2.3 μA/cm^2, c) long duration 21.6 ms with a pulse of 6 μA/cm^2 and d) long duration 35.6 ms with a pulse of 7 μA/cm^2.

Grill and Mortimer (1997) designed a pulse to excite deep neurons selectively. This was achieved by exploiting the nonlinear conductance properties of neuronal sodium channels. They found that a long-duration, subthreshold depolarizing pre-pulse followed by at least 100 microseconds of stimulus pulses can excite the deep neurons without exciting the neurons surrounding the electrode. The long duration of the pre-pulse decreases both sodium inactivation channel (h) and activation channel (m), which reduces the neurons' excitability by inactivating the sodium channel. As a result, the stimulus can reach deep neurons without excitation to neurons close to the electrode. In contrast, a short pre-pulse duration increases the neuron's excitability by reducing the sodium inactivation gate (h) at a constant rate and increasing the activation gate (m) significantly, resulting in the excitation of neurons during the pre-pulse duration.

Chapter 2 discusses that a pulse produced by a ramp can stimulate the deeper neurons in the brain selectively without exciting the closest neurons to the electrode (unpublished). Even with successful stimulation, the use of an electrode for deep brain stimulation has limitations, such as heating the electrode tip (Nitz et al., 2005) and inflammation caused by the reaction of the surrounding tissue (Hirshler, Polat and Biegon, 2010).

1.2 Electromagnetic Induction by a Microcoil

Magnetic stimulation therapy has become a highly effective treatment for many neurological conditions, such as depression (Rizvi and Khan, 2019). This technique involves using a coil placed near the nerves and passing an electrical current through the coil. In 1985, Dr. Anthony Barker et al. invented transcranial magnetic stimulation

(TMS) which requires a current passing through a coil held outside the skull with several kiloamps lasting a few hundred microseconds, and his device was able to stimulate the motor cortex in the brain (Barker et al., 1985). This current causes a change in the magnetic field which results in an induced electric field that can stimulate the nerves when it meets the neuron's threshold, helping alleviate pain like chronic low back pain (Ambriz-Tututi et al., 2016), reduce seizures, and improve other neurological symptoms (Wyszkowska, Jankowska, and Gas, 2019).

With an emphasis on how electrode shape influences nerve activation, Frank Rattay's mathematical model studies the stimulus-response behavior of nerve axon or muscle fibers when activated using extracellular electrodes (Rattay, 1989). He introduced the idea of an activating function, which is essential knowledge for understanding the activation of nerve fibers. The second derivative of the extracellular potential V_e with respect to the length x ($\frac{\partial^2 V}{\partial x^2}$) is necessary for this function to work. He discovered that monopolar electrodes, among other electrode configurations, such as bipolar, ring, and monopolar electrodes, efficiently regulate the number of fibers activated as the stimulus intensity increases. This is accomplished by positioning the return electrode, also known as ground, at a distance that does not affect the extracellular potential along the stimulated fiber, and the active electrode close to the target region. Thus, the activating function for different electrode configurations may be predicted by his model simulations.

In 1990, Roth and Basser extended Rattay's work. They explained the physics behind nerve fiber stimulation by electromagnetic induction, and explained how an

electric field that arises from a coil can stimulate the neurons (Roth and Basser, 1990). Their calculations obey the 1-D cable equation:

$$V - \lambda^2 \frac{\partial^2 V}{\partial x^2} + \tau \frac{\partial V}{\partial t} = -\lambda^2 \frac{\partial E_x}{\partial x}, \tag{1.1}$$

where V is the transmembrane potential, E_x is the component of the electric field induced along the axon, λ is the length constant, τ the time constant, and $-\lambda^2 \frac{\partial E_x}{\partial x}$ is the source term (the activating function). The electric field arising from a coil can be calculated, depending on the number of coil turns N and the change of the current with time dI/dt (Roth and Basser, 1990):

$$\mathbf{E} = -N \frac{\mu_0}{4\pi} \frac{dI}{dt} \int \frac{d\mathbf{l}}{R}. \tag{1.2}$$

An analytical solution of Eq. (1.2) can be found for a line segment (Roth et al. 1991). If the coil geometry is the same except for the size, the electric field one coil radius below a 10 mm coil is the same as the electric field one coil radius below a 10 μm coil because the integral in Eq. (1.2) is dimensionless, which means that its value is independent of the length scale. As a rule of thumb we can estimate the electric field using Eq. (1.3), but it is vital to say what units E and dI/dt are given in (E in V/m, and dI/dt in A/μs)

$$E = 0.1\, N \frac{\partial I}{\partial t}\ . \tag{1.3}$$

Roth and Basser's (1990) model describes in detail the analysis of excitation of a long nerve axon. They found that the spatial gradient of the induced electric field component parallel to the fiber, dE_x/dx, governs nerve stimulation, as in Eq. (1.1). Also, they demonstrated that many factors can impact stimulation, such as the coil's position, orientation, shape, the stimulating circuit's resistance, capacitance, and initial voltage.

In 1992, Nilsson et al. (1992) conducted experiments to test Roth and Basser's prediction of the location of nerve stimulation. They used mathematical modeling to calculate the derivative of the electric field dE_x/dx along the nerve fiber. They found that a negative value of dE_x/dx indicates that the electric field is decreasing in the direction of the nerve fiber, which leads to depolarization. They predicted that the stimulation site occurs where dE_x/dx is negative and largest in magnitude. It indicates a significant gradient can depolarize the nerve and fire an action potential. Their experiments confirmed the prediction that dE_x/dx corresponds most to the location of excitation (the "virtual cathode"), which is critical in the magnetic stimulation of peripheral nerves.

In 1993, Maccabee et al. performed comprehensive experiments employing magnetic coils to stimulate straight and bent peripheral nerves in vitro (Maccabee et al., 1993). The induced electric E_x field and its spatial derivative dE_x/dx (the activating function) were measured and calculated. Like Nilsson et al. (1992), Maccabee et al. (1993) verified that the cause of nerve excitation in a long axon is the spatial gradient of the electric field. In contrast, for a bent nerve the threshold decreases and excitation occurs at the bend (Maccabee et al., 1993). In addition, Nagarajan and Durand (1993) discovered that shorter axons were easier to excite than longer ones, and "hot spots" might also result from other variables, including the truncation of an axon at its distal or proximal end. So, depending on the neuron's geometry and the distance to the target nerve, either the electric field from electromagnetic induction or the spatial electric field gradient may be the main source of nerve stimulation.

When it comes to using TMS, there are some limitations to remember. For example, the electric field can weaken as the distance from the coil increases, as noted in

several studies (Deng et al., 2013; Epstein et al., 1990; Thielscher and Kammer, 2004). Additionally, deeper parts of the brain may not receive as much stimulation due to the diminishing electric field, and various factors can impact the effectiveness of TMS (Aberra et al., 2020). It is also worth noting that TMS requires a high current in the coil (typically a few kiloamps) and can be challenging to focus on specific neuronal targets (Wagner et al., 2007). Many of these challenges can be overcome by designing a smaller implanted coil with a lower current, making it an appealing option compared to conventional electrodes and TMS coils. However, recent work by Lee et al. (2016) designed a single-turn microcoil to stimulate the cortex neurons. They were clearly exciting neurons, but what is the mechanism of the excitation? Lee et al. claim that a single-turn microcoil with a few milliamps can produce enough electric field to stimulate the neurons but other studies accomplished stimulation only when using larger currents. Bonmassar et al. (2012), Park et al. (2018), and Yoshikawa et al. (2022) all used coils with multiple turns and carrying currents above 2 A with a suitable frequency and at a reasonable distance from the coil.

The critical concept to understand microcoil stimulation is the electric field that the coil can produce. It can be affected by multiple factors, including the strength of the current and its frequency, the distance between the coil and the nerve, the number of turns, and the properties of the surrounding tissues. In Chapter 3, calculating the electric field and its gradient arising from different microcoils is discussed. We conclude that microcoil magnetic stimulation using a single-turn microcoil with a current of a few milliamps is not possible, and some other mechanism must be responsible for excitation.

Chapter 3 was published in the *IEEE Transactions of Biomedical Engineering* (Alzahrani and Roth, 2023).

1.3 Capacitive Coupling

The research conducted by Lee et al. (2016) suggested that magnetic stimulation could cause neural excitation using a single-turn microcoil with a current of 1 mA. However, Alzahrani and Roth (2023) predicted that the electric field generated by such microcoil is too weak to excite a neuron. Alzahrani and Roth (2023) suggested that rather than electromagnetic induction, capacitive coupling might be causing neural excitation in Lee et al.'s experiments. Capacitive effects are often used to stimulate a nerve via electrodes (Cogan, 2008). Even if the electrode is electrically insulated from the surrounding tissue, current can still flow through the electrode capacitance. An advantage of capacitive stimulation is to prevent physical contact between the electrode and the tissue, which could otherwise cause electrical short circuits, tissue injury, or electrochemical reactions. The electrode is designed to allow a current pulse to pass, while the capacitor blocks the flow of direct current to ensure that the electrode does not interact with the tissue. These electrodes usually connect the stimulating circuit to a grounded tissue site. In most cases, the electrode capacitance is connected in series, so a second grounded electrode is needed to supply the current's return path. Chapter 4 presents a model of stimulation that is quite different than a series capacitance, and provides a new insight into the mechanisms underlying neural capacitive stimulation. The model is similar to the cable model for a nerve axon, except the "membrane" conductance is assumed to be zero, and coil is modeled as a straight length of wire with a radius of *a*

and a length of *2L* surrounded by an extracellular tissue with a radius of *b*. As the current passes through the wire, it produces an electric field in the surrounding tissue, assuming a capacitive coupling between the wire and the tissue.

This method calculated the electric field in the tissue following the traditional cable model derivation (Hobbie and Roth, 2015; Wu and Wikswo, 1997) using the same parameters that Lee et al. (2016) used in their work. The electric field arising from capacitive coupling is larger than the electric field from magnetic induction, implying that capacitive coupling may be the cause of excitation in Lee et al.'s experiment. Chapter 4 discusses the calculation of this model in more detail. The results were published in the journal *Applied Sciences* (Alzahrani and Roth, 2024a).

1.4 Electric Field Versus the Activating Function for Neural Excitation

Some researchers have examined utilizing the electric field gradient dE_x/dx to establish the membrane threshold (Lee et al., 2016; Lee et al., 2019; Sugai et al., 2020), while others have used the electric field (Minusa et al., 2019). One important factor determining whether to use electric field E_x or its gradient dE_x/dx is the distance between the coil and the target neurons. In TMS, the distance *b* between the coil and the neuron is much larger than the analogous distance for a microcoil. In TMS with its large value of *b*, dE_x/dx is the dominant mechanism. In contrast when analyzing a microcoil, *b* decreases and the gradient dE_x/dx becomes high, So the threshold value of dE_x/dx increases. Chapter 5 analyzes this issue in more detail. This research was published in the journal *Applied Sciences* (Alzahrani and Roth, 2024b).

CHAPTER TWO

SELECTIVE DEEP STIMULATION OF NEURONS IN THE BRAIN

2.1 Introduction

Neural stimulation is often performed using electrodes on the scalp surface. In general, the stimulus strength is stronger for neurons located shallow in the brain, nearer the electrode, and is weaker for more distant, deep neurons. Our goal is to find a way to selectively excite deep neurons while not activating shallow neurons.

Our hypothesis is that a stimulus waveform consisting of a long, weak ramp followed by a brief, stronger main pulse can selectively excite deep neurons. The purpose of the ramp is to render shallow neurons refractory, so they cannot respond to the main pulse, while the distant neurons are not made refractory and can be excited by the pulse. To test this hypothesis, we perform numerical simulations of a neuron's response to a stimulus.

2.2 Methods

We use the Hodgkin & Huxley model to represent the electrical properties of the nerve (Fig. 2.1).

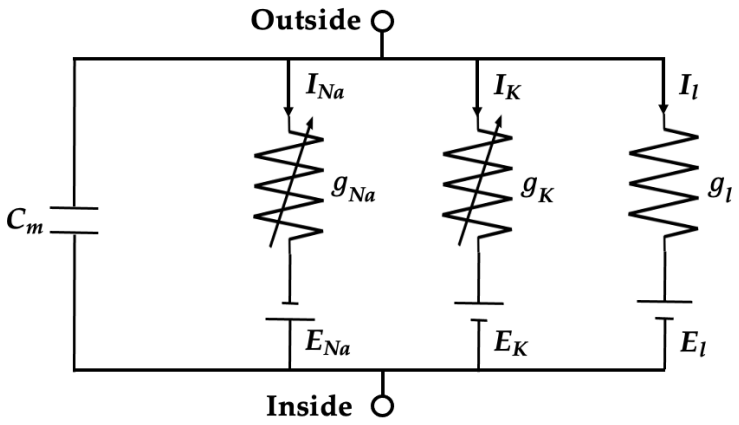

Fig. 2.1: Electrical equivalent circuit for a short segment of squid giant axon. Capacitor (capacitance per unit area C_m of the cell membrane); variable resistors (voltage-dependent Na^+ and K^+ conductance per unit area, g_{Na}, g_K); fixed resistor (voltage-independent leakage conductance per unit area g_l); batteries (reversal potentials for Na^+, K^+, leakage: E_{Na}, E_K, E_l); membrane potential $V = V_{in} - V_{out}$; arrows (current densities I_{Na}, I_K and I_l).

The equivalent RC circuit for the nerve membrane shown in Fig. 2.1 is governed by

$$I = C_m \frac{dV}{dt} + I_i, \tag{2.1}$$

where I is the total membrane current density (inward current positive), I_i is the ionic current density, V is the membrane potential (depolarization positive), C_m is the membrane capacity per unit area (assumed constant), and t is time.

The ionic current has three terms, $I_i = I_{Na} + I_K + I_l$, where

$$I_{Na} = g_{Na} m^3 h[V - V_{Na}], \quad I_K = g_K n^4 [V - V_K], \quad I_l = g_l [V - V_l]. \tag{2.2}$$

Equation (2.1) becomes

$$I = C_m \frac{dV}{dt} + g_K n^4 (V - V_K) + g_{Na} m^3 h (V - V_{Na}) + g_l (V - V_l), \tag{2.3}$$

where the variables *n*, *m*, and *h*—representing the opening and closing of ion channels—are governed by

$$\frac{dn}{dt} = \frac{n_\infty - n}{\tau_n}, \qquad \frac{dm}{dt} = \frac{m_\infty - m}{\tau_m}, \qquad \frac{dh}{dt} = \frac{h_\infty - h}{\tau_h}. \tag{2.4}$$

According to the Hodgkin-Huxley model (modern notation) the values of α, β and the gate values are given by

$$\alpha_n = 0.01\frac{V+55}{1-\exp\left(-\frac{V+55}{10}\right)}, \qquad \alpha_m = 0.1\frac{V+40}{1-\exp\left(-\frac{V+40}{10}\right)}, \qquad \alpha_h = 0.07\exp\left(-\frac{V+65}{20}\right), \tag{2.5}$$

$$\beta_n = 0.125\exp\left(-\frac{V+65}{80}\right), \quad \beta_m = 4\exp\left(-\frac{V+65}{18}\right), \qquad \beta_h = \frac{1}{1+\exp\left(-\frac{V+35}{10}\right)}, \tag{2.6}$$

$$n_\infty = \frac{\alpha}{\alpha+\beta}, \qquad \tau = \frac{1}{\alpha+\beta}. \tag{2.7}$$

The model parameters from Hodgkin and Huxley (1952) are given in Table 2.1.

Table 2.1. Parameters of the Hodgkin-Huxley model.

Symbol	Parameter	Value
g_{Na}	Maximum sodium conductance per unit area	120 mS cm^{-2}
g_K	Maximum potassium conductance per unit area	36 mS cm^{-2}
g_l	Leakage conductance per unit area	0.3 mS cm^{-2}
E_{Na}	Sodium Nernst reversal potential	50 mV
E_K	Potassium Nernst reversal potential	–77 mV
E_l	Leakage Nernst reversal potential	–54.387 mV
C_m	Membrane capacitance per unit area	1 μF cm^{-2}

The external current was a pulse preceded by a ramp with duration t_{ramp} and maximum strength *B*, as shown in (Fig. 2.2). Except for very strong stimuli, the ramp is

too slow and weak to excite an action potential. The pulse is responsible for exciting an action potential and has strength A and duration d. The pulse was stronger than the ramp by a factor of A/B = 2.3, 2.5 and 3. The MATLAB code for performing the calculation is given in the Appendix A.

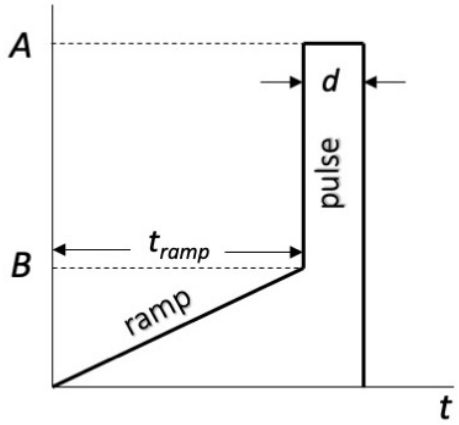

Fig. 2.2: The external pulse. The ramp affects the excitability of the transmembrane potential, and the pulse excites the neuron.

2.3 Results

For d = 0.5 ms, t_{ramp} = 130 ms, and A/B = 2.5, the membrane behavior has four types of responses depending on A. A weak stimulus (A = 8.5 μA/cm^2) is subthreshold (Fig. 2.3a). For a moderately strong stimulus (A = 12.6 μA/cm^2), the main pulse excites an action potential (Fig. 2.3b). For a strong stimulus (A = 16.5 μA/cm^2), the ramp makes the axon refractory, so the main pulse does not excite an action potential (Fig. 2.3c). A very strong stimulus (A = 17.6 μA/cm^2) triggers an action potential during the ramp before the main pulse (Fig. 2.3d).

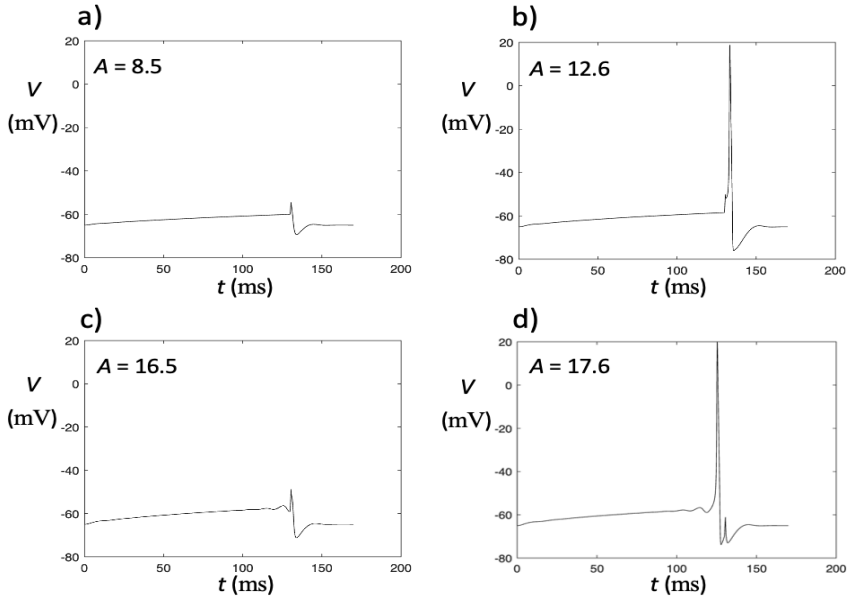

Fig. 2.3: The neuron response to stimulus strengths: a) weak, b) moderate, c) strong, and d) very strong. The pulse begins at t_{ramp}=130 ms.

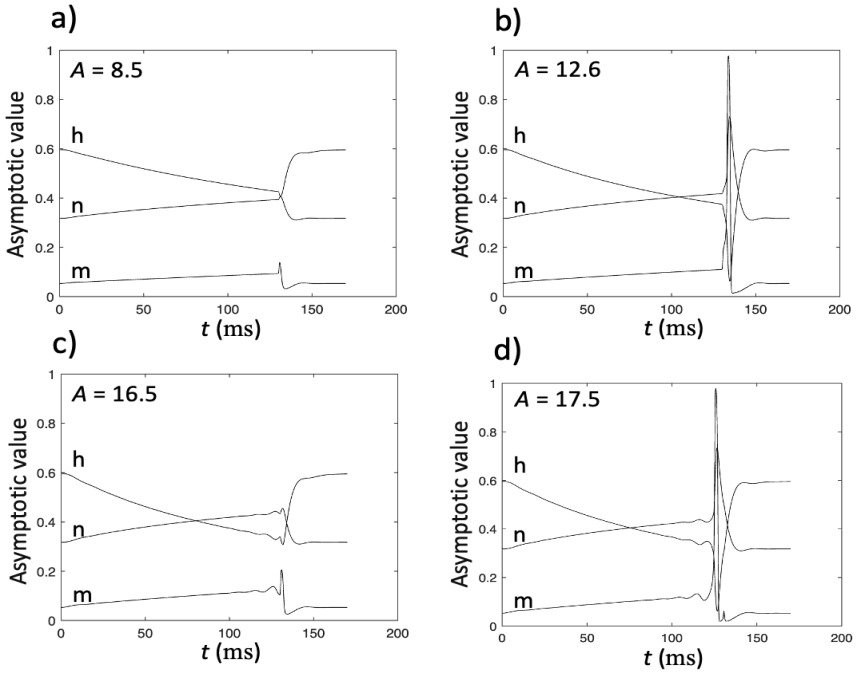

Fig. 2.4: The membrane gates response to stimulus strengths: a) weak stimulus, b) moderate stimulus, c) strong stimulus, and d) very strong stimulus.

Figure 2.4 shows the membrane gates corresponding to the same values of stimulus strengths shown in Fig. 2.3. For strong stimuli, *h* (the sodium channel inactivation gate) falls to a lower value just before the pulse in Fig 2.4c than that in Fig. 2.4b, and *n* (the potassium channel activation gate) rises to a higher value. Both of these changes make the axon more refractory. For very strong stimuli, the ramp excites an action potential before the main pulse (Fig. 2.4d).

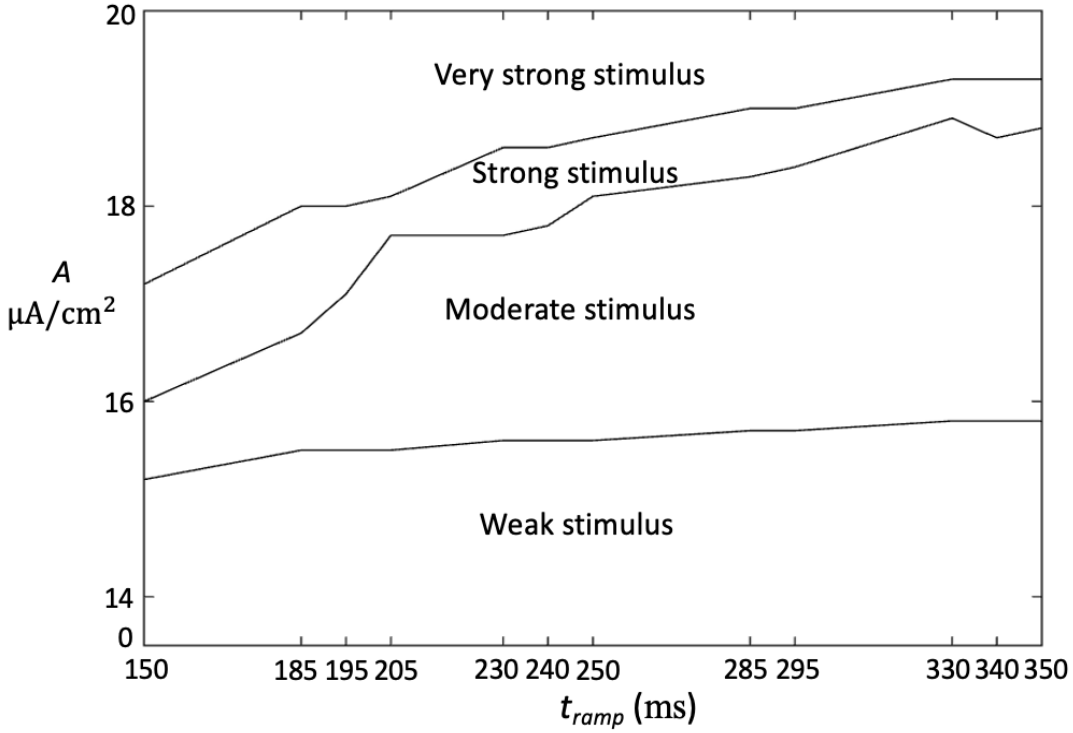

Fig. 2.5: The neuron behavior in response to stimulus strength *A* when the pulse is bigger than the ramp $A/B = 2.3$, as a function of t_{ramp}. Weak and strong stimuli do not excite neurons, but moderate stimuli do. Very strong stimuli trigger an action potential before the main pulse.

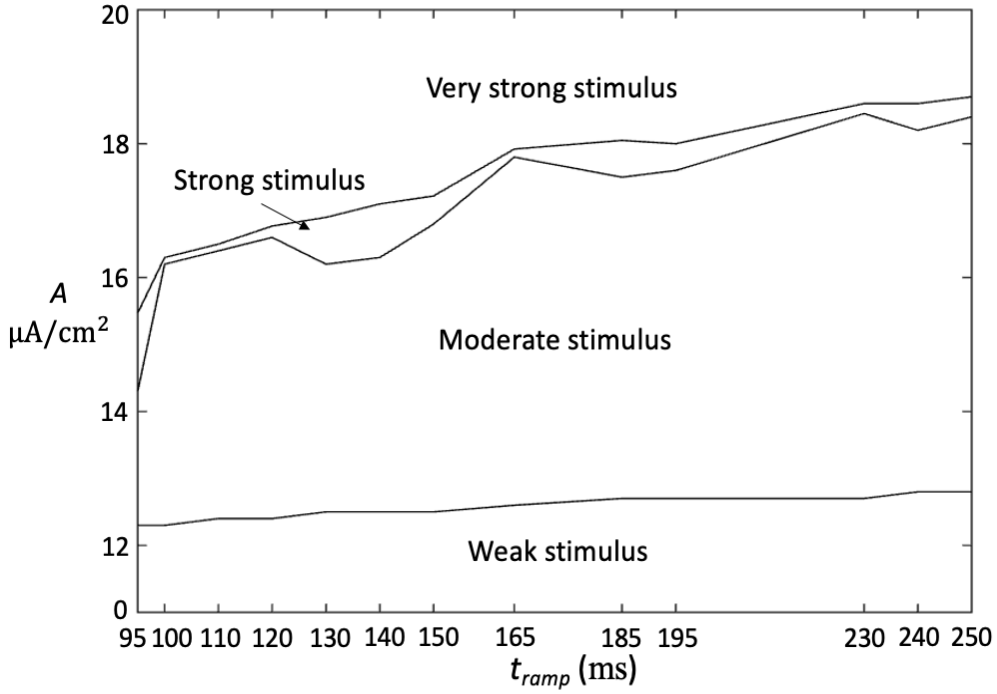

Fig. 2.6: The neuron behavior in response to stimulus strength A when the pulse is bigger than the ramp $A/B = 2.5$, as a function of t_{ramp}. Weak and strong stimuli do not excite neurons, but moderate stimuli do. Very strong stimuli trigger an action potential before the main pulse.

For the technique to be useful, the strong stimulus region should be as large as possible, and the threshold for a very strong stimulus should be high. The strong region is largest for $A/B = 2.3$. We tried smaller ratios of A/B, but the ramp makes the threshold very high for all stimulus strength in some regions, so the pulse does not excite the membrane. In the other regions, the ramp raises the membrane potential above the threshold, and the pulse excites an action potential for both moderate and strong stimulus. We see signs of an oscillation in threshold strength with time, which is most obvious Fig. 2.6.

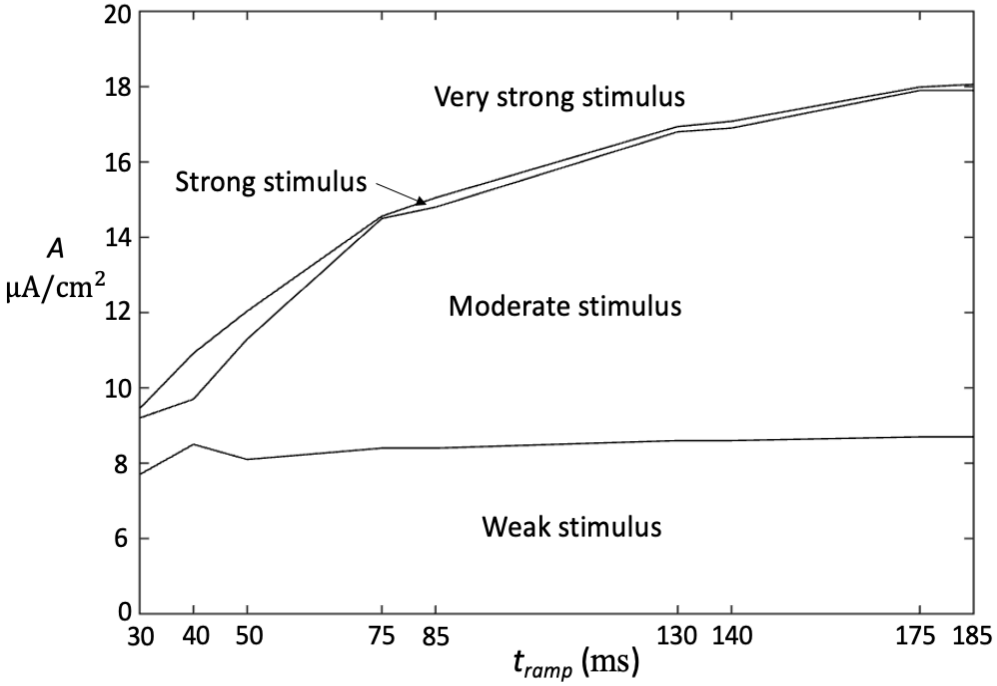

Fig. 2.7: The neuron behavior in response to stimulus strength A when the pulse is bigger than the ramp $A/B = 3$, as a function of t_{ramp}. Weak and strong stimuli do not excite neurons, but moderate stimuli do. Very strong stimuli trigger an action potential before the main pulse.

2.4 Discussion

We have examined neural stimulation using a stimulus ramp followed by a brief pulse. We have identified cases where a moderate stimulus strength excites an action potential, but a strong stimulus strength does not. For strong stimuli, the behavior of the ion channel gates indicates that the ramp makes the neuron refractory, so the subsequent pulse cannot excite an action potential.

In a cortical stimulator, the strength of the stimulus falls off with depth into the brain, but the ratio of ramp strength to pulse strength should remain the same. Therefore, our analysis focused on stimuli having a fixed ratio A/B. In Figs. 2.5–2.7, the distance from the stimulating electrode to the neuron will decrease as the strength A increases.

This method allows the stimulus from an electrode on the scalp surface to excite a deep neuron in the brain selectively. In other words, a deep neuron can be stimulated without exciting the neurons that are above it, closer to the electrode. The mechanism is that the stronger stimuli during the ramp renders the nearby neurons refractory.

A limitation of this study is that the region of strong stimulation is narrow, and depends sensitively on the neuron parameters. If the stimulus just below the electrode is too strong, it will excite the neurons during the ramp. Nevertheless, this study suggests that stimulating deep neurons selectively may be possible using a ramp-pulse stimulus. We hope that our simulations will motivate an experimental study of this method of neural stimulation.

CHAPTER THREE

THE ELECTRIC FIELD INDUCED BY A MICROCOIL DURING MAGNETIC STIMULATION

3.1 Introduction

During transcranial magnetic stimulation, a changing magnetic field induces an electric field that excites neurons in the brain (Roth et al., 1991). Traditionally, transcranial magnetic stimulation is performed by passing current pulses through a coil with a radius of several centimeters held outside the head. Typically, the current pulse through the coil has a duration of a few hundred microseconds and a strength of several kiloamps. Recently, Lee et al. (2016) claimed they could perform high-spatial-resolution magnetic stimulation using a smaller, implanted microcoil carrying less than a tenth of an amp of current. Their article is only one of many in the last decade that have examined using microcoils to stimulate the brain (Bonmassar et al., 2012; Lee and Fried, 2015; Park et al. 2018; Lee et al., 2019; Sugai et al., 2020; Ye et al., 2023).

This chapter aims to calculate the electric field during magnetic stimulation produced by a microcoil. Lee et al. (2016) predicted that a millimeter-sized, single-turn coil carrying a milliamp current produces an electric field large enough to excite a neuron. Our goal is to test that hypothesis by calculating the electric field produced by a microcoil accurately, to determine if it is large enough to excite a neuron.

3.2 Methods

We first analyzed the electric field induced by the microcoil shown in Fig. 3.1a, similar to that used by Lee et al. (2016) to stimulate the neocortex. The electric field can be calculated by

$$\mathbf{E} = -N\frac{\mu_0}{4\pi}\frac{dI}{dt}\int\frac{d\mathbf{l}}{R}, \tag{3.1}$$

where N is the number of turns in the coil, μ_0 is a constant ($4\pi \times 10^{-7}$ H/m), $I(t)$ is the current in the coil, $d\mathbf{l}$ is an element along the coil path, and R is the distance between the coil element and the field point where the electric field $\mathbf{E}$ is calculated. If we approximate the coil as a polygon, then for each side Equation (3.1) can be written as

$$\mathbf{E} = -N\frac{\mu_0}{4\pi}\frac{dI}{dt}\frac{\boldsymbol{\delta}}{\delta}\left\{\sinh^{-1}\left[\frac{\frac{\delta}{2R}+\cos\varphi}{\sin\varphi}\right]-\sinh^{-1}\left[\frac{-\frac{\delta}{2R}+\cos\varphi}{\sin\varphi}\right]\right\}, \tag{3.2}$$

where $\sinh^{-1}$ is the inverse of the hyperbolic sine function, $\boldsymbol{\delta}$ is a vector along one element of the coil, $\boldsymbol{R}$ is the vector from the field point to the midpoint of the element, and φ is the angle between $\boldsymbol{R}$ and $\boldsymbol{\delta}$ (Roth et al., 1991).

The parameters we used in our calculation are defined in Fig. 3.1a for the square-microcoil used by Lee et al. (2016). The microcoil is a single-turn (N = 1), square loop (500 μm per side), carrying a current with an amplitude of 1 mA. The time course of the coil current is half a period of a 3-kHz sine wave. The electric field was calculated at a distance z = 0.3 μm above the plane of the coil, corresponding to the thickness of the insulating layer separating the coil from the neural tissue.

In addition, we analyzed Lee et al.'s "asymmetric" microcoil (Fig. 3.1b), with the same parameters used for the square microcoil, except for the geometry of the coil. The asymmetric microcoil is 1000 µm long and 100 µm wide, but narrows to 50 µm by the end of the last 200 µm of the microcoil. We also examined Lee et al.'s (2019) W-microcoil (Fig. 3.1c). This microcoil is a single-turn and is shaped like a W with a length of 500 µm and a width of 70 µm. The current is 1 mA with a frequency of 5 kHz, and the electric field is calculated in a plane 15 µm above the coil. Finally, we used the parameters of Sugai et al. (2020) to study their V-microcoil shown in (Fig. 3.1d). It has a single-turn, is 500 µm long and 100 µm wide, carries a current with an amplitude of 78 mA and has a stimulation frequency of 100 Hz. Sugai et al. (2020) did not report the distance from the microcoil to the plane where the electric field was calculated, so we assume z = 30 µm.

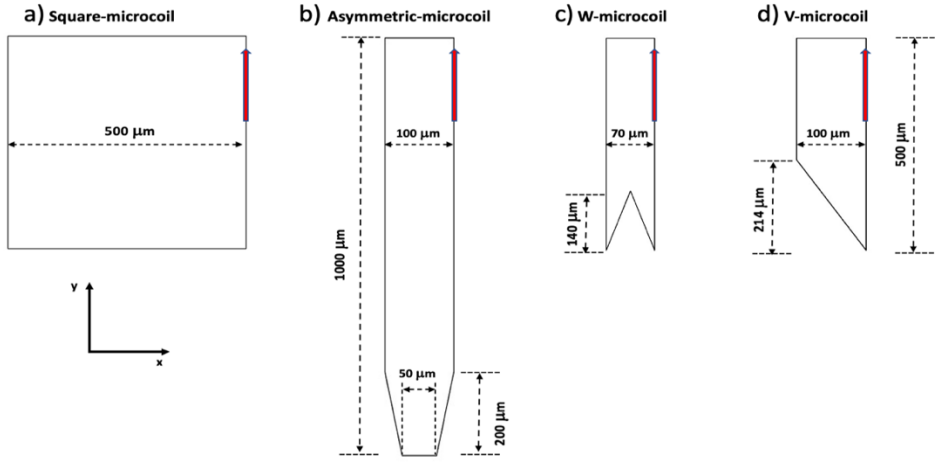

Fig. 3.1: Microcoil designs. a) A square microcoil (Lee et al., 2016), b) an asymmetric microcoil (Lee et al., 2016), c) a W-shaped microcoil (Lee et al., 2019), and d) a V-shaped microcoil (Sugai et al., 2020).

3.3 Results

We calculated the electric field for each side of the microcoil shown in Fig. 3.1a and added them together to get the total electric field **E** (for details, see Appendix B). Figure 3.2 (a) and (b) shows the distribution of the *x*-component of the electric field, E_x, and its gradient, dE_x/dx. The peak electric field arising from the square coil carrying a current of 1 mA is 26 μV/m (Fig. 3.3c), and the peak electric field gradient is 3.6 V/m^2 (Fig. 3.3d), at $y = -250$ μm. The field and its gradient are different than Lee et al. (2016) found in their calculations. They obtained a value of dE_x/dx of approximately 50,000 V/m^2, which differs from our value by more than a factor of ten thousand. To obtain their gradient, we would need to use a current near 14 A, a different frequency, or multiple coil turns.

We calculated the electric field and its gradient for Lee's asymmetric coil (Fig. 3.1b) using the same parameters as in Lee et al. (2016). We found similar results as in Fig. 3.2. Figure 3.3 (a) and (b) shows the distribution of the *x*-component of the electric field, E_x, and its gradient, dE_x/dx. The peak electric field, E_x, was 21 μV/m (Fig. 3.3c), and the peak electric field gradient, dE_x/dx, was 3.6 V/m^2 (Fig. 3.3d) at $y = -500$ μm. Lee et al. calculated a peak electric field of a few volts per meter, implying that their results are about a factor of 100,000 larger than ours; their peak electric field gradient was about 10,000 larger than ours (see their Fig. 2a).

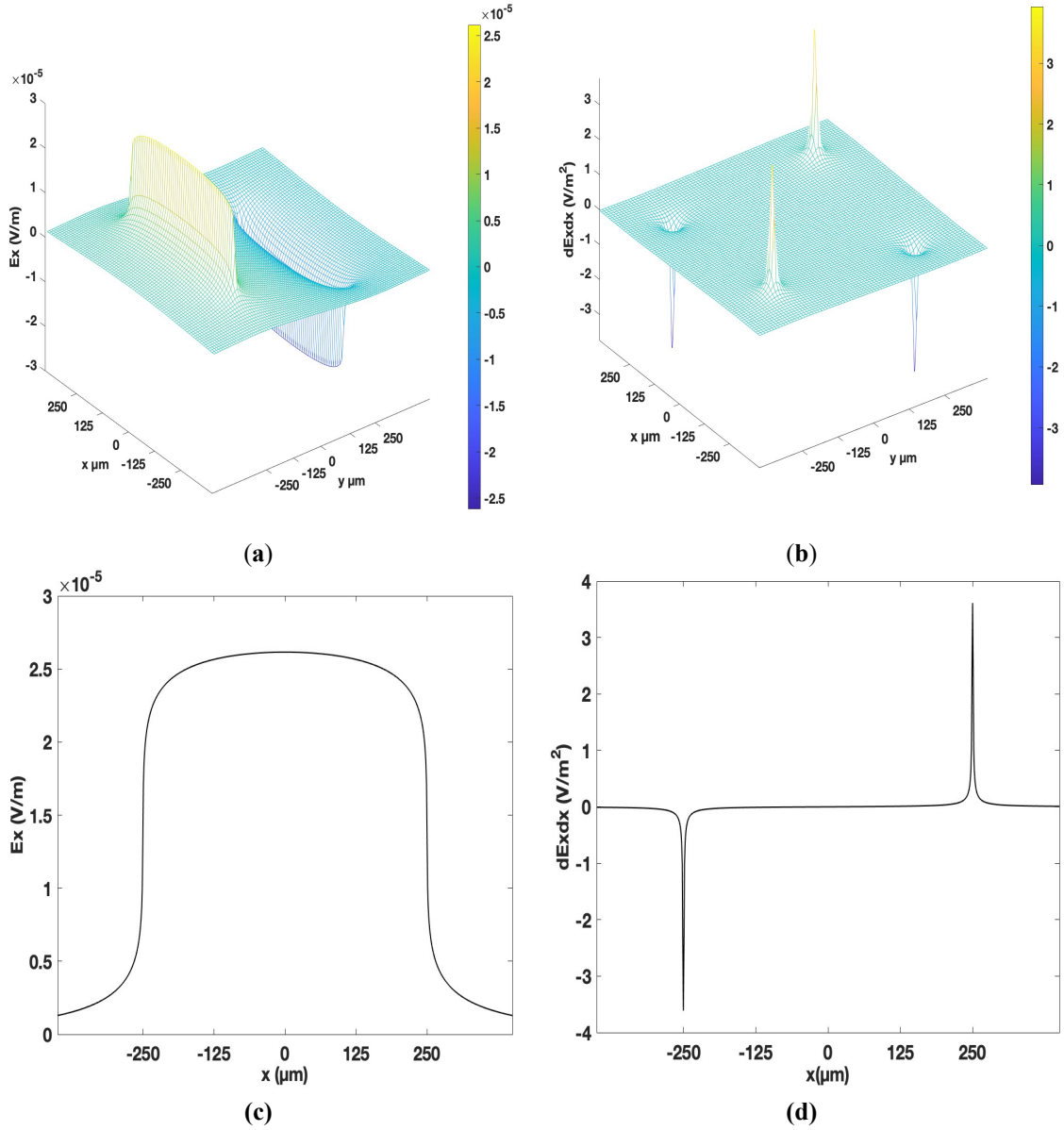

Fig. 3.2: Square microcoil. a) The distribution of the electric field E_x in the plane z = 0.3 µm above the plane of the coil, b) The distribution of dE_x/dx, c) The electric field E_x peak value of 26 µV/m, and d) the magnitude of dE_x/dx has a peak of 3.6 V/m^2

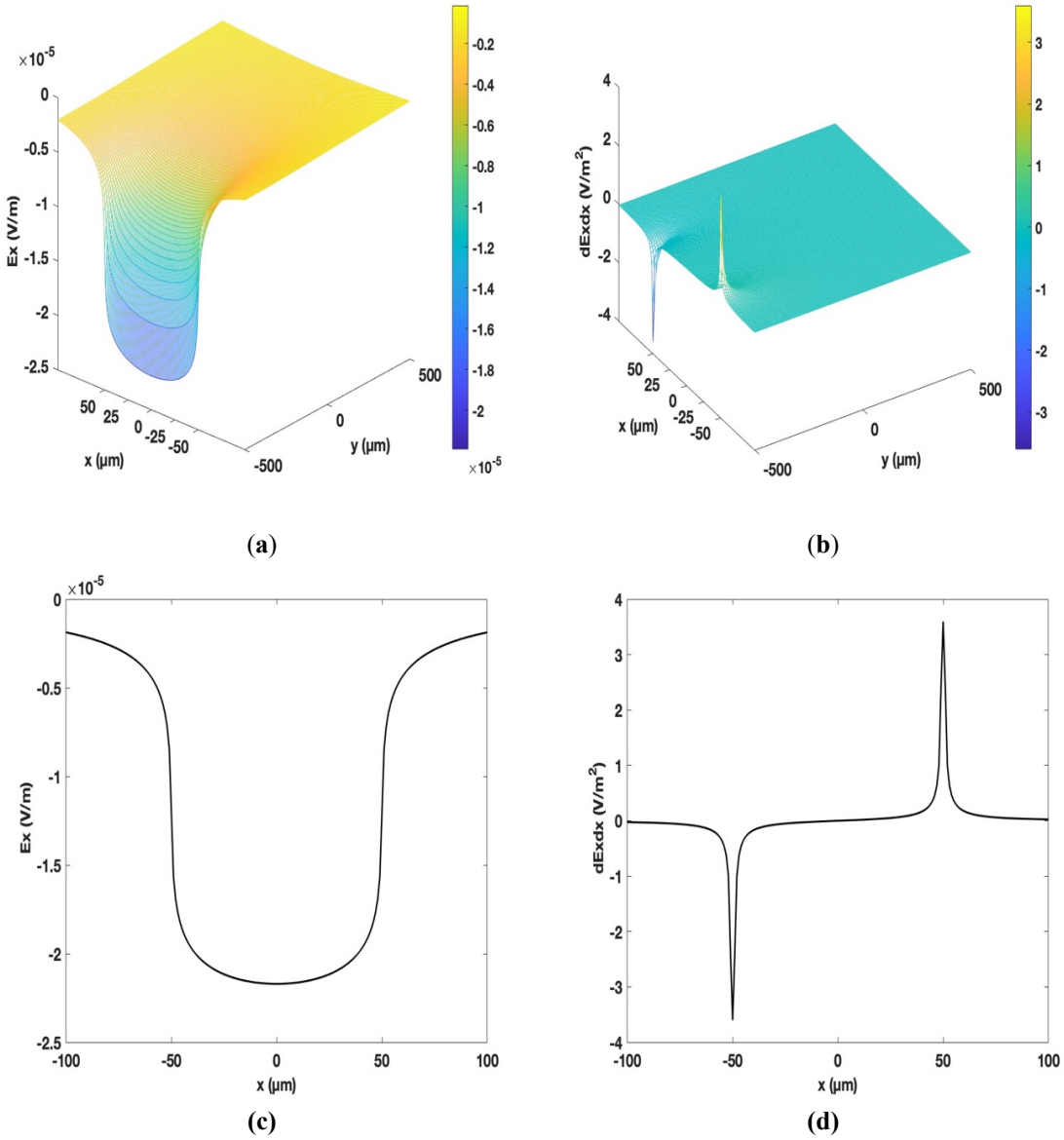

Fig. 3.3: Asymmetric coil. a) The distribution of the electric field E_x in the plane z = 0.3 μm above the plane of the coil, b) The distribution of dE_x/dx, c) The electric field E_x peak value of 21 μV/m, and d) the magnitude of dE_x/dx has a peak of 3.6 V/m^2.

In another study, Lee et al. (2019) claimed that the spatial gradient could exceed 11,000 V/m^2 for their W-coil (Fig. 3.1c), using a current with a frequency of 5 kHz and a strength of 1 mA, and calculating the electric field in a plane 15 μm above the coil. When we repeated their calculation, we found a peak gradient dE_x/dx of 0.077 V/m^2 at $y = -103$ μm (Fig. 3.4a), and dE_y/dy of 0.338 V/m^2 at $x = -25$ μm (Fig. 3.4b).

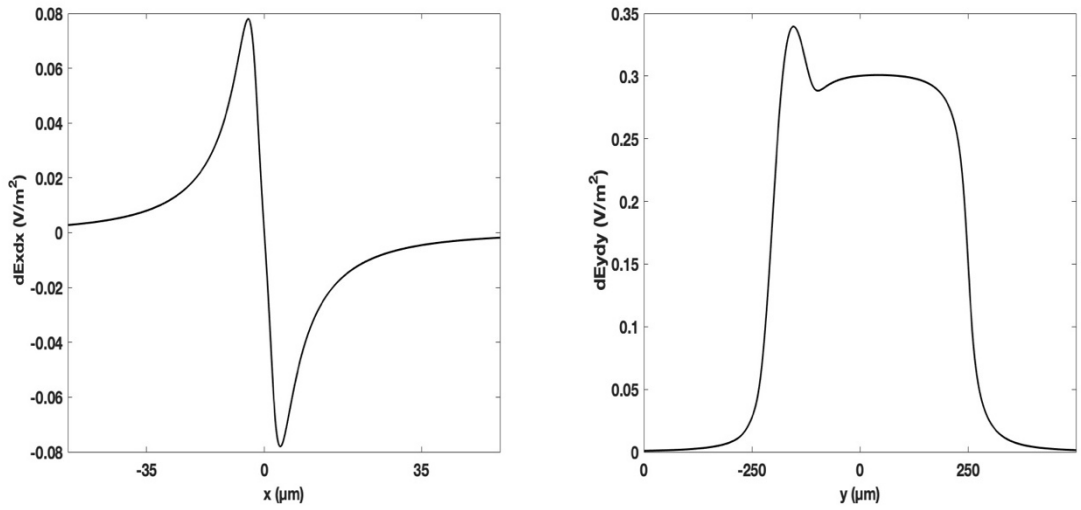

(**a**) (**b**)

Fig. 3.4: W-coil. a) The gradient field dE_x/dx peak value of 0.077 V/m^2, b) The gradient field dE_y/dy peak value of 0.338 V/m^2.

Finally, we also repeated Sugai et al.'s (2020) calculation for a V-coil (Fig. 3.1d). Their coil current is 78 mA, with a frequency 100 Hz, but they did not mention the distance from the plane of the coil to where they calculated the electric field (we assume a value of 30 μm). Using their current with a frequency of 1 kHz, we obtain a peak electric field in the x direction at $y = -150$ μm, E_x, of 86 μV/m (Fig. 3.5a), a peak gradient, dE_x/dx, of 0.619 V/m^2 at $y = -90$ μm (Fig. 3.5b), a peak electric field in the y

direction at x = 7 μm, E_y, of 126 μV/m (Fig. 3.5 (c)), and a peak gradient at y = –27 μm, dE_y/dy, of 2.9 V/m^2 (Fig. 3.5 (d)).

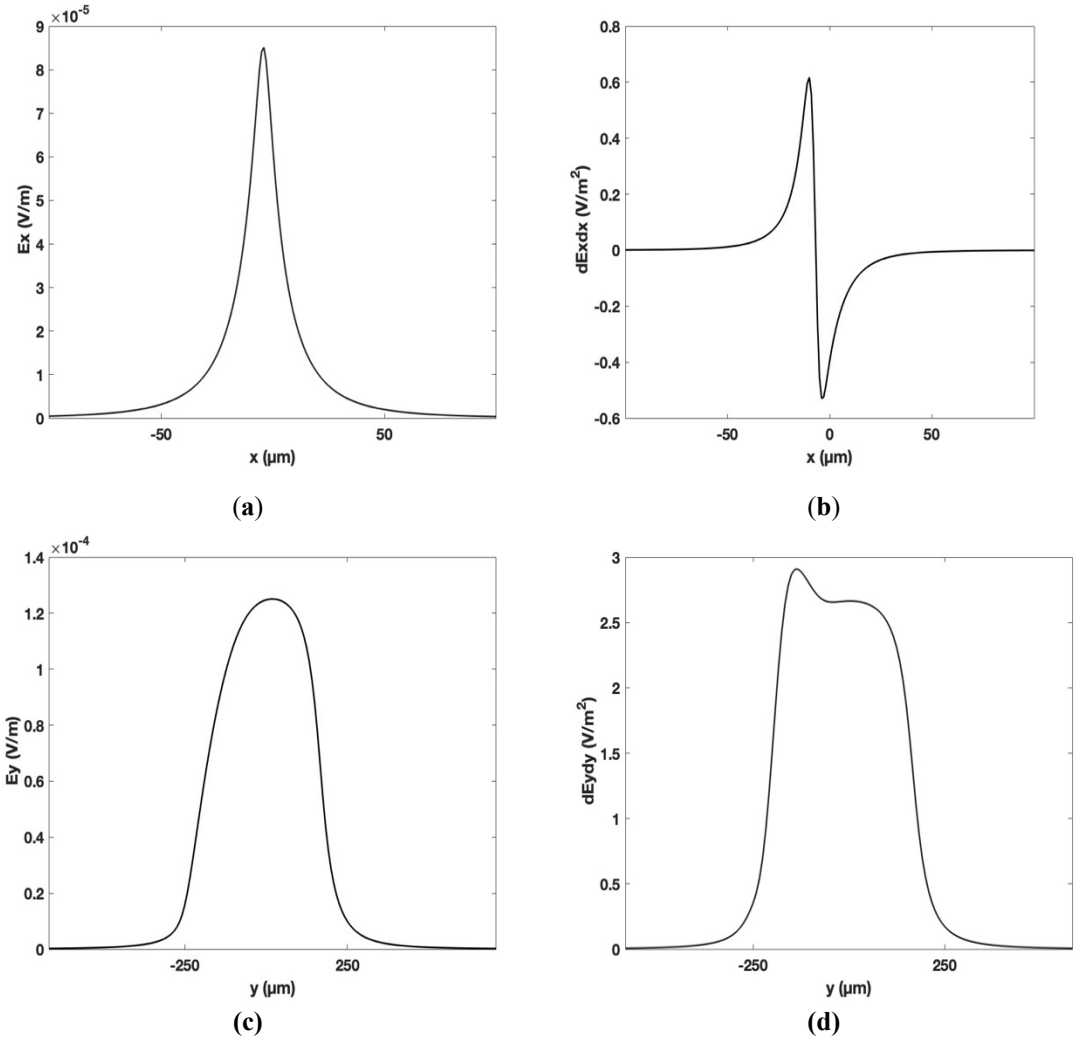

Fig. 3.5: V-coil. a) The electric field E_x peak value of 86 μV/m, and b) the magnitude of dE_x/dx has a peak of 0.619 V/m^2, c) The electric field E_y peak value of 126 μV/m, and d) the magnitude of dE_y/dy has a peak of 2.9 V/m^2.

In addition, Sugai et al. (2020) used a higher frequency to more accurately map the electric field distribution. When we used their current of 20 mA and frequency of 30

MHz, we find a peak electric field, E_x, of 0.66 V/m, a peak gradient, dE_x/dx, of 4790 V/m^2, a peak electric field, E_y, of 1 V/m, and a peak gradient, dE_y/dy, of 22,522 V/m^2. Sugai et al. (2020) claim their maximum value of the gradient is 23,800 V/m^2. So, in their high-frequency study, their calculated electric field gradient is similar to ours.

3.4 Discussion

Our calculations indicate that the electric field induced by the microcoil in Fig. 3.1(a) is 0.000026 V/m, which is five orders of magnitude weaker than calculated by Lee et al. (2016). We also found an electric field gradient on the order of 3.6 V/m^2, which is four orders of magnitude smaller than Lee et al. calculated. In Roth et al. (1991), the order-of-magnitude electric field induced by current in a coil is given by

$$E = 0.1\, N\, \frac{\partial I}{\partial t} \tag{3.3}$$

where $\frac{\partial I}{\partial t}$ has units of A/μs and E is in V/m. Using a current of 1 mA, with a frequency of 3 kHz, passed through a one turn coil, Eq. (3.3) implies that the electric field should be on the order of 2 μV/m. This estimate is similar to, but somewhat smaller than, our result, but is dramatically smaller than the report by Lee et al. (2016). Equation (3.3) is based on Eq. (3.1), but the integral is not included. Roth et al. (1991) note that the integral is dimensionless, meaning that its value is independent of the length scale: the electric field one coil radius below a 10 mm coil is the same as the electric field one coil radius below a 0.1 mm coil, assuming the geometry is the same except for the length scale. Having the coil closer to the nerve is exactly counterbalanced by having a smaller coil.

Many authors studying microcoils emphasize the gradient of the electric field, rather than the electric field itself, as the relevant quantity. The focus on dE_x/dx arises from a study by Roth and Basser (1990), which derived the cable equation governing the transmembrane potential along a nerve axon. That analysis found that the source term in the cable equation (called the "activating function") is dE_x/dx. Applying this result to brain stimulation has two limitations. 1) The transmembrane potential should be nearly proportional to dE_x/dx when the electric field varies gradually over distances similar to the axon length constant (about 1 mm). This is the case for magnetic stimulation using a large coil held centimeters from the nerve, but not for an implanted microcoil. When the induced electric field varies dramatically over one length constant, the relationship between the transmembrane potential and the activation function is more complex (see Chapter 5). 2) The activating function derived by Roth and Basser (1990) is appropriate for long, straight axons, such as in peripheral nerves. In the brain, the neurons have irregular shapes, their axons can change direction, and often the axon terminates on other neurons (Roth, 1994). In these cases, the electric field may determine neural excitation instead of the activating function (Maccabee et al., 1993). Our calculations, therefore, show both the electric field and its gradient. Although the electric field does not depend on the length scale used in the calculation, the electric field gradient does depend on the length scale. This may explain why reported dE_x/dx values are in somewhat better agreement with our results than are reported E_x values. Regardless of if we use E_x or dE_x/dx, our calculations indicate the stimulus is considerably less than that found in other studies.

The threshold for neural excitation is on the order of 10 V/m (Tranchina and Nicholson, 1986; Hause, 1975; Roth, 1994), although weaker fields, as low as 0.1 V/m, may change the spontaneous firing rate in a neural network (Francis et al., 2003). Our calculated value of E_x is 26 μV/m, equal to 0.000026 V/m, which falls nearly a factor of a million below the 10 V/m threshold. Clever coil geometries might increase the electric field strength slightly, but that is unlikely to make up such a large difference in field strength. Lee et al. (2016) used a coil current of 1 mA in their calculations, but in experiments they used a coil current more like 50 mA. This significantly larger coil current still leaves the electric field over a factor of one thousand too weak to trigger neural activation.

Some microcoil studies did not report the distance from the plane of the coil to the plane where the electric field was calculated. To compare our results to Lee et al.'s (2016) study, we used a distance of 300 nm, which is smaller than the size of a neuron and smaller than the width of the coil wire. This small distance means that our calculated electric field overestimates the actual electric field experienced by a neuron, making the discrepancy between our results and Lee et al.'s (2016) even greater.

Different values of current and numbers of turns were used in previous studies. Bonmassar et al. (2012), Park et al. (2018), and Yoshikawa et al. (2022) all used coils with more turns and carrying larger currents than did Lee et al. (2016), and found results similar to what we calculate.

Our calculations indicate that Lee et al. (2016) and Lee et al. (2019) could not have excited the neurons by magnetic stimulation; the electric field is too weak. Two questions remain unresolved. First, why are our calculations and those of Lee et al.

(2016) so different? We do not have a good answer to this question, but we include our calculation in Appendix B and our computer code in Appendixes C, D, E and F, so anyone can check our results. Second, Lee et al. (2016) were clearly exciting neurons. If the mechanism of excitation was not magnetic stimulation, then what was it? Capacitive coupling may be the cause of excitation (see Chapter 4).

CHAPTER FOUR

THE STIMULATION OF A NERVE BY A CURRENT PULSE THROUGH MICROCOIL VIA CAPACITIVE COUPLING

4.1 Introduction

Magnetic stimulation therapy has become a highly effective treatment for many neurological conditions, such as depression (Rizvi and Khan, 2019). In 1985, Dr. Anthony Barker et al. invented transcranial magnetic stimulation, TMS, in which a current passes through a coil held outside the head, with a strength of several kiloamps lasting a few hundred microseconds, and his device was able to stimulate the motor cortex in the brain (Barker et al., 1985). This current caused a change in the magnetic field, which resulted in an induced electric field (electromagnetic induction) that could stimulate a neuron when it reached its threshold for firing an action potential, helping and improving neurological symptoms (Wyszkowska, Jankowska, and Gas, 2019) such as depression (Yesavage et al., 2018) and Alzheimer's disease (Koch et al. 2018). Despite the widespread use of TMS therapy, it has poor spatial resolution, which makes it challenging to activate selectively the deeper targeted regions of the brain and achieve a focused stimulation (Bonmassar et al., 2012; Ridding and Rothwell, 2007; Wagner et al., 2007; Syrek and Bărbulescu, 2017).

Recently, microcoil technology has been a significant development in magnetic stimulation therapy (Liu et al., 2023; Ye et al., 2023; Lee et al., 2023; Tian et al., 2023; Jeong et al., 2021). (The term “microcoil” is often used, although these devices do not necessarily have a circular shape like a traditional “coil” but rather sometimes appear to

be more like a bent wire.) Unlike traditional TMS, microcoils induce a highly localized and precise electric field, making it easier to stimulate specific brain regions (Park et al., 2013). The improvement in spatial resolution comes at the cost of implanting the microcoil, which makes its use more invasive. Nevertheless, for some applications the advantage of an increase in spatial resolution may override the disadvantage of implantation.

Researchers have made considerable progress in constructing microcoils with various sizes, shapes, and configurations. In 2012, Bonmassar et al. designed a microcoil with a radius of 500 micrometers and a height of 1 mm, made from 21 turns of copper wire placed 300 micrometers above the soma of an isolated ganglion cell (Bonmassar et al., 2012). When a few amps of current were passed through this microcoil it produced a strong enough electric field to stimulate neurons effectively. Since then, other researchers have designed different microcoils requiring several amps of current and multiple coil turns to stimulate neurons (Park et al., 2018; Yoshikawa et al., 2022). This development of small, implantable microcoil technology has opened up new possibilities in treating neurological conditions, offering a new approach to magnetic stimulation therapy. The critical concept in understanding microcoil stimulation is the electric field that it can produce. It can be affected by multiple factors, including the strength of the current and its frequency, the distance between the coil and the nerves, the number of coil turns, and the properties of the surrounding tissues.

In 2016, Lee et al. designed a single-turn microcoil and they were able to stimulate neurons with only 40 mA current. They claimed that magnetic stimulation was the mechanism of this excitation (Lee et al., 2016). Alzahrani and Roth were skeptical

that magnetic stimulation was responsible for excitation because the induced electric field was too weak (Alzahrani and Roth, 2023; see Chapter 3). According to previous studies, the threshold for neuronal excitation is an electric field intensity of approximately 10 V/m (Hause, 1975; Tranchina and Nicholson, 1985). (However, weaker fields, as low as 0.1 V/m, may alter the spontaneous firing rate in a neural network (Francis et al., 2003)). Alzahrani and Roth suggested that capacitive coupling may be a more likely mechanism than magnetic stimulation (Alzahrani and Roth, 2023).

The primary purpose of this investigation is to calculate the electric field in the brain during neural stimulation using capacitive coupling. This paper presents an analysis of the electric field induced by capacitive coupling by utilizing the parameters from Lee et al.'s (2016) study. We aim to provide a detailed calculation of the electric field generated by this method. Additionally, our study compares the results of the capacitive coupling analysis to the electric field expected during magnetic stimulation. With the increasing use of microcoil technologies in medical and therapeutic applications, the findings of this study provide insights into the mechanisms of exciting neurons.

4.2 Methods

We model the stimulating coil as a straight length of copper wire of radius *a* and length *2L*, surrounded by a tissue of radius *b* (we assume $b >> a$). The copper has conductivity σ_i and the surrounding tissue has conductivity σ_e. The resistance per unit length of the wire is then $r_i = 1/(\sigma_i \pi a^2)$ and of the surrounding space is $r_e = 1/(\sigma_e \pi b^2)$. The two are coupled capacitively. The wire insulation has a capacitance per unit area $C = \frac{\kappa \varepsilon_o}{d}$, determined by the dielectric constant of the insulator κ and its

thickness *d*. We assume the resistance of the insulation is infinite. This model for the wire is essentially the same as the cable model for a nerve axon, except that we take the "membrane" conductance to be zero. Figure 4.1 illustrates the model.

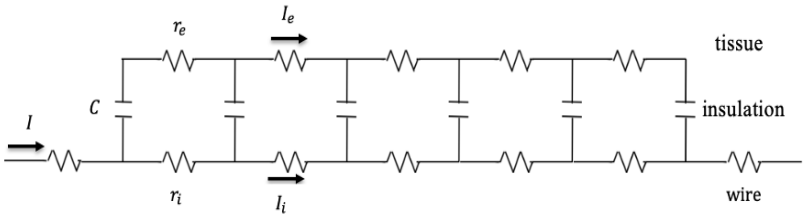

Fig. 4.1: A model of a wire coupled to the surrounding tissue by a capacitance. The current in the wire is I_i, the wire resistance per unit length is r_i, the current in the tissue is I_e, the tissue resistance per unit length is r_e, the capacitance per unit area of the insulation is C, and the current applied to the wire at its ends is I.

Our analysis follows the traditional derivation of the cable equation (Wu and Wikswo, 1997). The position along the cable is denoted by x, with $x = 0$ at the center and $x = \pm L$ at the ends. Time is denoted t. To derive an equation governing the voltages in the wire, V_i, and in the surrounding tissue, V_e, consider a section of the wire of length Δx. The wire current, I_i, entering this section from the left is $I_i(x)$ and the current leaving this section on the right is $I_i(x+\Delta x)$. The current exiting the wire through the capacitance is $C\,\partial(V_i - V_e)/\partial t$ times the wire's surface area $2\pi a \Delta x$. Taking the limit as Δx goes to zero, this relationship becomes $-\frac{\partial I_i}{\partial x} = 2\pi a C \frac{\partial (V_i - V_e)}{dt}$. In the copper the current and voltage are related by Ohm's law, $I_i = -\frac{1}{r_i}\frac{\partial V_i}{\partial x}$, so this equation becomes $\frac{1}{r_i}\frac{\partial^2 V_i}{\partial x^2} = 2\pi a C \frac{\partial (V_i - V_e)}{dt}$. A similar relationship can be derived for the tissue space, but a minus sign is introduced

because capacitive current exiting the wire is entering the tissue. We can rearrange these expressions and define a diffusion constant as $D = \frac{1}{2\pi aC(r_i+r_e)}$, resulting in the pair of differential equations:

$$\frac{\partial}{\partial t}(V_i - V_e) = D\left(\frac{r_i+r_e}{r_i}\right)\frac{\partial^2 V_i}{\partial x^2} \quad \text{and} \quad \frac{\partial}{\partial t}(V_i - V_e) = -D\left(\frac{r_i+r_e}{r_e}\right)\frac{\partial^2 V_e}{\partial x^2}\,. \tag{4.1}$$

Next, we introduce two new voltages—the voltage across the insulation, V, and a weighted average voltage, ψ—defined by

$$V = V_i - V_e \quad \text{and} \quad \psi = V_i + \frac{r_i}{r_e}V_e\ . \tag{4.2}$$

which can be inverted to give V_i and V_e in terms of V and ψ

$$V_i = \frac{r_e}{r_i+r_e}\left(\psi + \frac{r_i}{r_e}V\right) \quad \text{and} \quad V_e = \frac{r_e}{r_i+r_e}(\psi - V)\,. \tag{4.3}$$

You can use Eqs. (4.1) and (4.2) to show that $V(x,t)$, the voltage across the insulation, obeys the diffusion equation, and $\psi(x,t)$, a weighted average of the wire and tissue voltages, obeys a one-dimensional version of Laplace's equation

$$\frac{\partial V}{\partial t} = D\frac{\partial^2 V}{\partial x^2} \quad \text{and} \quad \frac{\partial^2 \psi}{\partial x^2} = 0\,. \tag{4.4}$$

Our introduction of the diffusion constant earlier was motivated by its appearance in the diffusion equation for the voltage difference across the wire capacitance.

We assume a sinusoidal stimulus current (the system is driven by a current source, not a voltage source), $I(t) = I_o \sin(\omega t)$, where $\omega = 2\pi f$ and f is the frequency. The

diffusion time can be defined as L^2/D and is the same as the RC time constant of the wire: the resistance $(r_i + r_e)L$ times the capacitance $C2\pi aL$.

For $t < 0$, the initial condition is $V = \psi = 0$. At the ends $x = \pm L$, all the current is in the wire and none is in the tissue, implying

$$\frac{\partial V_e}{\partial x} = 0 \qquad \text{and} \qquad \frac{\partial V_i}{\partial x} = -I_o r_i \sin(\omega t) \; . \tag{4.5}$$

In terms of V and ψ, these boundary conditions become

$$\frac{\partial V}{\partial x} = -r_i I_o \sin(\omega t) \quad \text{and} \quad \frac{\partial \psi}{\partial x} = -r_i I_o \sin(\omega t) \; . \tag{4.6}$$

The equation for $\psi(x,t)$ in Eq. (4.4) can be solved analytically,

$$\psi(x,t) = -r_i I_o \sin(\omega t) x \; . \tag{4.7}$$

The diffusion equation for *V(x,t)* in Eq. (4.4) must be solved numerically (Press et al., 1992). The derivatives are approximated using finite differences with space step Δx and time step Δt

$$V(x, t + \Delta t) = V(x,t) + D\frac{\Delta t}{\Delta x^2}[V(x + \Delta x, t) + V(x - \Delta x, t) - 2V(x,t)] \; . \tag{4.8}$$

The calculation must satisfy the stability criterion

$$\frac{4D\Delta t}{\Delta x^2} \leq 1 \; . \tag{4.9}$$

The parameters we used in the calculation are given in Table 1, selected to approximately match those used experimentally by Lee et al. (2016). They imply $D = 1.8$ m^2/s, $r_i = 850$ Ω/m and $r_e = 320\ M\Omega$/m. Clearly $r_i << r_e$ as you would expect. The DC resistance of the coil is 1.7 Ω. The capacitance per unit area is $C = 0.00011$ F/m^2. This is about a hundred times smaller than the capacitance of the cell membrane, 0.01 F/m^2 or $1\ \mu F/cm^2$, because the insulation thickness, 300 nm, is nearly a hundred times greater than the thickness of a cell membrane. The diffusion time is 0.56 μs. In the calculation, we used Δx = 0.1 mm and Δt = 0.001 μs, implying the quantity on the left side of Eq. (4.9) is 0.72 and the calculation is stable.

Table 4.1: Parameters used in the calculation (from Lee et al., 2016).

Parameters	**Definition**	**Value**	**Unit**
κ	Insulation dielectric constant	3.8	-
σ_e	Tissue conductivity	0.1	$(\Omega\text{m})^{-1}$
σ_i	Wire conductivity	60 x 10^6	$(\Omega\text{m})^{-1}$
d	Insulation thickness	300	nm
a	Wire radius	2.5	μm
b	Tissue radius	0.1	mm
L	Half the wire length	1	mm
I_o	Amplitude of applied current	1	mA
f	Frequency	3	kHz

Using a MATLAB program (R2022b), we calculated the electric field generated by the model shown in Fig. 4.1. The current in the wire was 1 mA with a frequency of 3 kHz. The voltage in the wire V_i and the tissue V_e varied as a function of time and space, and we expressed this variation using the functions ψ and V in terms of V_i and V_e. After

determining the values of ψ and V using the parameters outlined in Table 1, we could calculate the voltage along the wire V_i and the voltage in the tissue V_e. Finally, we calculated the electric field E in the tissue by taking the gradient of V_e. The MATLAB program used to perform the calculation is given in Appendix G.

4.3 Results

When we calculate the voltages, we find that ψ and V are nearly the same: they are both approximately linear in x (Fig. 4.2), and both are nearly sinusoidal in time (Fig. 4.3). This behavior occurs because the diffusion time (L^2/D = 0.56 μs) is much less than the period of the applied current (333 μs). The voltage difference between the ends of the wire, ΔV_i, is nearly equal to $\Delta\psi$ for $r_e >> r_i$, so from Fig. 4.2 we see that the voltage difference is about 1.7 mV. The voltage in the tissue, V_e, is approximately the difference between ψ and V, which is difficult to determine from Figs. 4.2 and 4.3 but is not zero (Fig. 4.4). It has a maximum amplitude at the ends of the coil and a maximum slope at the center. The magnitude of the electric field in the tissue is about 4 mV/m at $x = 0$.

The time course for V_e and E (Fig. 4.5) are approximately proportional to $\cos(\omega t)$. Therefore, the tissue electric field is 90 degrees out of phase with the coil current. Because the initial condition is $V_e = 0$, the tissue potential rises abruptly near $t = 0$ (Fig. 4.6). In about one microsecond (roughly the diffusion time) it reaches its asymptotic behavior.

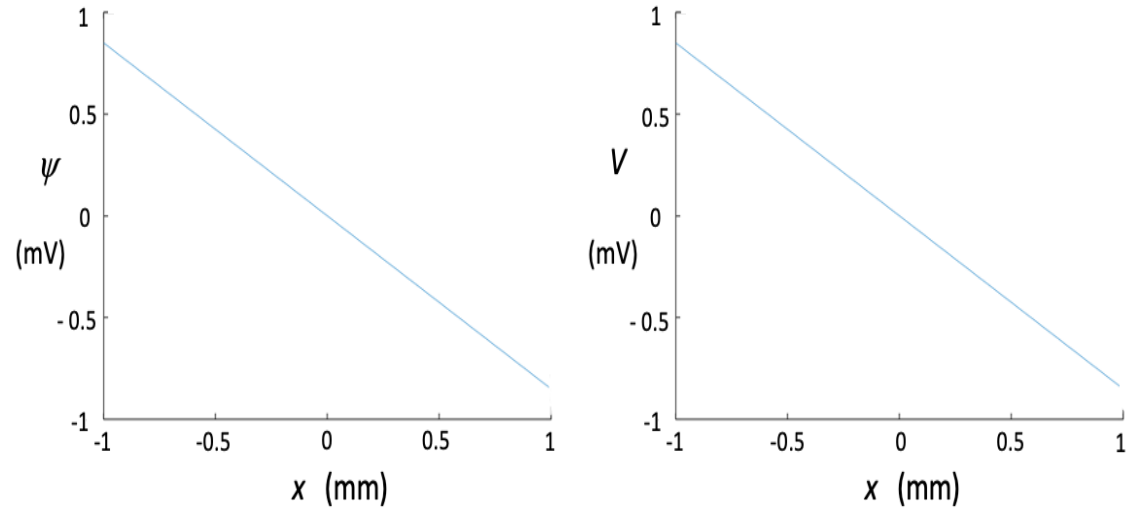

(**a**) (**b**)

Fig. 4.2: a) The weighted average voltage ψ and b) the voltage across the insulation V as functions of position x at time t = 83 μs (the time of the peak of the first phase of the sine wave).

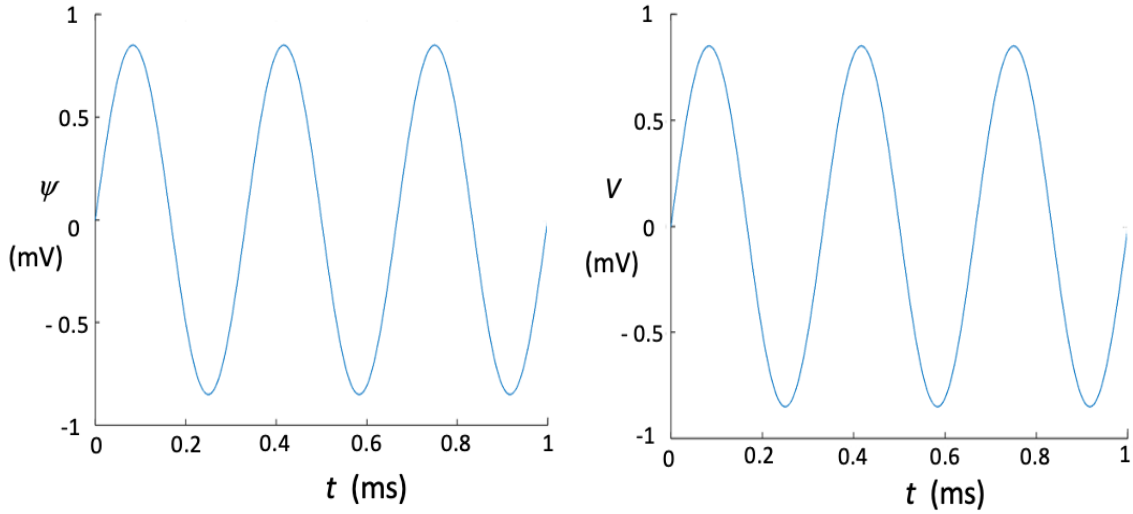

(**a**) (**b**)

Fig. 4.3: a) The weighted average voltage ψ and b) the voltage across the insulation V as functions of time t at position x = –10 mm (the left end of the wire).

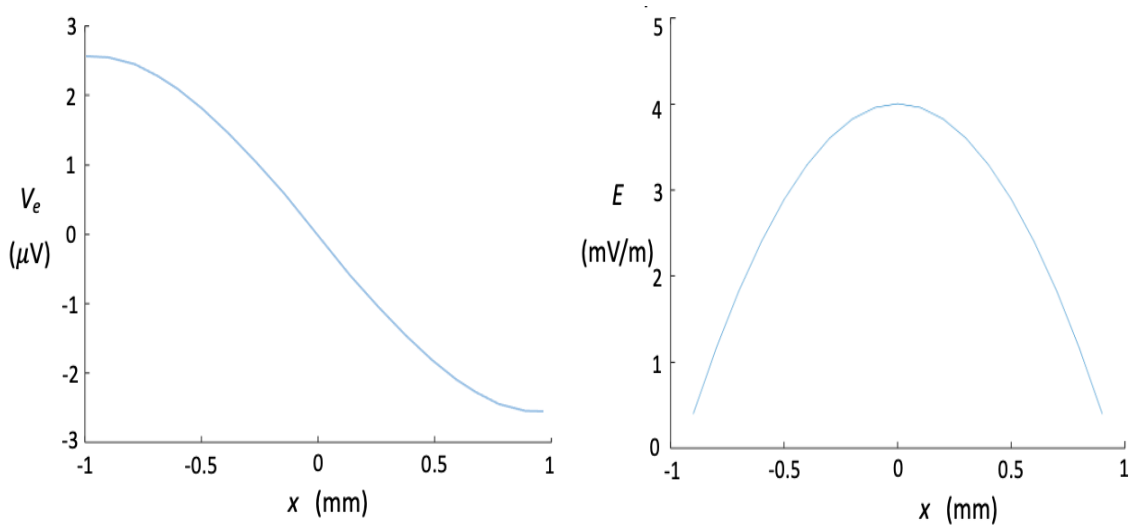

(**a**) (**b**)

Fig. 4.4: a) The voltage in the tissue V_e and b) the tissue electric field E as functions of position x at time t = 333 μs.

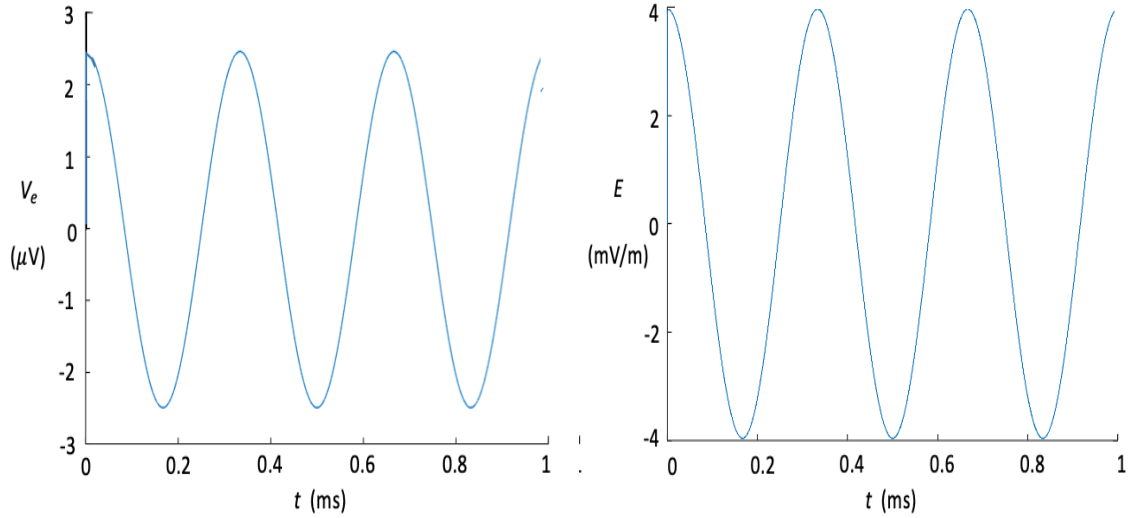

(**a**) (**b**)

Fig. 4.5: a) The voltage in the tissue, V_e, at position x = –10 mm and b) the tissue electric field, E, at position x = 0; both as functions of time t.

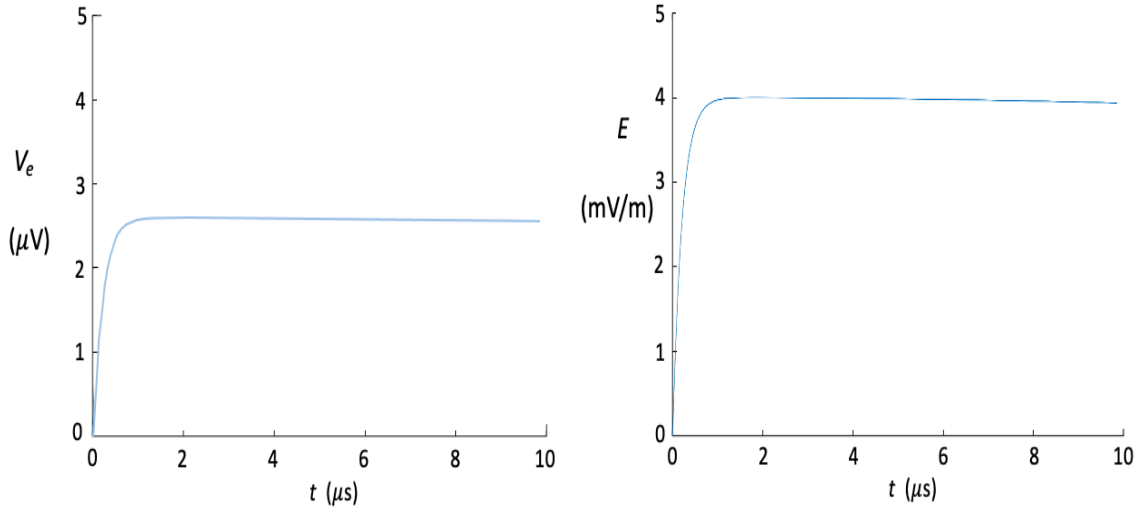

(**a**) (**b**)

Fig. 4.6: a) The voltage in the tissue, V_e, at position $x = -10$ mm and b) the tissue electric field, E, at position $x = 0$; both as functions of time t. This is the same data as in Fig. 4.5, but over a shorter range of time.

The voltage drop across the tissue is about 0.005 mV, compared to a drop of 1.7 mV in the wire. The tissue voltage drop, and therefore the tissue electric field, is so small because of the high resistance of the current path through the tissue (about 640,000 Ω) compared to that through the wire (1.7 Ω). Neither the tissue conductivity nor the radius of the cylindrical tissue space is known accurately, and the tissue conductivity may be heterogeneous (Syrek, 2019) . Figure 4.7 shows the peak electric field strength as a function of the tissue resistance per unit length, r_e.

Lee et al. performed a test to determine if capacitive currents were important by passing a large transient current to burn a small portion of the coil, leaving an open circuit (Lee et al., 2016). We can simulate this experiment by dramatically increasing r_i. When we set $r_i = 30$ MΩ/m, we found that the electric field was 143,385 mV/m.

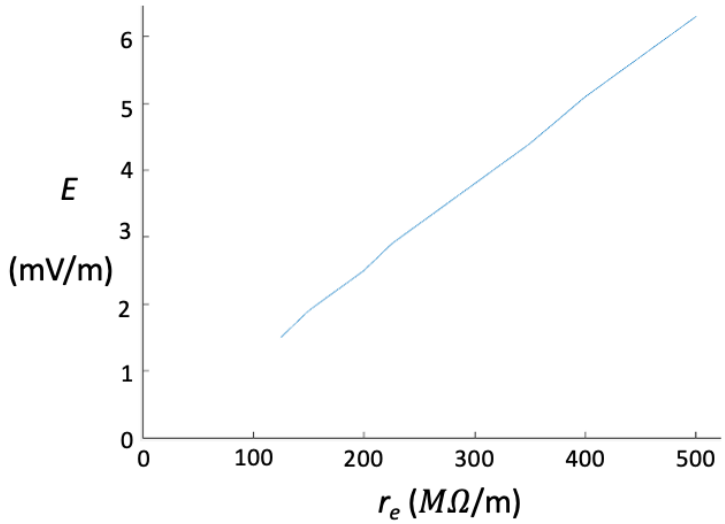

Fig. 4.7: The peak tissue electric field intensity, E, as function of the tissue resistance per unit length, r_e.

The stability criterion defined earlier slows the numerical calculation because it implies a very small-time step. We had to use a time step (0.001 μs) that is more than 100,000 times shorter than the period of the stimulation current (333 μs). Except for a brief time when the stimulus first turns on (Fig. 4.6), the electric field in the tissue follows a sinusoidal time course. Therefore, to a good approximation we could calculate the electric field analytically for a sinusoidal current that extends over all time. Assume $V_e \ll V_i$ and $r_i \ll r_e$. In that case, from Eq. (4.3) $V_i = \psi$ and the second expression in Eq. (4.1) becomes

$$\frac{\partial \psi}{\partial t} = -D \frac{\partial^2 V_e}{\partial x^2}. \tag{4.10}$$

Since ψ is known from Eq. (4.7), we can simply integrate Eq. (4.10) to get an approximate analytical expression for the tissue voltage,

$$V_e \approx \frac{r_i}{D} I_0 \omega \cos(\omega t) \left[\frac{x^3}{6} - \frac{L^2 x}{2}\right], \tag{4.11}$$

and for the tissue electric field

$$E \approx \frac{r_i}{D} I_0 \omega \cos(\omega t) \left[\frac{L^2}{2} - \frac{x^2}{2}\right]. \tag{4.12}$$

At $x = 0$, the amplitude of the electric field is thus $\frac{L^2 r_i \omega}{2D} I_0$, which agrees fairly well with Fig. 4.5. We have performed several numerical simulations and found them to be consistent with this approximate analytical analysis. For instance, our calculations indicate that the electric field intensity in the tissue is proportional to the frequency. Figure 4.7 indicates the electric field is proportional to the tissue resistance per unit length, which follows from the factor of the diffusion constant in the denominator of our analytical solution.

In traditional transcranial magnetic stimulation, the current through the coil is not sinusoidal but instead is delivered as a pulse. We have performed a simulation using a current pulse through the wire with an amplitude of 1 mA, a rise time of 100 μs, and a subsequent decay of about 1 ms (Fig. 4.8). The electric field in the tissue rises abruptly to a peak 0.7 μs after the pulse begins, and then decays and changes sign, but with a low amplitude. The peak amplitude of the electric field is about 50 mV/m, which is somewhat larger than found during a simulation with a sinusoidal current because of the abrupt rise of the pulse. In other words, during a Fourier analysis frequencies greater than 3 kHz contribute to the rapid rise of the current waveform.

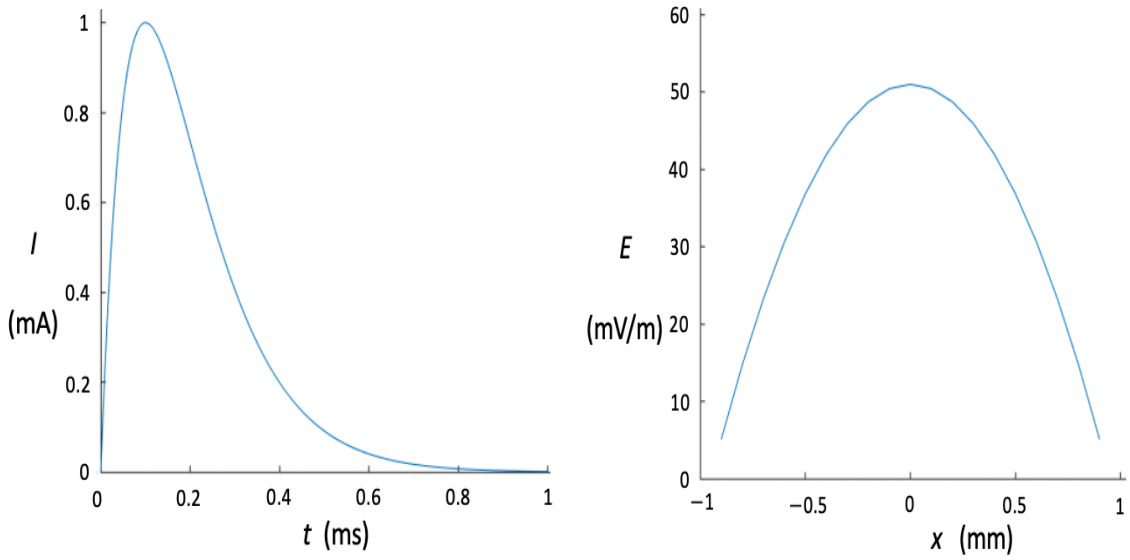

(**a**) (**b**)

Fig. 4.8. a) The current, *I*, applied to the wire as a function of time, *t*, and b) the peak tissue electric field intensity, *E*, as a function of position, *x*, at time 0.7 μs.

4.4 Discussion

Capacitive effects are known to be important for stimulating electrodes (Cogan, 2008). Typically, such electrodes are either Faradaic (where a chemical reaction occurs at the interface between the wire and the tissue) or capacitive (where charging or discharging a charged double layer at the electrode surface allows the stimulating current to enter the tissue). However, these electrodes typically connect the stimulating circuit to a grounded tissue space. In other words, the electrode capacitance is in series with the wire injecting the stimulating current, and a second grounded electrode is required to provide the return path for the current. Our case is different. The wire capacitance is distributed in parallel along the length of the wire. Capacitive current passes out of the wire at one end and returns back into the wire at the other end. In essence, one end of the

wire acts as the cathode and the other end as the anode. This is a very different circuit than used when analyzing most stimulating electrodes; no separate ground electrode is required. Our model resembles, in fact, an undersea telegraph cable or an axon within a nerve more than the usual stimulating electrode.

This model shows that a wire passing a sinusoidal current with a frequency of 3 kHz and amplitude of 1 mA produces an electric field in the surrounding tissue of about 4 mV/m. This value of E is small compared to the value required for excitation of neurons in the brain. Hause found that the transmembrane potential produced in a single neuron in an electric field of 10 V/m can polarize a neuron by 6 to 8 mV, implying that threshold is on the order of 10 V/m, or 10,000 mV/m (Hause,1975). Our value of E is about 2500 less than this threshold. Therefore, the electric field induced by capacitive coupling for a 1 mA, 3 kHz current should be well below the strength needed for neural excitation. In their calculations Lee et al. used a nominal value of 1 mA for the current, but in their experiments, they found thresholds on the order of 40 mA (Lee et al., 2016). A current of 40 mA would increase our calculated electric field up to 160 mV/m, bringing the stimulus closer to the expected threshold, within a factor of about 60.

For long, straight axons, the "activating function" dE_x/dx is often used as the source of electrical stimulation rather than the electric field itself. However, in the brain where axons bend and terminate, the electric field is more appropriate. The differences between these mechanisms are discussed in detail in (Roth, 1994).

Lee et al. assumed the electric field in the tissue was caused by magnetic stimulation, and calculated its amplitude to be about 1000 mV/m (Lee. et al. 2016).

However, using arguments like those presented by Alzahrani and Roth (2023; see Chapter 3), the electric field produced by magnetic stimulation should be on the order of

$$E \approx \frac{\mu_o}{4\pi} \frac{dI}{dt} \approx \frac{\mu_o}{4\pi} I_o 2\pi f \tag{4.13}$$

where μ_o is the permeability of free space (4π x 10^{-7} V s/(A m)). For I_o = 1 mA and f = 3 kHz, E should be on the order of 0.002 mV/m, which is nearly a factor of a million smaller than the value Lee et al. calculated (we have no explanation why their calculation gave such a large value because we do not have access to their computer code; the computer code for our magnetic stimulation calculation is given in Appendix G). In this case, the electric field from magnetic stimulation (0.002 mV/m) is more than a thousand times smaller than the electric field from capacitive coupling (4 mV/m), implying that capacitive coupling is the dominant mechanism. A more accurate calculation of the electric field arising during magnetic stimulation with a microcoil was performed by (Alzahrani and Roth, 2023; see Chapter 3) and they found the electric field to be about 0.026 mV/m at a distance just outside the coil insulation surface (0.3 μm from the coil).

How could you distinguish experimentally a model based on capacitive coupling from one based on magnetic stimulation? 1) Both predict an electric field proportional to the frequency and the amplitude of the applied coil current, and that are out of phase with the coil current. 2) Increasing the thickness of the insulation should decrease the capacitance, thereby increasing the diffusion constant making capacitive stimulation even more difficult. Magnetic stimulation, on the other hand, should not be affected by the thickness of the insulation. 3) The electric field produced by capacitive stimulation is

sensitive to the tissue resistance (Fig. 4.7), but the electric field induced by magnetic stimulation is not. 4) If the wire were made from silver instead of copper, then r_i would be smaller. This would decrease the electric field via capacitive stimulation, but (assuming a current source) this would not affect magnetic stimulation. 5) Increasing the wire gauge and thus decreasing the wire radius would increase r_i, which would increase the electric field caused by capacitive stimulation. There would be no effect of wire gauge during magnetic stimulation (again, assuming a current source). 6) The coil could be wound using more turns. This would have a complicated influence during capacitive stimulation, because it would couple the individual windings capacitively. For magnetic stimulation, increasing the number of windings would increase the magnetic field (assuming a current source so any changes in coil resistance or inductance do not affect the current). 7) Finally, the length of the coil leads (L) would play a major role in capacitive stimulation, but less or no role during magnetic stimulation.

To examine some of these effects in more detail, if you make the wire thinner (decrease a), you will increase r_i. But assuming that r_i is still much smaller than r_e and that you are driving the coil with a current source, increasing r_i should increase the magnitude of the tissue electric field, making it easier to stimulate (essentially you increase the voltage drop along the wire). For instance, when the resistance r_i becomes equal to the resistance of the tissue r_e, the peak of the electric field will be huge, about 1,500,000 mV/m. Note, however, that as you increase r_i while using a current source, the voltage produced by the source will grow. The current source must be powerful enough to produce such a voltage or else letting r_i become large in our calculation is unrealistic. Nevertheless, the best way to stimulate neurons in the brain may be to use two electrodes,

an anode and a cathode, with a gap ($r_i = \infty$), as is often used in traditional electric stimulation (Cogan, 2008).

Increasing the resistance of the tissue space, r_e, would decrease D and increase the electric field in the tissue (Fig. 4.7). For instance, making r_e ten times larger, r_e= 3200 MΩ/m, will increase the electric field in the tissue to be 40 mV/m. The radius of the cylinder of tissue, b, is the least well known parameter in our model. A more accurate calculation would treat the tissue as a volume conductor and determine the distribution of the tissue voltage and electric field as a function of position. In that case, the average electric field in the tissue may be smaller than what we calculate, but its peak value adjacent to the insulation may be larger.

Our calculation only approximates the physical situation examined by Lee et al., 2016. Their coil was not a straight wire, but bent into a hairpin loop. We assumed the tissue exists in a 0.1 mm radius cylinder surrounding the wire, which is probably the most arbitrary assumption in our calculation. The electric field in the tissue is almost certainly not independent of distance from the wire, as we have assumed in our one-dimensional model. All these assumptions will impact the predicted electric field in the tissue. However, our main conclusion is that the electric field in the tissue is over one thousand times larger for capacitive stimulation than for magnetic stimulation. Our assumptions would need to account for three orders of magnitude difference, but it is not clear if accounting for these assumptions would make the electric field larger or smaller.

The predicted electric field in the tissue is a factor of 60 less than what we would expect for the threshold for neural stimulation. Some combination of our assumptions and an error in the estimation of threshold as 10,000 mV/m might raise our predicted tissue

electric field to threshold level. For instance, a hairpin loop may result in the tissue voltage drop occurring over the distance between the two parallel wires (0.1 mm) rather than over the length of the wire (2 mm), thereby raising the electric field in the tissue significantly. The evidence is convincing that Lee et al. were somehow exciting neurons in their experiment (Lee et al., 2016) but it is difficult to imagine what other mechanisms could be active besides capacitive coupling and magnetic stimulation.

It is useful to examine the case of a hairpin loop in the wire in more detail. Assume that the wire, instead of being straight, takes a 180° bend (Fig. 4.9).

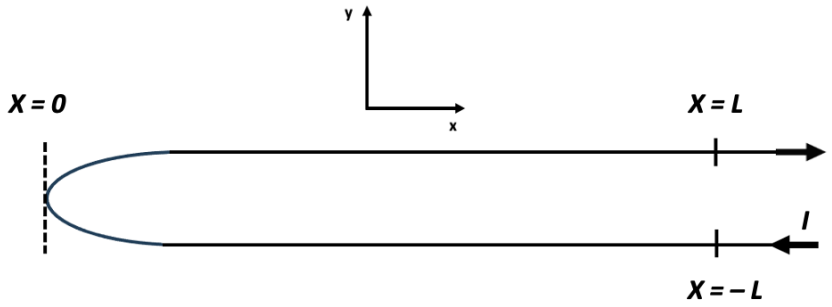

Fig. 4.9. A wire undergoes 180° bend.

We start the analysis where we derived the equation

$$\frac{1}{r_i}\frac{\partial^2 V_i}{\partial x^2} = 2\pi a C \frac{\partial}{\partial t}(V_i - V_e)\,, \tag{4.14}$$

we assume V_e is small, then

$$\frac{1}{r_i}\frac{\partial^2 V_i}{\partial x^2} = 2\pi a C \frac{\partial V_i}{\partial t}\,, \tag{4.15}$$

and

$$V_i = -I_0 r_i x \sin\omega t \ . \tag{4.16}$$

Now, what will be the electric field caused by this wire? The capacitance times unit area C times the rate of change $\frac{\partial V_i}{\partial t}$ is just the current density J passing through the wire insulation. Close to the wire, the radial current density leaving the tissue should be J, so the radial electric field just outside the wire is J/σ_e, where σ_e is the conductivity of the extracellular space. This means

$$E = -\frac{I_0 C r_i x \omega \cos\omega t}{\sigma_e} \ . \tag{4.17}$$

The electric field will point radially out, from one wire to the other. It will be largest at $x = L$ near the end of the shaft of the electrode, and zero near the hairpin turn. We have all the parameters we need to calculate its magnitude from the above equation. We get a peak electric field of 18 mV/m. This value is over four times what we found for a wire without a hairpin loop. Therefore, the geometry of the coil and surrounding tissue affects the tissue electric field.

Our model makes specific predictions about microcoil stimulation of the brain via capacitive coupling. We hope that our results will motivate experiments to test these predictions.

CHAPTER FIVE

THE DIFFERENCE BETWEEN TRADITIONAL MAGNETIC STIMULATION (TMS) AND MICCROCOIL STIMULATION MECHANISMS

5.1 Introduction

For years, magnetic stimulation has been studied and used to stimulate brain neurons, monitor brain function (Barker et al., 1991) and treat neurological diseases such as Alzheimer's (Wyszkowska, Jankowska and Gas 2019). Barker et al. invented Transcranial Magnetic Stimulation (TMS) and their device was able to stimulate the human motor cortex (Barker et al., 1985). The device consists of a large coil held a few centimeters outside the scalp and requires a kiloamp pulse of current passing through the coil, which induces an electric field *E* in the brain by electromagnetic induction. This non-invasive method causes less pain than electrical stimulation using electrodes on the scalp. TMS has been utilized to improve neurological symptoms for depression (Yesavage et al., 2018) and Alzheimer's disease (Koch et al., 2018).

Roth and Basser (1990) developed a mathematical model that explains the physics behind nerve stimulation through electromagnetic induction. Their model incorporated several key components: (1) circuit analysis; the stimulating coil and current source were modeled as a series RLC circuit, allowing for the prediction of the coil's current over time; (2) electromagnetic induction; Maxwell's equations were used to calculate the induced electric field and its gradient based on the coil geometry and the time course of the coil current; (3) cable theory; they derived a source term for the cable equation representing the nerve fiber that contained the gradient of the electric field; and (4) the

Hodgkin-Huxley model; this model of ion channel kinetics simulated the nerve fiber's response to the induced electric field, considering the fiber's membrane capacitance, voltage-dependent membrane conductance, and intracellular resistance. By integrating these four components, they could predict the transmembrane potential of a nerve fiber in response to an induced electric field.

Fundamentally, Roth and Basser showed that the electric field's gradient dE_x/dx (the activating function, where x is the distance along the fiber) is responsible for neural excitation (Roth and Basser, 1990). This gradient can either hyperpolarize or depolarize the membrane. Once the gradient depolarizes the axon's transmembrane potential to a threshold value, the nerve fires an action potential that then propagates along the fiber. Maccabee et al. (1993) performed experiments using a peripheral nerve and verified that the cause of nerve excitation is the spatial derivative of the induced electric field.

Recently, an implanted microcoil has been proposed for magnetic stimulation of the brain (Bonmassar et al., 2012; Lee et al., 2016; Park et al., 2018; Lee et al., 2019; Sugai et al., 2020; Ye and Barret, 2021; Ye et al., 2023). The microcoil uses the same mechanism as TMS (electromagnetic induction) except the coil is littler, the current is weaker, and the distance between the coil and targeted nerve is smaller. The development of microcoils began when Bonmassar et al. constructed a 500 μm diameter and 1 mm high coil composed of 21 turns of copper wire positioned 300 μm above the soma of an isolated ganglion cell (Bonmassar et al., 2012). This method has sparked significant interest in the research community. Subsequently, researchers have developed and designed many microcoils with different geometries, shapes, sizes (Lee and Fried, 2015; Park et al., 2018; Lee et al., 2019; Minusa et al., 2019; Bernardo et al., 2019; Sugai et al.,

2020; Ye and Barret, 2021; Yoshikawa, 2022; Liu et al., 2023; Saha et al., 2024; Saha et al., 2024).

Understanding the electric field generated by a coil through electromagnetic induction is crucial to predicting the threshold for stimulation. The induced electric field can be influenced by many factors, such as the number of coil turns, the distance between the coil and the target neuron, and the frequency of the current (Alzahrani and Roth, 2023; see Chapter 3). Some researchers have used the electric field E to determine the membrane threshold (Minusa et al., 2019), while others have used the electric field gradient dE_x/dx (Lee et al., 2016; Lee and Fried, 2015; Lee et al., 2019; Sugai et al., 2020). In this chapter, we follow the analysis by Roth and Basser and assume the electric field gradient is responsible for stimulation.

Roth and Basser analyzed magnetic stimulation of a long, straight axon using a large coil, for which a threshold value of dE_x/dx characterized excitation (Roth and Basser, 1990). This same analysis has been applied to microcoils, where the spatial distribution of the electric field varies over distances that are short compared to the length constant that appears in the cable equation. However, no studies have been performed to determine if the value of dE_x/dx found for large coils is applicable when stimulating with microcoils. Our hypothesis is that the threshold value of the electric field gradient dE_x/dx depends on the spatial distribution of dE_x/dx. A threshold value of dE_x/dx appropriate for transcranial magnetic stimulation using a centimeter-sized coil may be grossly inappropriate for stimulation using a 10-micon-sized microcoil. We test this hypothesis using mathematical modeling and computer simulation.

5.2 Methods

We will analyze microcoil stimulation in two ways: first using a spatial frequency analysis, and second by analyzing an active nerve axon using a typical electric field distribution.

5.2.1 Spatial Frequency Analysis

The goal in this section is to write the cable equation, including the activating function, using Fourier analysis: expressing the mathematical functions as sums of sines and cosines of different spatial frequency. We then show that terms with high spatial frequency—meaning those terms that vary over short distances—are suppressed (that is, filtered out) of the solution for the transmembrane potential.

Our model is based on the cable equation, which describes the axon as a long cable having an intracellular resistance and a membrane conductance and capacitance. We start with the activating function, $S = -\lambda^2 \frac{\partial E_x}{\partial x}$, in the cable equation (Roth and Basser, 1990):

$$V - \lambda^2 \frac{\partial^2 V}{\partial x^2} + \tau \frac{\partial V}{\partial t} = S, \tag{5.1}$$

where λ is the axon length constant and τ is its time constant. Typically, λ is on the order of 0.1 centimeters and τ is about 1 millisecond. We assume that the system is in steady state (this restrictive assumption is relaxed in the next section), so the time derivative is zero. As the first step in Fourier analysis, we examine the behavior of an activating function in the form of a sine wave with a single spatial frequency *k*,

$$S = S_0 \sin(kx), \tag{5.2}$$

Although a sinusoidal source is not characteristic of magnetic stimulation, any spatial distribution of dE_x/dx can be expressed using Fourier analysis, so a sinusoidal source is nevertheless useful.

To determine the transmembrane potential V, we assume a solution of Eq. (5.1) of the form

$$V = V_0 \sin(kx)\,. \tag{5.3}$$

We plug (5.2) and (5.3) into (5.1) and find

$$V_0 \sin(kx) + \lambda^2 k^2 V_0 \sin(kx) = S_0 \sin(kx), \tag{5.4}$$

so,

$$V_0 = \frac{S_0}{1+k^2\lambda^2}\,. \tag{5.5}$$

The induced voltage depends on the membrane length constant and the spatial frequency. For $k\lambda << 1$ (the activating function S is nearly uniform over distances that are greater than the length constant)

$$V_0 = S_0\,. \tag{5.6}$$

For $k\lambda >> 1$ (the activating function changes over distances that are small compared to the length constant)

$$V_0 = \frac{S_0}{k^2\lambda^2}\,. \tag{5.7}$$

5.2.2 Active Nerve Axon

The cable equation (Eq. 5.1) illustrates how the induced electric field interacts with the neuron but does not fully capture the kinetics of nerve stimulation. To improve on our model, we add a mathematical representation of the ion channels in the nerve membrane. These channels behave nonlinearly, so a linear process like Fourier analysis is no longer appropriate. Instead, we solve the cable equation, including the ion channels, numerically.

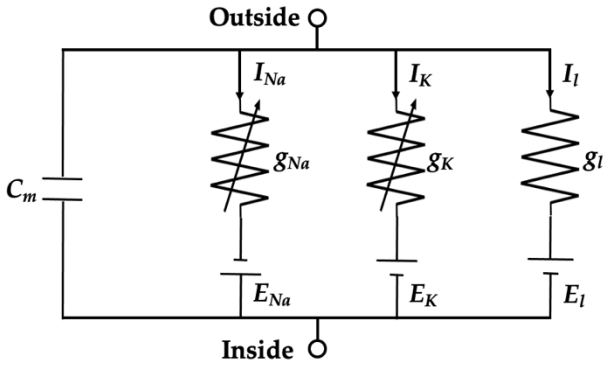

Fig. 5.1: Electrical equivalent circuit for a short segment of squid giant axon. Capacitor (capacitance per unit area C_m of the cell membrane); variable resistors (voltage-dependent Na^+ and K^+ conductance per unit area, g_{Na}, g_K); fixed resistor (voltage-independent leakage conductance per unit area g_l); batteries (reversal potentials for Na^+, K^+, leakage: E_{Na}, E_K, E_l); membrane potential $V = V_{in} - V_{out}$; Arrows (current densities I_{Na}, I_K and I_l).

The Hodgkin-Huxley model as shown in Fig. 5.1 allows us to calculate the stimulation and propagation of action potentials numerically (Hodgkin and Huxley, 1952). The sodium, potassium, and leak ionic current densities are

$$I_{Na} = g_{Na}m^3h[V - E_{Na}], \quad I_K = g_k n^4[V - E_K], \quad I_l = g_l[V - E_l], \tag{5.8}$$

where the dimensionless variables n, m, and h represent the opening and closing of ion channels, and vary between 0 and 1. Differential equations of first order determine these gating variables:

$$\frac{\partial m}{\partial t} = \alpha_m(1 - m) - \beta_m m, \quad \frac{\partial h}{\partial t} = \alpha_h(1 - h) - \beta_h h, \quad \frac{\partial n}{\partial t} = \alpha_n(1 - n) - \beta_n n. \tag{5.9}$$

The values of the rate constants α and β (in 1/ms) are functions of V (mV) and are given by

$$\alpha_n = 0.01\frac{V+55}{1-\exp\left(-\frac{V+55}{10}\right)}, \alpha_m = 0.1\frac{V+40}{1-\exp\left(-\frac{V+40}{10}\right)}, \ \alpha_h = 0.07\exp\left(-\frac{V+65}{20}\right), \tag{5.10}$$

$$\beta_n = 0.125\exp\left(-\frac{V+65}{80}\right), \ \beta_m = 4\exp\left(-\frac{V+65}{18}\right), \quad \beta_h = \frac{1}{1+\exp\left(-\frac{V+35}{10}\right)}. \tag{5.11}$$

With no source of external current, the Hodgkin-Huxley equation for V is

$$C_m\frac{dV}{dt} + g_k n^4(V - E_K) + g_{Na}m^3h(V - E_{Na}) + g_l(V - E_l) = 0. \tag{5.12}$$

When we plug the Hodgkin-Huxley equation (5.12) into the modified cable equation (5.1) it becomes

$$\frac{a}{2R_i}\frac{\partial^2 V}{\partial x^2} - (I_{Na} + I_k + I_l) = C_m \frac{\partial V}{\partial t} + \frac{a}{2R_i}\frac{\partial E_x}{\partial x}(x,t), \tag{5.13}$$

where a is the axon radius and R_i is the intracellular resistivity. We solve equation (5.13) numerically using the parameters in Table 5.1.

Table 5.1: The parameters for simulation of the (Hodgkin and Huxley, 1952) model.

Symbol	Parameter	Value
g_{Na}	Maximum sodium conductance per unit area	120 mS cm^{-2}
g_K	Maximum potassium conductance per unit area	36 mS cm^{-2}
g_l	Leakage conductance per unit area	0.3 mS cm^{-2}
E_{Na}	Sodium Nernst potential	50 mV
E_K	Potassium Nernst potential	–77 mV
E_l	Leakage Nernst potential	–54.387 mV
C_m	Membrane capacitance per unit area	1 μF cm^{-2}
R_i	Intracellular resistivity of the axoplasm	0.0354 kΩ cm
a	the radius of the axon	0.0238 cm

Equation (5.14) expresses the time course of the current in the coil $I(t)$ that induces the electric field $E(t)$. It consists of a rapid rise and then an exponential decay with time constant τ_{coil}. We take τ_{coil} to be 0.1 ms, typical of a magnetic stimulation pulse (Fig. 5.2a). The induced electric field varies as the derivative of the coil current. It is biphasic, with a brief, strong positive phase, followed by a longer, weaker negative phase (Fig. 5.2b)

$$I(t) = t\, \mathrm{e}^{-\frac{t}{\tau_{coil}}}, \tag{5.14}$$

$$\frac{dI}{dt}(t) = \left(1 - \frac{t}{\tau_{coil}}\right) \mathrm{e}^{-\frac{t}{\tau_{coil}}}. \tag{5.15}$$

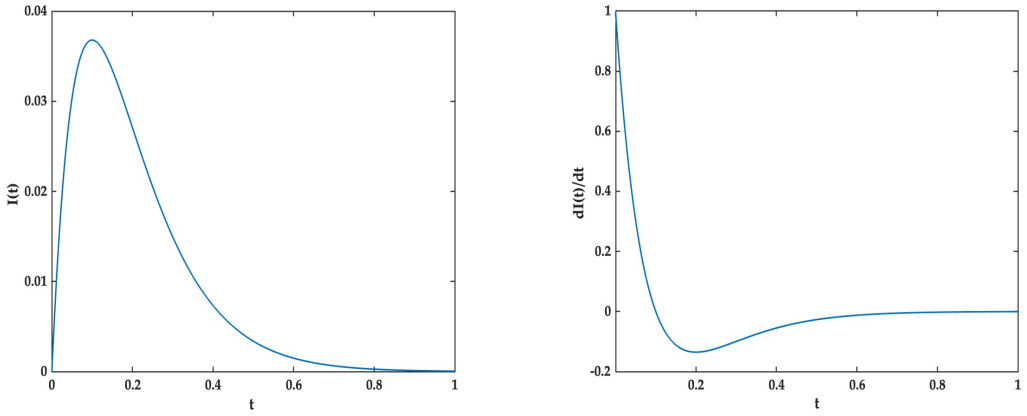

(**a**) (**b**)

Figure. 5.2: (a) The coil current *I(t),* and (b) its time derivative, normalized so that *dI*/*dt* at $t = 0$ is one. The coil current is monophasic with a fast rise and slower decay. The induced electric field is proportional to *dI/dt*, which is biphasic with a strong positive phase lasting about 0.1 ms followed by a slower, weaker negative phase.

Furthermore, we assume the normalized spatial distribution of the electric field is given by

$$\frac{b^2}{b^2+x^2}, \tag{5.16}$$

where *b* indicates the spatial extent of the electric field in centimeters and varies with coil size, and *x* is the position along the axon. The electric field is largest at $x = 0$ and decays over a distance *b* (Fig. 5.3a). The spatial distribution of the activating function is proportional to the spatial derivative of the function in Eq. 5.16. It is zero at $x = 0$, and is positive to the left of $x = 0$ and negative to the right (Fig. 5.3b)

$$\frac{-2b^2x}{(b^2+x^2)^2}. \tag{5.17}$$

Thus, the expression for the activating function is

$$dE_x/dx = Q\left[\left(1-\frac{t}{\tau}\right)\mathrm{e}^{-\frac{t}{\tau}}\right]\left[\frac{-2b^2x}{(b^2+x^2)^2}\right], \tag{5.18}$$

where Q is the peak electric field at time $t = 0$ and position $x = 0$. Calculating the threshold corresponds to varying Q.

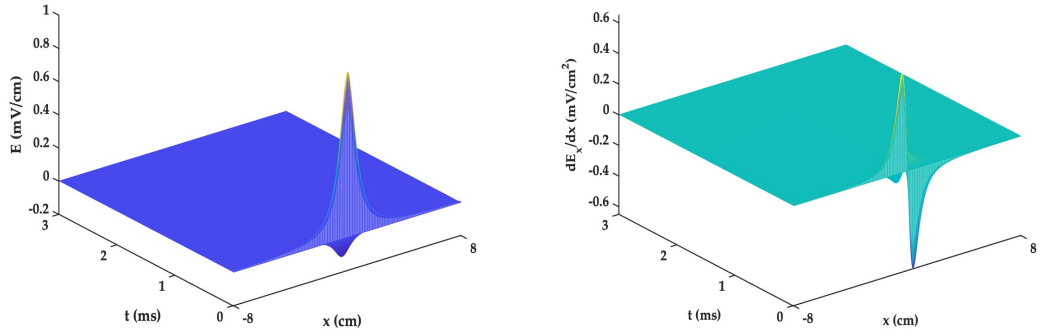

(**a**) (**b**)

Fig. 5.3: (a) The electric field E, and (b) the spatial derivative of the electric field, dE_x/dx, as functions of time t and space x, for $Q = 1$ mV/cm and $b = 1$ cm. The electric field is large at the origin ($x = 0$) and decays to half its value by $x = \pm b$. In time, the electric field follows the time course of a biphasic pulse, like dI/dt in Fig. 5.2b. The gradient of the electric field is zero at the origin and large on either side of the origin, positive in one direction and negative in the other.

We express our results in terms of the peak value of dE_x/dx required for excitation. We started by taking the expression for dE_x/dx as a function of x, then calculated its derivative and set it equal to zero to determine the value of x corresponding to the peak value of dE_x/dx, which we found to be $x_{peak} = 0.577\ b$. Substituting this value

into the equation for dE_x/dx, we obtained $(dE_x/dx)_{peak} = 0.65\ Q/b$. We observed that the value of b influences the peak of the electric field gradient; as b decreases, similar to the distance between the nerve and the microcoil, the spatial gradient of the electric field becomes larger. The value of Q/b decreases significantly as the distance between the nerve and TMS increases as shown in Table. 5.2.

To solve Eq. (5.13), we approximated the partial differential equation using finite differences, with a space step Δx and a time step Δt

$$\frac{a}{2R_i}\frac{V(x-\Delta x,t)-2V(x,t)+V(x+\Delta x,t)}{\Delta x^2} - (I_{Na} + I_k + I_l) = C_m\frac{V(x,t+\Delta t)-V(x,t)}{\Delta t} + \frac{a}{2R_i}\frac{\partial E_x}{\partial x}(x,t). \quad (5.19)$$

We used an explicit method to solve the equation (we used the gates and voltage at time t to determine the new transmembrane potential at time $t+\Delta t$). Similarly, Eq (5.9) for the gate constants n, m, and h were solved using a finite difference approximation. Because we use an explicit method, the value of the time step had to be small enough to ensure the stability of the solution. We generally used a value of $\Delta t = 0.0002$ ms, which is far smaller than the time associated with the upstroke of the action potential, and is small compared to the rise time of the coil current. We also had to ensure that the space step was small compared to the length constant of the axon, the spatial length of the action potential upstroke, and the parameter b characterizing the extent of the applied electric field. At the same time, we had to use a long enough fiber so that the fiber ends (sealed) did not affect stimulation. Typically, we assumed the fiber was 12 cm long and used 400 space points, implying a space step of $\Delta x = 0.03$ cm. For some simulations, we had to

adjust the number of space nodes and the fiber length to better represent a longer or shorter fiber.

We solved numerically the equation of propagation, the coil current, and the distribution of spatial electric field and its gradient by the using a computer program written for MATLAB R2024 a. The MATLAB code is given in Appendix (H).

5.3 Results

5.3.1 Spatial Frequency Analysis

In steady state the analytical solution of the cable equation shows that the transmembrane potential depends on the spatial frequency *k,* Eq. (5.5). In traditional magnetic stimulation, the stimulating electric field varies over centimeters, so k is about 1 cm^{-1}. The length constant is on the order of a millimeter, $\lambda = 0.1$ cm. Therefore, $k\lambda << 1$ and the transmembrane potential is equal to S_0. During microcoil stimulation, the electric field varies over tenths of a millimeter, so k is about 100 cm^{-1} and $k\lambda >> 1$. The transmembrane potential is smaller than S_0, so a stronger stimulus is needed to excite the nerve. As a result, we cannot use S_0 from traditional magnetic stimulation to estimate threshold for microcoil stimulation. Figure 6.4 represents the relation between induced transmembrane potential and the spatial frequency k.

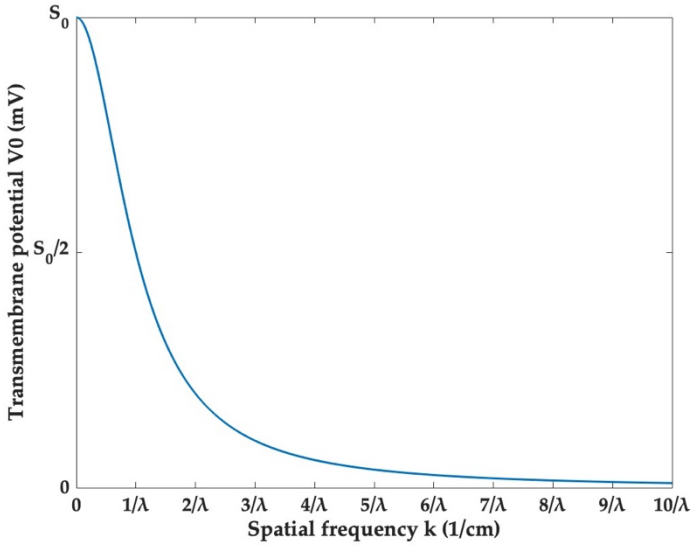

Fig. 5.4: The transmembrane potential as function of spatial frequency k (Eq. (5.5)). For low values of k the transmembrane potential is relatively large but at high values of k it is much smaller, suggesting that excitation is easier at small spatial frequencies.

5.3.2 Active Nerve Axon

The numerical solution of equation (5.13) demonstrates how the interaction between the activating function and the Hodgkin-Huxley membrane model leads to the propagation of an action potential (Fig. 5.5). Initially, the passive response resembles the activating function, and is proportional to the derivative of the electric field dE_x/dx. Then, after about a 2-ms delay (latency), the action potential fires at the point where dE_x/dx is positive and propagates in two directions (left and right). The simulation in Fig. 5.5 is for a stimulus just above threshold; stronger stimuli have a shorter latency. The action potential has a peak of about +40 mV, and propagates about 5 cm in 5 ms, for a speed of approximately 1 cm/ms. After about 2 ms, the action potential repolarizes, becomes

refractory, and finally returns to rest. This behavior is all consistent with that observed by Hodgkin and Huxley (1952). Because we are primarily interested in the all-or-nothing excitation of the action potential, we did not study the recovery and refractoriness associated with repolarization.

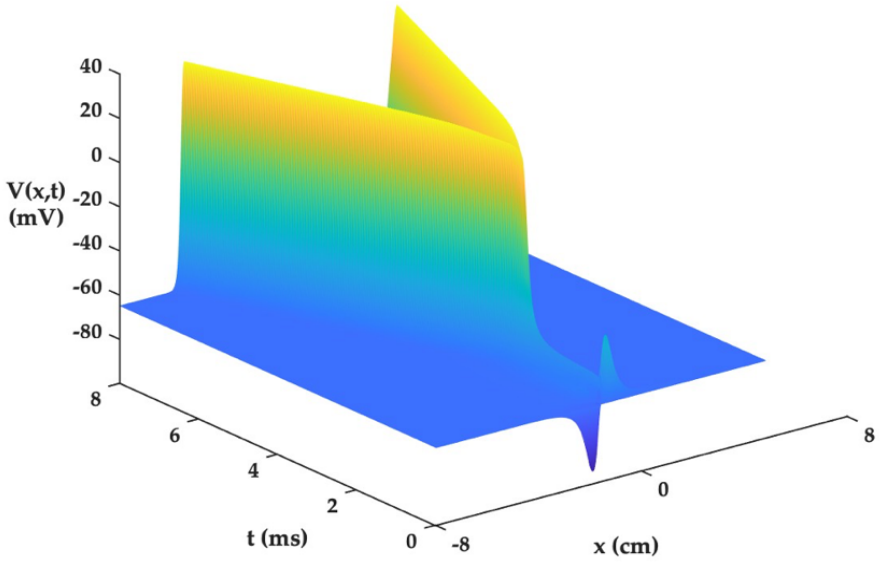

Fig. 5.5: The propagation of the action potential due to the activating function, for b = 1 cm and Q = 4089 mV/cm. Near t = 0 the transmembrane potential is proportional to the activating function. However, by t = 2 ms, the depolarization reaches threshold and triggers an action potential, which then propagates in both directions away from its stimulation site. A slightly weaker stimulus would not have excited an action potential; excitation is an all-or-none phenomenon.

Our main result is presented in Fig. 5.6 and Table 5.2, which show that the activating function is affected by the spatial length b of the electric field gradient. When b decreases, which is similar to reducing the coil size and the distance between the

microcoil and the targeted neuron, the threshold peak of the electric field gradient increases. However, when the electric field distribution is several centimeters or more (as during transcranial magnetic stimulation), increasing *b* has little influence on the threshold peak of the electric field gradient (Table 5.2).

Table 5.2: The calculations of dE_x/dx_{peak} for a wide range of *b*.

***b* (cm)**	***Q* (mV/cm)**	dE_x/dx_{peak} **(mV/cm^2)**
100	285,197	1853
30	85,763	1858
10	28,911	1877
3	9674	2094
1	4089	2665
0.3	2415	5229
0.1	2445	15881
0.03	4166	90,195
0.01	9393	610,084

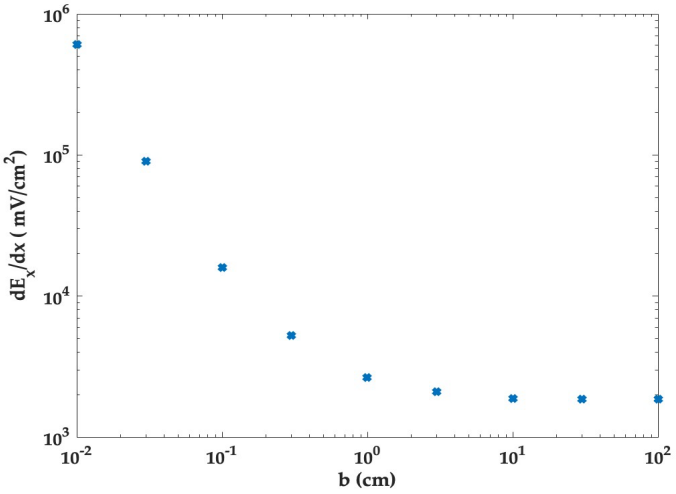

Fig. 5.6. A log-log plot of the threshold electric field gradient as function of spatial length *b*. For large values of *b* (greater than about 1 cm) the threshold value of dE_x/dx is constant, but for smaller values of *b* (less than about 1 cm) the threshold rises as *b* is made smaller.

5.4 Discussion

When analyzing magnetic stimulation with a microcoil, many researchers assume excitation will occur if the electric field gradient, dE_x/dx, reaches a threshold value. For instance, both Lee et al. (2016) and Sugai et al. (2020) claim that excitation will occur if dE_x/dx reaches 11,000 V/m^2 (1100 mV/cm^2), and justify this value by citing Maccabee et al. (1993) who used a coil with a diameter of about 4 cm. Our results indicate that you should not assume a threshold value obtained from studies of traditional magnetic stimulation if you are using a microcoil. Figure 5.6 indicates that the threshold value of dE_x/dx is elevated by a factor of one hundred or more when using a microcoil (note the log-log scales on this plot).

In our spatial frequency analysis, summarized in Eq. (5.5) and Fig. 5.4, the spatial frequency k affects the threshold. When the spatial frequency is small compared to the reciprocal of the length constant, the membrane potential V_0 is proportional to the activating function dE_x/dx. In that situation, using a threshold value of dE_x/dx from another study with a different sized coil would be reasonable. However, once the spatial frequency increases so it is large compared to the reciprocal of the length constant, the value of the appropriate threshold value of dE_x/dx rises, so it is not reasonable to use a threshold value from an experiment with $k\lambda << 1$ to analyze an experiment with $k\lambda >> 1$. This conclusion is reinforced by Fig. 5.6, which shows the threshold value of dE_x/dx as a function of the parameter b, which will be similar to the coil size or the coil-axon distance. As b decreased from 100 to 0.01 cm, the threshold value of dE_x/dx increased by a factor of 300, suggesting that this variation of the threshold value is not a small effect.

Based on their plots of dE_x/dx versus x, the value of b that corresponds to the microcoil size used by Lee et al. (2016) and Sugai et al. (2020) is probably 0.01 cm or even smaller (perhaps as low as 0.001 cm = 10 μm). We do not have good data for the length constant λ of their neurons (which are usually on the order of a millimeter), so it is difficult to predict exactly by how much the threshold value should be multiplied when using a microcoil, but clearly the increase will be significant.

There are similarities between our results and the traditional strength-duration curve often considered in electrical neural stimulation. A generic equation describing the strength-duration curve is

$$I = I_{\text{rheobase}}\left(1 + \frac{d_{\text{chronaxie}}}{d}\right), \tag{5.20}$$

where I is the threshold stimulus current strength, d is the pulse duration, I_{rheobase} is the rheobase current (the threshold stimulus current strength for a long duration pulse) and $d_{\text{chronaxie}}$ is the chronaxie (the minimum stimulus duration that can excite a neuron with a stimulus of twice rheobase). A short duration pulse ($d << d_{\text{chronaxie}}$) requires a much stronger stimulus than a long duration pulse ($d >> d_{\text{chronaxie}}$). The strength-duration curve arises because the neuron has its own time constant, τ. If the stimulus duration d is longer than τ (that is, if $d >> \tau$), then the threshold value of the stimulus (the rheobase) is a constant, independent of duration. However, for short duration stimuli ($d << \tau$) the membrane voltage does not have time to respond to the brief stimulus and the threshold value rises.

Our strength-spatial extent curve in Fig. 5.6 for magnetic stimulation is analogous to the strength-duration curve for electrical stimulation, if we replace the stimulus duration d by the spatial extent of the stimulus b, and the time constant τ by the length constant λ. Our results in Fig. 5.6 have a "spatial rheobase" dE_x/dx value for large values of the spatial extent b. At small values of b, the value of dE_x/dx rises. If we wanted to define a "spatial chronaxie" (the value of b for which the threshold value of dE_x/dx rises by a factor of two) it would be about half a centimeter (Table 5.2).

In a broader context, our results suggest that magnetic stimulation using a microcoil may be more difficult than previous studies have suggested. When this result is combined with our prior work showing that the electric field during microcoil stimulation may have been overestimated in early studies (Alzahrani and Roth, 2023 see Chapter 3), it casts doubt on the feasibility of microcoil magnetic stimulation, at least for stimulation using relatively weak current pulses (less than an amp). We have previously suggested that capacitive coupling may explain stimulation with a microcoil better than magnetic induction (Alzahrani and Roth, 2024 see Chapter 4). However, our results suggest that capacitive stimulation would also be suppressed when applied over a short distance. Nerve axons have their own characteristic length and time constants. When stimuli are applied over distances short compared to the length constant or in pulse durations that are short compared to the time constant, excitation becomes more difficult.

One limitation of our analysis is that we assume the stimulus during magnetic stimulation depends on dE_x/dx, as suggested by Roth and Basser's theoretical analysis of the cable equation (Roth and Basser, 1990) and Maccabee et al.'s experiments using long nerves and large coils (Maccabee et al., 1993). Maccabee et al.'s threshold value for

dEx/dx was for magnetic stimulation of a long, straight, uniform peripheral nerve “like that modeled by Roth and Basser”. However, their experiments also studied the excitation in bent peripheral nerves during magnetic stimulation, and their findings suggested that excitation mechanism is different at a bend compared to a straight nerve segment. Their experiments implied that an inhomogeneity caused by, say, the bending of the nerve may lead to an excitation "hot spot" where the threshold was determined by the electric field rather than its gradient as was the case for straight nerves. Nagarajan, Durand, and Warman analyzed the influence of magnetic stimulation on neuronal structures of finite length and varying geometries, including bending, branching, and termination (Nagarajan, Durand, and Warman 1993). They found that shorter axons were more easily excited than longer ones, and other factors, such as the truncation of an axon at its distal or proximal end, could also lead to "hot spots." Our analysis assumes the axon is uniform, straight, and long, so there are no such “hot spots.” If this is not the case (as it might not be for neurons in the brain), the entire idea of using dE_x/dx to characterize the threshold may be erroneous. Our analysis in this paper does not resolve the issue of E_x versus dE_x/dx for the stimulation of a neuron in the brain. We merely claim that if you assume dE_x/dx is the relevant parameter for neural stimulation, then the threshold value of dE_x/dx depends on the size of the coil, especially during microcoil stimulation.

Our analysis has several additional limitations. We used the Hodgkin-Huxley model to represent the behavior of a nerve axon. This model, derived using data from a squid axon, is useful as a generic model of neural excitation, and was the model used by Roth and Basser in their original study of magnetic stimulation (Roth and Basser, 1990). However, this model may not be appropriate for a mammalian neuron. One reason for

doing the spatial frequency analysis in addition to the Hodgkin and Huxley calculation is that the spatial frequency analysis is based on the cable equation with a fixed membrane conductance. The fact that the spatial frequency analysis gives the same qualitative insights as does the Hodgkin-Huxley model gives us confidence that our results will have wide validity. We also used the continuous form of the cable equation, which is appropriate for unmyelinated axons. In a myelinated axon, the discrete locations of the nodes may not be important when propagation or stimulation occurs over many nodes, but may play a larger role when stimulating locally with a microcoil. As both our spatial frequency analysis and the Hodgkin-Huxley analysis assume an unmyelinated axon, additional research is needed to determine how relevant our results are to a myelinated axon. In the Hodgkin-Huxley calculation, we assume generic functions for the time course of the coil current and the spatial distribution of dE_x/dx. While both are typical of magnetic stimulation, neither exactly represents the coil current and the spatial distribution of the electric field. Microcoils are meant to be implanted in the body or the brain. The act of implantation may disrupt or injure the neurons, and we have not accounted for any such injury in our analysis. Finally, our model makes predictions about neural stimulation that have not yet been verified experimentally. One of our main goals is to motivate experiments to test our predictions.

CHAPTER SIX

CONCLUSION AND FUTURE WORK

Over the years, neuromodulation procedures have been beneficial and offer more precise therapies in treating many brain disorders. Although the future of brain stimulation methods we covered in this dissertation is promising, advances in computational modeling will be crucial in optimizing it. Therefore, we discussed different methods of exciting a nerve membrane. Most of our discussion is related to brain stimulation mechanisms and how to achieve this, especially in transcranial magnetic stimulation and microcoil stimulation.

First, we suggested that a ramp followed by a pulse in the Hodgkin-Huxley model excites the deep neurons in the brain selectively. So, this pulse can stimulate without exciting the neurons above it, closer to the electrode. Technically, deep neurons can be selectively excited by a stimulus pulse that consists of a lengthy, weak ramp followed by a short, stronger main pulse. Since the deeper neurons are not made refractory and can be stimulated by the main pulse, the ramp's goal is to make the shallow neurons refractory, meaning that the closer neurons can not respond to the main pulse. We use a numerical calculation to study the neuron reaction to a stimulus to test this hypothesis, and we conclude that moderate stimulus strength excites an action potential, but a strong stimulus strength does not. So, stimulating deep neurons in the brain selectively may be possible using a ramp-pulse stimulus waveform.

We varied the amplitude of the ramp versus the pulse in our analysis (A/B), but there are many other parameters that could influence our results. Future studies could

examine slower or longer ramps or stimulus pulses, or different shaped waveforms (perhaps a long weak constant pulse instead of a ramp, followed by a brief strong pulse), or even a ramp of opposite sign. The number of possibilities is endless. Our goal would be to optimize the waveform so excitation for moderate sized pulses is encouraged while excitation by strong pulses is discouraged. If such a waveform is discovered, it may be a significant contribution to scalp excitation of the brain.

Second, we analyzed and calculated the electric field and its gradient arising from different microcoils, and we concluded that Lee et al. (2016) and Lee et al. (2019) could not have excited neurons by magnetic stimulation; the induced electric fields are too weak. Two questions remain unresolved. First, why are our calculations and those of Lee et al. so different? We do not have a good answer, but our computer code is in Appendixes C, D, E and F, so that anyone can check our results. Second, Lee et al. were clearly exciting neurons. If the excitation mechanism was not magnetic stimulation, what was it? The cause might be capacitive coupling.

The goal of our analysis of Lee et al.'s results is to indicate to the research community that this commonly cited study may contain erroneous results. Magnetic stimulation with a microcoil may ultimately be possible, but researchers who design such devices need to have an accurate understanding of how these devices work. Also, the National Institutes of Health and other funding agencies have awarded considerable funding to the development of microcoils for magnetic stimulation, and it is essential that these funding agencies understand the limitations of this technique.

Third, a microcoil can precisely target specific brain regions, allowing for more localized stimulation with fewer side effects. But here, capacitive coupling may be the

mechanism of brain stimulation in this case. Capacitive coupling using 1 mA predicts a small electric field relative to what we would expect for the neural threshold (10,000 mV/m). Lee et al. observed that 40 mA currents were required for neural excitation, making our predicted electric field about 60 times smaller than the expected threshold (Lee et al., 2016). Some combination of invalid assumptions in our calculation, such as the presence of a hairpin loop along the wire so the voltage drop occurs between the two parallel wires rather than along the entire wire length, and an overly conservative value of the neural threshold may explain the discrepancy between the predicted and expected excitation threshold. Regardless of the electric field strength relative to the excitation threshold, our primary prediction is that the electric field caused by capacitive coupling should be much larger than the electric field induced by magnetic stimulation.

The capacitive coupling method is more effective than the magnetic induction method. The results of this model provide insights into the mechanisms of neuronal excitation, which is relevant given the increasing application of microcoil technology in therapeutic and medicinal applications. Our capacitive coupling model might be utilized and considered in the future designing of microcoils.

A key limitation of our capacitive coupling model is it does not include a more realistic representation of the surrounding volume conductor. An extension of our study would be to couple our cable-like model for the coil wire to a finite-element model for the volume conductor, including a realistic description of the coil geometry. While such a finite element calculation is beyond the scope of this dissertation, it would be the next logical step for this research.

Finally, we investigate the differences in neural stimulation threshold values between traditional magnetic and microcoil stimulation. So, we analyze the activating function required for stimulation using two methods: spatial frequency analysis and active membrane analysis with the Hodgkin-Huxley model. We find that microcoils, which are significantly smaller than traditional coils, have a higher stimulation threshold when the spatial frequency is high, or the spatial extent of the activating function is small.

Our results show that even with long, straight nerve fibers, you should not use a threshold value of dE_x/dx in a microcoil experiment obtained from a traditional magnetic stimulation experiment with a large coil. The threshold value must be scaled to account for the spatial extent of the dE_x/dx distribution. Magnetic stimulation is inherently more difficult for microcoils than traditional large coils for the same reason that electrical stimulation is more difficult for short-duration stimulus pulses than long-duration pulses. The nerve axon has its own time and space constants, and if the pulse duration or the extent of the *dEx/dx* distribution is smaller than these constants, the threshold for stimulation will rise. For microcoil stimulation, the rise can be dramatic. When utilizing transcranial magnetic stimulation, a threshold value of dE_x/dx suitable for stimulation differs from that of a 10-micron-sized microcoil. Therefore, a threshold value of dE_x/dx that is suitable for stimulation with a centimeter-sized coil is completely incorrect for a microcoil.

Future studies could analyze neurons that had curving fibers, bends, and terminations to see in more detail how under what conditions dE_x/dx is the critical parameters for excitation. For a small coil, a nerve axon only needs to be straight and uniform for a short distance near the coil to appear like an infinitely long, straight fiber.

The question of what conditions must to be met for dE_x/dx to be the appropriate measure of stimulation strength needs to be examined in more detail.

Many of the chapters in this dissertation contain some additional limitations. For instance, Chapters 2 and 5 use the Hodgkin-Huxley model for neural stimulation of a squid giant axon. Historically this is the first and most important such model, but additional models have been developed that may be more appropriate for mammalian neurons or myelinated axons. In fact, while myelination might be safely ignored in traditional magnetic stimulation, it may be a more serious issue for microcoil stimulation, where the size of the coil is small compared to the distance between nodes of Ranvier.

Finally, all of the chapters analyze neural stimulation using computer simulation. They can be thought of as providing hypotheses for testing experimentally. Of course, the value of these studies will be determined by how well these predictions are verified in experiments.

APPENDIX A

MATLAB CODE USED FOR THE NUMERICAL ANALYSIS IN CHAPTER TWO

```
m = 1; % membrane capacitance

dt = 0.0001; % time step

ENa = 50;

EK = -77;

El =-54.387;

gNamax = 120; %max conductances

gKmax = 36;

glmax = 0.3;

niter = 60000; % max number of iterations

% Initial conditions

vm(1) = -65; % initial membrane voltage

V(1) = vm;

% calculating alphas and betas for the initial membrane voltage

alpn = 0.01*(vm+55)/(1-exp(-(vm+55)/10));

alpm = 0.1*(vm+40)/(1-exp(-(vm+40)/10));

alph = 0.07*exp(-0.05*(vm+65));

betn = 0.125*exp(-(vm+65)/80);

betm = 4*exp(-0.0556*(vm+65));

beth = 1/(1+exp(-0.1*(vm+35)));

% intial m,n & h
```

```
n(1) = alpn/(alpn+betn);

m(1) = alpm/(alpm+betm);

h(1) = alph/(alph+beth);

time=0;

Iext2(1)=0;

% the loop for calculation of membrane voltage dynamics is here.

for i = 1:niter,

 i

   time=time+dt;

   T=3;

   A=4;

   %I=1;

   if       (time>0 && time<=T)

   Iext2(i+1)=A*(i*1*dt)/T;

   elseif     (time>T && time<=T+0.5)

   Iext2(i+1)=3*A;

   elseif time>T+0.5

    Iext2(i+1)=0;

   end

   dm = dt*(alpm*(1-m(i))-betm*m(i));

   dn = dt*(alpn*(1-n(i))-betn*n(i));

   dh = dt*(alph*(1-h(i))-beth*h(i));

   m(i+1) = m(i) + dm;
```

```
 n(i+1) = n(i) + dn;
 h(i+1) = h(i) + dh;
 gNa = gNamax*m(i)^3*h(i);
 gK = gKmax*n(i)^4;
 gl = glmax;
 INa = gNa*(vm-ENa);
 IK = gK*(vm-EK);
 Il = gl*(vm-El);
dvm = (dt/cm)*(Iext2(i+1)-( INa + IK + Il));
 vm = vm + dvm;
 V2(i+1) = vm;
 alpn = 0.01*(vm+55)/(1-exp(-(vm+55)/10));
 alpm = 0.1*(vm+40)/(1-exp(-(vm+40)/10));
 alph = 0.07*exp(-0.05*(vm+65));
 betn = 0.125*exp(-(vm+65)/80);
 betm = 4*exp(-0.0556*(vm+65));
 beth = 1/(1+exp(-0.1*(vm+35)));
 end
tim = dt*(1:niter+1);
6001
plot(tim,V2);
xlabel('time in ms');   ylabel('v_m mv');
```

APPENDIX B

THE CALCULATIONS ANALYSIS IN CHAPTER THREE

1. SQUARE COIL

The calculation of the electric field is based on Eq. (3.2) for square coil.

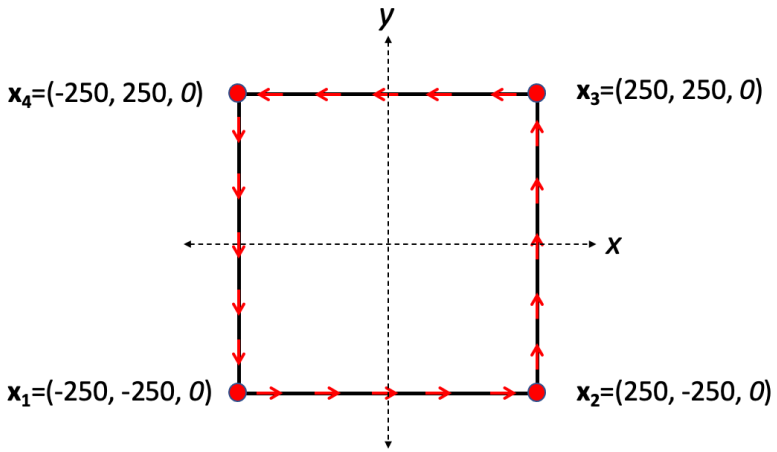

A square microcoil 500 μm per side. The red arrows show the direction of the current flows in the coil. The distance from coil to the plane where the electric field is calculated is b = 0.3 μm and the length of each side is 500 μm.

We calculated the electric field in the plane z = b as the following:

Side 1

Side 1 will be the bottom side (along y = –250 and x= –250). The endpoints of this side are $\mathbf{x}_1$ and $\mathbf{x}_2$, or $\mathbf{x}_1$ = –250 **i** –250 **j** and $\mathbf{x}_2$ = 250 **i** –250 **j**. The vector $\boldsymbol{\delta}$ is defined as

$$\boldsymbol{\delta} = \mathbf{x}_1 - \mathbf{x}_2 = -500\ \mathbf{i}\ ,$$

where **i**, **j**, and **k** are unit vectors in the *x*, *y*, and *z* directions. The point **r** is where the electric field is calculated.

$$\mathbf{r} = x\,\mathbf{i} + y\,\mathbf{j} + b\,\mathbf{k}\ .$$

The vector **R** is defined as

$$\mathbf{R} = \mathbf{r} - (\mathbf{x_1} + \mathbf{x_2})/2 = (x - 500/2)\,\mathbf{i} + y\,\mathbf{j} + b\,\mathbf{k}\ .$$

The magnitudes of $\boldsymbol{\delta}$ and **R** are

$$\delta = |\boldsymbol{\delta}\,| = 500,$$

$$R = |\,\mathbf{R}\,| = \text{sqrt}\,[\,(x - 500/2)^2 + y^2 + z^2],$$

The angle φ is the angle between **R** and $\boldsymbol{\delta}$,

$$\varphi = \mathbf{R}^{*}\boldsymbol{\delta}/Rd = (x - 500/2) \,/\, \text{sqrt}\,[\,(x - 500/2)^2 + y^2 + z^2]\ .$$

Finally, the electric field is calculated using Eq. (2)

$$\boldsymbol{E} = -N\frac{\mu_0}{4\pi}\frac{dI}{dt}\frac{\boldsymbol{\delta}}{\delta}\left\{\sinh^{-1}\left[\frac{\frac{\delta}{2R} + \cos\varphi}{\sin\varphi}\right] - \sinh^{-1}\left[\frac{-\frac{\delta}{2R} + \cos\varphi}{\sin\varphi}\right]\right\},$$

Side 2

Repeat above but with

$$\mathbf{x_2} = 250\ \mathbf{i} - 250\ \mathbf{j},$$

$$\mathbf{x_3} = 250\ \mathbf{i} + 250\ \mathbf{j},$$

Side 3

Repeat above but with

$$\mathbf{x_3} = 250\ \mathbf{i} + 250\ \mathbf{j},$$

$$\mathbf{x_4} = -250\ \mathbf{i} + 250\ \mathbf{j},$$

Side 4

Repeat above but with

$$\mathbf{x_4} = -250\ \mathbf{i} + 250\ \mathbf{j},$$

$$\mathbf{x_1} = -250\ \mathbf{i} - 250\ \mathbf{j},$$

Add the contributions for the four sides to get the total electric field.

2. ASYMMETRIC COIL

The calculation of the electric field is based on Eq. (3.2) for asymmetric coil.

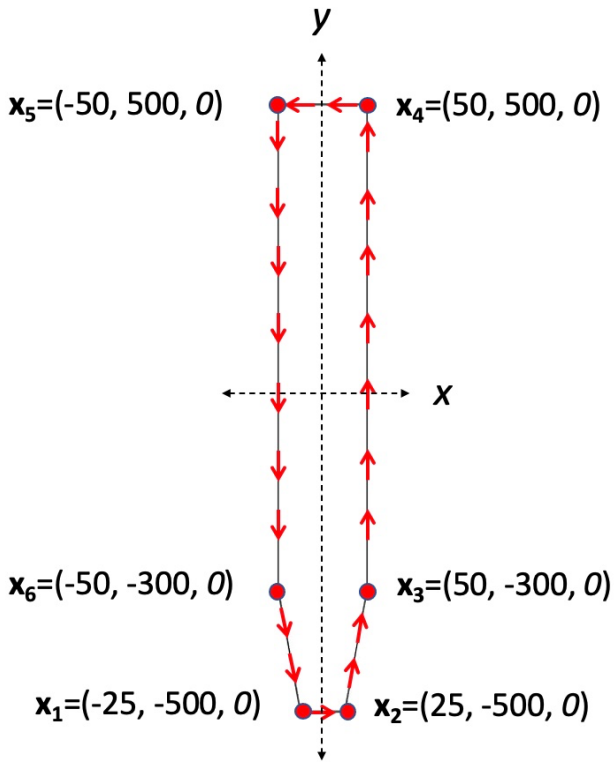

An asymmetric microcoil is 1000 μm long and 100 μm wide but narrows to 50 μm at the end of the last 200 μm of the coil. The red arrows show the direction of the current flows in the coil. The distance from coil to the plane where the electric field is calculated is b = 0.3 μm.

We calculated the electric field in the plane $z = b$. It is similar to the square microcoil, except for the coil geometry.

3. V-COIL

The calculation of the electric field is based on Eq. (4.2) for V-coil.

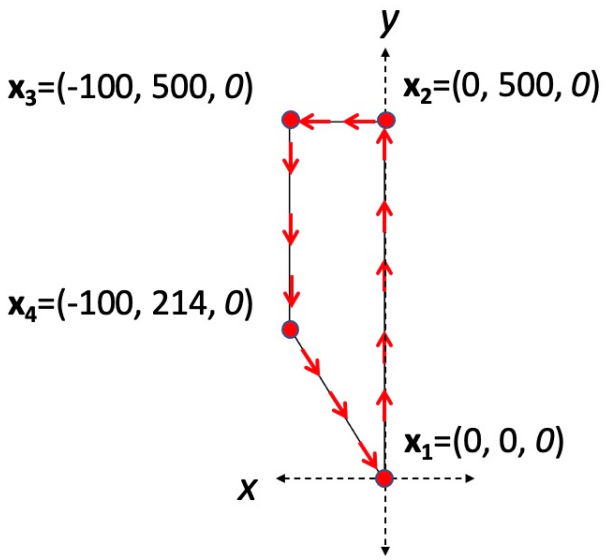

V- microcoil is 5000 μm long and 100 μm wide. The red arrows show the direction of the current flows in the coil. The distance from coil to the plane where the electric field is calculated is b = 30 μm.

We calculated the electric field in the plane $z = b$. It is similar to the square microcoil, except for the coil geometry.

4. W-COIL

The calculation of the electric field is based on Eq. (4.2) for W-coil.

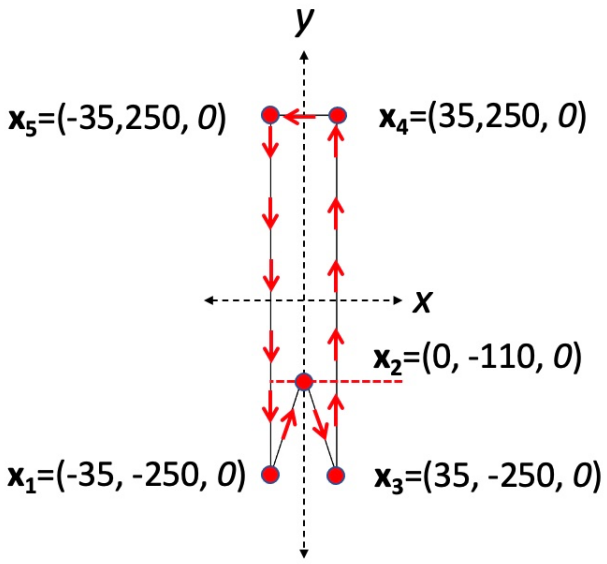

W- microcoil is 5000 μm long and 70 μm wide. The red arrows show the direction of the current flows in the coil. The distance from coil to the plane where the electric field is calculated is b = 15 μm.

We calculated the electric field in the plane $z = b$. It is similar to the square microcoil, except for the coil geometry.

APPENDIX C

MATLAB CODE USED FOR THE NUMERICAL ANALYSIS IN CHAPTER THREE

FOR A SQUARE COIL

```
N=100;
I=1e-3*(18850);
K=1e-7;
dx=10e-6;
dy=10e-6;
Z=300e-9;
for i=1:N
x(i)=(i-N/2)*dx;
y(i)=(i-N/2)*dy;
end
x1=[-250e-6  -250e-6  0]; % Rectangular start point %
x2=[250e-6  -250e-6  0];
x3=[250e-6 250e-6  0];
x4=[-250e-6 250e-6   0];
delta1=x1-x2;
delta2=x2-x3;
delta3=x3-x4;
delta4=x4-x1;
for i=1:N
```

```
for j=1:N
Ex(i,j)=0;
Ey(i,j)=0;
Ez(i,j)=0;
r=[x(i) y(j) Z];
    %%%%%%% Side 1 %%%%%%%
R1=r-(x1/2+x2/2);
Rm1=sqrt(R1(1)^2+R1(2)^2+R1(3)^2);
d1=sqrt(delta1(1)^2+delta1(2)^2+delta1(3)^2);
q1=d1/(2*Rm1);
phi1=acos((R1(1)*delta1(1)+R1(2)*delta1(2)+R1(3)*delta1(3))/(Rm1*d1));
M1=cos(phi1); N1=sin(phi1);
V1=[delta1/d1];
Ex(i,j)=Ex(i,j) - K*I*V1(1)*(asinh((q1+M1)/N1)-asinh((-q1+M1)/N1));
Ey(i,j)=Ey(i,j) - K*I*V1(2)*(asinh((q1+M1)/N1)-asinh((-q1+M1)/N1));
Ez(i,j)=Ez(i,j) - K*I*V1(3)*(asinh((q1+M1)/N1)-asinh((-q1+M1)/N1));
    %%%%%%% Side 2 %%%%%%%
R2=r-(x2/2+x3/2);
Rm2=sqrt(R2(1)^2+R2(2)^2+R2(3)^2);
d2=sqrt(delta2(1)^2+delta2(2)^2+delta2(3)^2);
q2=d2/(2*Rm2);
phi2=acos((R2(1)*delta2(1)+R2(2)*delta2(2)+R2(3)*delta2(3))/(Rm2*d2));
M2=cos(phi2);  N2=sin(phi2);
```

```
V2=[delta2/d2];
Ex(i,j)=Ex(i,j) - K*I*V2(1)*(asinh((q2+M2)/N2)-asinh((-q2+M2)/N2));
Ey(i,j)=Ey(i,j) - K*I*V2(2)*(asinh((q2+M2)/N2)-asinh((-q2+M2)/N2));
Ez(i,j)=Ez(i,j) - K*I*V2(3)*(asinh((q2+M2)/N2)-asinh((-q2+M2)/N2));
    %%%%%%%% Side 3 %%%%%%%%
R3=r-(x3/2+x4/2);
Rm3=sqrt(R3(1)^2+R3(2)^2+R3(3)^2);
d3=sqrt(delta3(1)^2+delta3(2)+delta3(3)^2);
q3=d3/(2*Rm3);
phi3=acos((R3(1)*delta3(1)+R3(2)*delta3(2)+R3(3)*delta3(3))/(Rm3*d3));
M3=cos(phi3);  N3=sin(phi3);
V3=delta3/d3;
Ex(i,j)=Ex(i,j) - K*I*V3(1)*(asinh((q3+M3)/N3)-asinh((-q3+M3)/N3));
Ey(i,j)=Ey(i,j) - K*I*V3(2)*(asinh((q3+M3)/N3)-asinh((-q3+M3)/N3));
Ez(i,j)=Ez(i,j) - K*I*V3(3)*(asinh((q3+M3)/N3)-asinh((-q3+M3)/N3));
    %%%%% Side 4%%%%%%%
R4=r-(x4/2+x1/2);
Rm4=sqrt(R4(1)^2+R4(2)^2+R4(3)^2);
d4=sqrt(delta4(1)^2+delta4(2)^2+delta4(3)^2);
q4=d4/(2*Rm4);
phi4=acos((R4(1)*delta4(1)+R4(2)*delta4(2)+R4(3)*delta4(3))/(Rm4*d4));
M4=cos(phi4); N4=sin(phi4);
V4=delta4/d4;
```

```
Ex(i,j)=Ex(i,j) - K*I*V4(1)*(asinh((q4+M4)/N4)-asinh((-q4+M4)/N4));

Ey(i,j)=Ey(i,j) - K*I*V4(2)*(asinh((q4+M4)/N4)-asinh((-q4+M4)/N4));

Ez(i,j)=Ez(i,j) - K*I*V4(3)*(asinh((q4+M4)/N4)-asinh((-q4+M4)/N4));

   %%%%%%%%%%%%%%%%%%%%%%%%%%%%%%%%%%%

end

 end

for i=2:N-1

for j=1:N

dExdx(i,j) = ( Ex(i+1,j) - Ex(i-1,j) )/(2*dx);

end

end

for j=1:N

dExdx(1,j) = ( Ex(2,j) - Ex(1,j) )/dx;

dExdx(N,j) = ( Ex(N,j) - Ex(N-1,j) )/dx;

end
```

APPENDIX D

MATLAB CODE USED FOR THE NUMERICAL ANALYSIS IN CHAPTER THREE

FOR ASSYMETRIC COIL

```
N=100;
I=1e-3*2*pi*3000;
K=1e-7;
dx=1e-6;
dy=1e-6;
dz=0;
Z=300e-9;
for i=1:N
x(i)=(i-N/2)*dx;
 y(i)=(i)*dy;
end
x1=[-50e-6  500e-6  0]; % V coil %
x2=[-50e-6  -300e-6   0];
x3=[-25e-6   -500e-6    0];
x4=[25e-6   -500e-6     0];
x5=[50e-6 -300e-6    0];
x6=[50e-6 500e-6    0];
delta1=x1-x2;
delta2=x2-x3;
```

```
delta3=x3-x4;

delta4=x4-x5;

delta5=x5-x6;

delta6=x6-x1;

for i=1:N

  for j=1:N

Ex(i,j)=0;

Ey(i,j)=0;

Ez(i,j)=0;

r=[x(i) y(j) Z];

%%%%%%% Side 1 %%%%%%%

R1=r-(x1/2+x2/2);

Rm1=sqrt(R1(1)^2+R1(2)^2+R1(3)^2);

d1=sqrt(delta1(1)^2+delta1(2)^2+delta1(3)^2);

q1=d1/(2*Rm1);

phi1=acos((R1(1)*delta1(1)+R1(2)*delta1(2)+R1(3)*delta1(3))/(Rm1*d1));

M1=cos(phi1); N1=sin(phi1);

V1=[delta1/d1];

Ex(i,j)=Ex(i,j) - K*I*V1(1)*(asinh((q1+M1)/N1)-asinh((-q1+M1)/N1));

Ey(i,j)=Ey(i,j) - K*I*V1(2)*(asinh((q1+M1)/N1)-asinh((-q1+M1)/N1));

Ez(i,j)=Ez(i,j) - K*I*V1(3)*(asinh((q1+M1)/N1)-asinh((-q1+M1)/N1));

%%%%%%% Side 2 %%%%%%%

R2=r-(x2/2+x3/2);
```

```
Rm2=sqrt(R2(1)^2+R2(2)^2+R2(3)^2);
d2=sqrt(delta2(1)^2+delta2(2)^2+delta2(3)^2);
q2=d2/(2*Rm2);
phi2=acos((R2(1)*delta2(1)+R2(2)*delta2(2)+R2(3)*delta2(3))/(Rm2*d2));
M2=cos(phi2);   N2=sin(phi2);
V2=[delta2/d2];
Ex(i,j)=Ex(i,j) - K*I*V2(1)*(asinh((q2+M2)/N2)-asinh((-q2+M2)/N2));
Ey(i,j)=Ey(i,j) - K*I*V2(2)*(asinh((q2+M2)/N2)-asinh((-q2+M2)/N2));
Ez(i,j)=Ez(i,j) - K*I*V2(3)*(asinh((q2+M2)/N2)-asinh((-q2+M2)/N2));
%%%%%%%% Side 3 %%%%%%%%
R3=r-(x3/2+x4/2);
Rm3=sqrt(R3(1)^2+R3(2)^2+R3(3)^2);
d3=sqrt(delta3(1)^2+delta3(2)^2+delta3(3)^2);
q3=d3/(2*Rm3);
phi3=acos((R3(1)*delta3(1)+R3(2)*delta3(2)+R3(3)*delta3(3))/(Rm3*d3));
M3=cos(phi3);   N3=sin(phi3);
V3=delta3/d3;
Ex(i,j)=Ex(i,j) - K*I*V3(1)*(asinh((q3+M3)/N3)-asinh((-q3+M3)/N3));
Ey(i,j)=Ey(i,j) - K*I*V3(2)*(asinh((q3+M3)/N3)-asinh((-q3+M3)/N3));
Ez(i,j)=Ez(i,j) - K*I*V3(3)*(asinh((q3+M3)/N3)-asinh((-q3+M3)/N3));
%%%%% Side 4%%%%%%%
R4=r-(x4/2+x5/2);
Rm4=sqrt(R4(1)^2+R4(2)^2+R4(3)^2);
```

```
d4=sqrt(delta4(1)^2+delta4(2)^2+delta4(3)^2);
q4=d4/(2*Rm4);
phi4=acos((R4(1)*delta4(1)+R4(2)*delta4(2)+R4(3)*delta4(3))/(Rm4*d4));
M4=cos(phi4);   N4=sin(phi4);
V4=delta4/d4;
Ex(i,j)=Ex(i,j) - K*I*V4(1)*(asinh((q4+M4)/N4)-asinh((-q4+M4)/N4));
Ey(i,j)=Ey(i,j) - K*I*V4(2)*(asinh((q4+M4)/N4)-asinh((-q4+M4)/N4));
Ez(i,j)=Ez(i,j) - K*I*V4(3)*(asinh((q4+M4)/N4)-asinh((-q4+M4)/N4));
%%%%%%%%%%%%%%%%%%%%%%%%%%%%%%%%%%%%%%%%%%%
R5=r-(x5/2+x6/2);
Rm5=sqrt(R5(1)^2+R5(2)^2+R5(3)^2);
d5=sqrt(delta5(1)^2+delta5(2)^2+delta5(3)^2);
q5=d5/(2*Rm5);
phi5=acos((R5(1)*delta5(1)+R5(2)*delta5(2)+R5(3)*delta5(3))/(Rm5*d5));
M5=cos(phi5);   N5=sin(phi5);
V5=delta5/d5;
Ex(i,j)=Ex(i,j) - K*I*V5(1)*(asinh((q5+M5)/N5)-asinh((-q5+M5)/N5));
Ey(i,j)=Ey(i,j) - K*I*V5(2)*(asinh((q5+M5)/N5)-asinh((-q5+M5)/N5));
Ez(i,j)=Ez(i,j) - K*I*V5(3)*(asinh((q5+M5)/N5)-asinh((-q5+M5)/N5));
%%%%%%%%%%%%%%%%%%%%%%%%%%%%%%%%%%%%%%%%%%%
R6=r-(x6/2+x1/2);
Rm6=sqrt(R6(1)^2+R6(2)^2+R6(3)^2);
d6=sqrt(delta6(1)^2+delta6(2)^2+delta6(3)^2);
```

```
q6=d6/(2*Rm6);
phi6=acos((R6(1)*delta6(1)+R6(2)*delta6(2)+R6(3)*delta6(3))/(Rm6*d6));
M6=cos(phi6);   N6=sin(phi6);
V6=delta6/d6;
Ex(i,j)=Ex(i,j) - K*I*V6(1)*(asinh((q6+M6)/N6)-asinh((-q6+M6)/N6));
Ey(i,j)=Ey(i,j) - K*I*V6(2)*(asinh((q6+M6)/N6)-asinh((-q6+M6)/N6));
Ez(i,j)=Ez(i,j) - K*I*V6(3)*(asinh((q6+M6)/N6)-asinh((-q6+M6)/N6));
end
end
for i=2:N-1
for j=1:N
dExdx(i,j) = ( Ex(i+1,j) - Ex(i-1,j) )/(2*dx);
end
end
for j=1:N
dExdx(1,j) = ( Ex(2,j) - Ex(1,j) )/dx;
dExdx(N,j) = ( Ex(N,j) - Ex(N-1,j) )/dx;
end
for i=2:N-1
for j=1:N
dEydy(i,j) = ( Ey(i+1,j) - Ey(i-1,j) )/(2*dy);
end
end
```

```
for j=1:N
dEydy(1,j) = ( Ey(2,j) - Ey(1,j) )/dy;
dEydy(N,j) = ( Ey(N,j) - Ey(N-1,j) )/dy;
end
for i=2:N-1
for j=1:N
dEzdz(i,j) = ( Ez(i+1,j) - Ez(i-1,j) )/(2*dz);
end
end
for j=1:N
dEzdz(1,j) = ( Ez(2,j) - Ez(1,j) )/dx;
dEzdz(N,j) = ( Ez(N,j) - Ez(N-1,j) )/dx;
end
```

APPENDIX E

MATLAB CODE USED FOR THE NUMERICAL ANALYSIS IN CHAPTER FOUR

FOR V-COIL

```
N=1000;
I=20e-3*1*2*pi*30e6;
K=1e-7;
dx=10e-6;
dy=10e-6;
dz=0;
Z=30e-6;
for i=1:N
x(i)=(i-N/2)*dx;
 y(i)=(i-N/2)*dy;
end
x1=[0                0        0];
x2=[0             500e-6   0];
x3=[-100e-6     500e-6   0];
x4=[-100e-6       214e-6   0];
delta1=x1-x2;
delta2=x2-x3;
delta3=x3-x4;
delta4=x4-x1;
```

```
for i=1:N
  for j=1:N
Ex(i,j)=0;
Ey(i,j)=0;
Ez(i,j)=0;
r=[x(i) y(j) Z];
%%%%%%% Side 1 %%%%%%%
R1=r-(x1/2+x2/2);
Rm1=sqrt(R1(1)^2+R1(2)^2+R1(3)^2);
d1=sqrt(delta1(1)^2+delta1(2)^2+delta1(3)^2);
q1=d1/(2*Rm1);
phi1=acos((R1(1)*delta1(1)+R1(2)*delta1(2)+R1(3)*delta1(3))/(Rm1*d1));
M1=cos(phi1); N1=sin(phi1);
V1=delta1/d1;
Ex(i,j)=Ex(i,j) - K*I*V1(1)*(asinh((q1+M1)/N1)-asinh((-q1+M1)/N1));
Ey(i,j)=Ey(i,j) - K*I*V1(2)*(asinh((q1+M1)/N1)-asinh((-q1+M1)/N1));
Ez(i,j)=Ez(i,j) - K*I*V1(3)*(asinh((q1+M1)/N1)-asinh((-q1+M1)/N1));
%%%%%%% Side 2 %%%%%%%
R2=r-(x2/2+x3/2);
Rm2=sqrt(R2(1)^2+R2(2)^2+R2(3)^2);
d2=sqrt(delta2(1)^2+delta2(2)^2+delta2(3)^2);
q2=d2/(2*Rm2);
phi2=acos((R2(1)*delta2(1)+R2(2)*delta2(2)+R2(3)*delta2(3))/(Rm2*d2));
```

```
M2=cos(phi2);   N2=sin(phi2);

V2=delta2/d2;

Ex(i,j)=Ex(i,j) - K*I*V2(1)*(asinh((q2+M2)/N2)-asinh((-q2+M2)/N2));

Ey(i,j)=Ey(i,j) - K*I*V2(2)*(asinh((q2+M2)/N2)-asinh((-q2+M2)/N2));

Ez(i,j)=Ez(i,j) - K*I*V2(3)*(asinh((q2+M2)/N2)-asinh((-q2+M2)/N2));

%%%%%%% Side 3 %%%%%%%%

R3=r-(x3/2+x4/2);

Rm3=sqrt(R3(1)^2+R3(2)^2+R3(3)^2);

d3=sqrt(delta3(1)^2+delta3(2)^2+delta3(3)^2);

q3=d3/(2*Rm3);

phi3=acos((R3(1)*delta3(1)+R3(2)*delta3(2)+R3(3)*delta3(3))/(Rm3*d3));

M3=cos(phi3);   N3=sin(phi3);

V3=delta3/d3;

Ex(i,j)=Ex(i,j) - K*I*V3(1)*(asinh((q3+M3)/N3)-asinh((-q3+M3)/N3));

Ey(i,j)=Ey(i,j) - K*I*V3(2)*(asinh((q3+M3)/N3)-asinh((-q3+M3)/N3));

Ez(i,j)=Ez(i,j) - K*I*V3(3)*(asinh((q3+M3)/N3)-asinh((-q3+M3)/N3));

%%%%% Side 4%%%%%%%

R4=r-(x4/2+x1/2);

Rm4=sqrt(R4(1)^2+R4(2)^2+R4(3)^2);

d4=sqrt(delta4(1)^2+delta4(2)^2+delta4(3)^2);

q4=d4/(2*Rm4);

phi4=acos((R4(1)*delta4(1)+R4(2)*delta4(2)+R4(3)*delta4(3))/(Rm4*d4));

M4=cos(phi4);   N4=sin(phi4);
```

```
V4=delta4/d4;
Ex(i,j)=Ex(i,j) - K*I*V4(1)*(asinh((q4+M4)/N4)-asinh((-q4+M4)/N4));
Ey(i,j)=Ey(i,j) - K*I*V4(2)*(asinh((q4+M4)/N4)-asinh((-q4+M4)/N4));
Ez(i,j)=Ez(i,j) - K*I*V4(3)*(asinh((q4+M4)/N4)-asinh((-q4+M4)/N4));
%%%%%%%%%%%%%%%%%%%%%%%%%%%%%%%%%%%%%%%%%%%%%%%%%%%%%%%%%%%%%%
end
end
for i=2:N-1
  for j=1:N
    dExdx(i,j) = ( Ex(i+1,j) - Ex(i-1,j) )/(2*dx);
    end
    end
for j=1:N
dExdx(1,j) = ( Ex(2,j) - Ex(1,j) )/dx;
dExdx(N,j) = ( Ex(N,j) - Ex(N-1,j) )/dx;
end
for i=2:N-1
 for j=1:N
  dEydy(i,j) = ( Ey(i+1,j) - Ey(i-1,j) )/(2*dy);
    end
end
for j=1:N
dEydy(1,j) = ( Ey(2,j) - Ey(1,j) )/dy;
```

```
dEydy(N,j) = ( Ey(N,j) - Ey(N-1,j) )/dy;

end

for j=1:N

dEzdz(1,j) = ( Ez(2,j) - Ez(1,j) )/dx;

dEzdz(N,j) = ( Ez(N,j) - Ez(N-1,j) )/dx;

end
```

APPENDIX F

MATLAB CODE USED FOR THE NUMERICAL ANALYSIS IN CHAPTER FOUR

FOR W-COIL

```
N=1000;
I=1e-3*2*pi*5000;
K=1e-7;
dx=1e-6;
dy=1e-6;
dz=0;
Z=15e-6;
for i=1:N
x(i)=(i-N/2)*dx;
 y(i)=(i-N/2)*dy;
end
x1=[-35e-6  -250e-6  0]; % w coil %
x2=[0   -110e-6    0];
x3=[35e-6  -250e-6   0];
x4=[35e-6   250e-6     0];
x5=[-35e-6 250e-6    0];

delta1=x1-x2;
delta2=x2-x3;
```

```
delta3=x3-x4;
delta4=x4-x5;
delta5=x5-x1;
for i=1:N
  for j=1:N
Ex(i,j)=0;
Ey(i,j)=0;
Ez(i,j)=0;
r=[x(i) y(j) Z];
%%%%%%% Side 1 %%%%%%%
R1=r-(x1/2+x2/2);
Rm1=sqrt(R1(1)^2+R1(2)^2+R1(3)^2);
d1=sqrt(delta1(1)^2+delta1(2)^2+delta1(3)^2);
q1=d1/(2*Rm1);
phi1=acos((R1(1)*delta1(1)+R1(2)*delta1(2)+R1(3)*delta1(3))/(Rm1*d1));
M1=cos(phi1); N1=sin(phi1);
V1=[delta1/d1];
Ex(i,j)=Ex(i,j) - K*I*V1(1)*(asinh((q1+M1)/N1)-asinh((-q1+M1)/N1));
Ey(i,j)=Ey(i,j) - K*I*V1(2)*(asinh((q1+M1)/N1)-asinh((-q1+M1)/N1));
Ez(i,j)=Ez(i,j) - K*I*V1(3)*(asinh((q1+M1)/N1)-asinh((-q1+M1)/N1));
%%%%%%% Side 2 %%%%%%%
R2=r-(x2/2+x3/2);
Rm2=sqrt(R2(1)^2+R2(2)^2+R2(3)^2);
```

```
d2=sqrt(delta2(1)^2+delta2(2)^2+delta2(3)^2);
q2=d2/(2*Rm2);
phi2=acos((R2(1)*delta2(1)+R2(2)*delta2(2)+R2(3)*delta2(3))/(Rm2*d2));
M2=cos(phi2);   N2=sin(phi2);
V2=[delta2/d2];
Ex(i,j)=Ex(i,j) - K*I*V2(1)*(asinh((q2+M2)/N2)-asinh((-q2+M2)/N2));
Ey(i,j)=Ey(i,j) - K*I*V2(2)*(asinh((q2+M2)/N2)-asinh((-q2+M2)/N2));
Ez(i,j)=Ez(i,j) - K*I*V2(3)*(asinh((q2+M2)/N2)-asinh((-q2+M2)/N2));
%%%%%%% Side 3 %%%%%%%%
R3=r-(x3/2+x4/2);
Rm3=sqrt(R3(1)^2+R3(2)^2+R3(3)^2);
d3=sqrt(delta3(1)^2+delta3(2)^2+delta3(3)^2);
q3=d3/(2*Rm3);
phi3=acos((R3(1)*delta3(1)+R3(2)*delta3(2)+R3(3)*delta3(3))/(Rm3*d3));
M3=cos(phi3);   N3=sin(phi3);
V3=delta3/d3;
Ex(i,j)=Ex(i,j) - K*I*V3(1)*(asinh((q3+M3)/N3)-asinh((-q3+M3)/N3));
Ey(i,j)=Ey(i,j) - K*I*V3(2)*(asinh((q3+M3)/N3)-asinh((-q3+M3)/N3));
Ez(i,j)=Ez(i,j) - K*I*V3(3)*(asinh((q3+M3)/N3)-asinh((-q3+M3)/N3));
%%%%% Side 4%%%%%%%
R4=r-(x4/2+x5/2);
Rm4=sqrt(R4(1)^2+R4(2)^2+R4(3)^2);
d4=sqrt(delta4(1)^2+delta4(2)^2+delta4(3)^2);
```

```
q4=d4/(2*Rm4);
phi4=acos((R4(1)*delta4(1)+R4(2)*delta4(2)+R4(3)*delta4(3))/(Rm4*d4));
M4=cos(phi4);   N4=sin(phi4);
V4=delta4/d4;
Ex(i,j)=Ex(i,j) - K*I*V4(1)*(asinh((q4+M4)/N4)-asinh((-q4+M4)/N4));
Ey(i,j)=Ey(i,j) - K*I*V4(2)*(asinh((q4+M4)/N4)-asinh((-q4+M4)/N4));
Ez(i,j)=Ez(i,j) - K*I*V4(3)*(asinh((q4+M4)/N4)-asinh((-q4+M4)/N4));
%%%%%%%%%%%%%%%%%%%%%%%%%%%%%%%%
R5=r-(x5/2+x1/2);
Rm5=sqrt(R5(1)^2+R5(2)^2+R5(3)^2);
d5=sqrt(delta5(1)^2+delta5(2)^2+delta5(3)^2);
q5=d5/(2*Rm5);
phi5=acos((R5(1)*delta5(1)+R5(2)*delta5(2)+R5(3)*delta5(3))/(Rm5*d5));
M5=cos(phi5);   N5=sin(phi5);
V5=delta5/d5;
Ex(i,j)=Ex(i,j) - K*I*V5(1)*(asinh((q5+M5)/N5)-asinh((-q5+M5)/N5));
Ey(i,j)=Ey(i,j) - K*I*V5(2)*(asinh((q5+M5)/N5)-asinh((-q5+M5)/N5));
Ez(i,j)=Ez(i,j) - K*I*V5(3)*(asinh((q5+M5)/N5)-asinh((-q5+M5)/N5));
end
end
for i=2:N-1
for j=1:N
dExdx(i,j) = ( Ex(i+1,j) - Ex(i-1,j) )/(2*dx);
```

```
end
end
for j=1:N
dExdx(1,j) = ( Ex(2,j) - Ex(1,j) )/dx;
dExdx(N,j) = ( Ex(N,j) - Ex(N-1,j) )/dx;
end
for i=2:N-1
for j=1:N
dEydy(i,j) = ( Ey(i+1,j) - Ey(i-1,j) )/(2*dy);
end
end
for j=1:N
dEydy(1,j) = ( Ey(2,j) - Ey(1,j) )/dy;
dEydy(N,j) = ( Ey(N,j) - Ey(N-1,j) )/dy;
end
for i=2:N-1
  for j=1:N
dEzdz(i,j) = ( Ez(i+1,j) - Ez(i-1,j) )/(2*dz);
end
end
for j=1:N
dEzdz(1,j) = ( Ez(2,j) - Ez(1,j) )/dx;
dEzdz(N,j) = ( Ez(N,j) - Ez(N-1,j) )/dx; end
```

APPENDIX G

MATLAB CODE USED FOR THE NUMERICAL ANALYSIS IN CHAPTER FOUR

CAPACITIVE COUPLING

```
Nt=1000000;

Nx=21;

L=0.001;

U=zeros(Nt,Nx);

V=zeros(Nt,Nx);

Vi=zeros(Nt,Nx);

Ve=zeros(Nt,Nx);

deltat=0.000000001;

deltax=2*L/(Nx-1);

t(1)=0;

W=2*pi*3e3;

ri=850;

re=3.183e8;


k=3.8;

eo=8.85e-12;

d=300e-9;

a=2.5e-6;

C=k*eo/d;
```

```
D=1/(2*pi*a*C*(ri+re));
I=0.001;
c1=deltax*ri*I;
c2=deltat/deltax^2*D;
c3=ri*I;
for j=1:Nx
x(j)=-L+(j-1)*deltax;
V(1,j)=0;
U(1,j)=0;
end
ncount=0;
Ebig=0;
for i=2:Nt;
t(i)=t(i-1)+deltat;
for j=2:Nx-1;
V(i,j)=V(i-1,j)+c2*(V(i-1,j+1)+V(i-1,j-1)-2*V(i-1,j));
end
V(i,1)=V(i,2)+c1*sin(W*t(i));
V(i,Nx)=V(i,Nx-1)-c1*sin(W*t(i));
for j=1:Nx
U(i,j)=-c3*sin(W*t(i))*x(j);
end
for j=1:Nx
```

```
Ve(i,j)=(re/(ri+re))*(U(i,j)-V(i,j));

Vi(i,j)=(re/(ri+re))*(U(i,j)+(ri/re)*V(i,j));

end

for j=2:Nx-1

E(i,j)=-(Ve(i,j+1)-Ve(i,j-1))/(2*deltax);

end

if(E(i,(Nx+1)/2)>Ebig)

Ebig=E(i,(Nx+1)/2);

end

ncount=ncount+1;

if(ncount>99999)

i

ncount=0;

end

end

Ebig
```

APPENDIX H

MATLAB CODE USED FOR THE NUMERICAL ANALYSIS IN CHAPTER FIVE

ACTIVATION FUNCTION

```
Nt=100000;   % max number of time iterations
Nx=401;      %max number of space iterations
L=12;     % the length in cm
cm = 1;     % membrane capacitance in μF/cm^2
%ri=1e5;    %The resistance of the axon kOhm/cm
R2=0.0354;  %the specific resistance of the axoplasm in Kohm.cm
a=0.0238;   % The axon radius of in cm
b=1;        % Spatial width of the electric field in cm
dt= 0.001/5; % time step in ms
deltax=2*L/(Nx-1); % space step in cm
ENa = 50;   %Sodium Voltage
EK = -77;   % Potassium Voltage in mV
El =-54.387;    %Leakage Voltage in mV
gNamax = 120;   %max Sodium conductance in 1/(kOhm cm^2), or mS/cm^2, S=1/ohm,
or S=Amper/Volt.
gKmax = 36;     % %max potassium conductance in 1/(kOhm cm^2)
glmax = 0.3;    % max leakage conductance in 1/(kOhm cm^2)
% Initial conditions
vm(1,1) = -65; % initial membrane voltage in mV
```

```
V(1,1)=vm(1,1); %initial membrane voltage in mV
tau1=0.1;
time(1)=0;
Q=1; % Electric field strength in mV/cm
% calculating alphas and betas for the initial membrane voltage
alpn = 0.01*(vm+55)/(1-exp(-(vm+55)/10));
alpm = 0.1*(vm+40)/(1-exp(-(vm+40)/10));
alph = 0.07*exp(-0.05*(vm+65));
betn = 0.125*exp(-(vm+65)/80);
betm = 4*exp(-0.0556*(vm+65));
beth = 1/(1+exp(-0.1*(vm+35)));
% initial m,n & h
for j= 2:Nx,
x(j)=-L+(j-1)*deltax;
V(1,j)=-65;
n(1,j) = alpn/(alpn+betn);
m(1,j) = alpm/(alpm+betm);
h(1,j) = alph/(alph+beth);
end
for i=2:Nt;
time=time+dt;
Iext2(i)=time*2.71828^(-time/tau1);
E0(i)=Q*(1-time/tau1)*2.71828^-(time/tau1);
```

```
end
 for i=2:Nt
time=time+dt;
for j= 2:Nx-1,
E(i,j)=E0(i)*((b^2)/(b^2+x(j)^2));
dExdx(i,j)=E0(i)*(-2*(b^2)*x(j)/(b^2+x(j)^2)^2);
end
 end
% the loop for calculation of membrane voltage dynamics is here.
for i = 1:Nt,
time=time+dt;
for j= 2:Nx-1,
V(i+1,1)=V(i,2);
V(i+1,Nx)=V(i,Nx-1);
alpn = 0.01*(V(i,j)+55)/(1-exp(-(V(i,j)+55)/10));
alpm = 0.1*( V(i,j)+40)/(1-exp(-(V(i,j)+40)/10));
alph = 0.07*exp(-0.05*(V(i,j)+65));
betn = 0.125*exp(-(V(i,j)+65)/80);
betm = 4*exp(-0.0556*(V(i,j)+65));
beth = 1/(1+exp(-0.1*(V(i,j)+35)));
dm = dt*(alpm*(1-m(i,j))-betm*m(i,j));
dn = dt*(alpn*(1-n(i,j))-betn*n(i,j));
dh = dt*(alph*(1-h(i,j))-beth*h(i,j));
```

```
m(i+1,j) = m(i,j) + dm;

n(i+1,j) = n(i,j) + dn;

h(i+1,j) = h(i,j) + dh;

gNa = gNamax*m(i,j)^3*h(i,j);

gK = gKmax*n(i,j)^4;

gl = glmax;

INa = gNa*(V(i,j)-ENa);

IK = gK*(V(i,j)-EK);

Il = gl*(V(i,j)-El);

   dvm = (dt/cm)*-1*(INa + IK + Il)+((dt*a)/(2*R2*deltax*deltax*2*cm)*(V(i,j+1)-

2*V(i,j)+V(i,j-1)))-dExdx(i,j)*((dt*a)/(2*R2*cm)); %(V(i,j+1)-2*V(i,j)+V(i,j-1)))

V(i+1,j)=V(i,j)+dvm

 end

end
```

REFERENCES

Aberra AS, Wang B, Grill WM, Peterchev AV (2020) Simulation of transcranial magnetic stimulation in head model with morphologically-realistic cortical neurons. *Brain Stimulation*, *13(1)*, 175–189.

Alzahrani M, Roth BJ (2023) The electric field induced by a microcoil during magnetic stimulation. *IEEE Trans Biomed Eng, 70*, 3260–3262.

Alzahrani M, Roth BJ (2024) The calculation of maximum electric field intensity in brain tissue stimulated by a current pulse through a microcoil via capacitive coupling. *Applied Sciences*, *14*, 2994.

Alzahrani M, Roth BJ (2024) The Difference between Traditional Magnetic Stimulation and Microcoil Stimulation: Threshold and the Electric Field Gradient. *Applied Sciences*, *14,* 8349.

Ambriz-Tututi M, Alvarado-Reynoso B, Drucker-Colín R (2016) Analgesic effect of repetitive transcranial magnetic stimulation (rTMS) in patients with chronic low back pain. *Bioelectromagnetics*, *37*, 527–535.

Baker PF, Hodgkin AL, Shaw TI (1962) Replacement of the axoplasm of giant nerve fibres with artificial solutions. *The Journal of Physiology*, *164*(2), 330–354.

Barker AT, Jalinous R, Freeston IL (1985) Non-invasive magnetic stimulation of human motor cortex. *Lancet, 1*(8437), 1106–1107.

Barker AT (1991) An introduction to the basic principles of magnetic nerve stimulation. *J Clin Neurophysiol*, *8*, 26–37.

Bensmaia SJ, Miller LE (2014) Restoring sensorimotor function through intracortical interfaces: progress and looming challenges. *Nat Rev Neurosci*, *15*(5), 313-25.

Berger TW et al. (2001) Brain-implantable biomimetic electronics as the next era in neural prosthetics. *Proceedings of the IEEE*, *89*(7), 993-1012.

Bernardo R, Rodrigues A, Soares dos Santos MP, Cameiro P, Lopes A, Amaral JS, Amaral VS, Morais R (2019) Novel magnetic stimulation methodology for low-current implantable medical devices. *Med Eng Phys*, *73*, 77–84.

Bonmassar G, Lee SW, Freeman DK, Polasek M, Fried SI, Gale JT (2012) Microscopic magnetic stimulation of neural tissue. *Nat Commun, 3*, 921.

Cogan SF (2008) Neural stimulation and recording electrodes. *Annual Review of Biomedical Engineering*, *10*, 275–309.

Deng ZD, Lisanby SH, Peterchev AV (2014) Coil design considerations for deep transcranial magnetic stimulation. *Clin Neurophysiol*, *125*(6), 1202-1212.

Epstein CM, Schwartzberg DG, Davey KR, Sudderth DB (1990). Localizing the site of magnetic brain stimulation in humans. *Neurology*, *40*(4), 666–670.

Fang X, Duan S, Wang L (2021) Memristive Hodgkin-Huxley spiking neuron model for reproducing neuron behaviors. *Frontiers in Neuroscience*, *15*, 730566.

Francis JT, Gluckman BJ, Schiff SJ (2003) Sensitivity of neurons to weak electric fields. *J Neurosci*, *23*, 7255–7261.

Grill WM, Mortimer JT (1997) Inversion of the current-distance relationship by transient depolarization. *IEEE Transactions on Biomedical Engineering*, *44*(1), 1–9.

Hause L (1975) A mathematical model for transmembrane potentials secondary to extracellular fields. In *Electroanaesthesia: Biomedical and Biophysical Studies*, ed. A Sances Jr, SJ Larson, 176–200. New York: Academic.

Hirshler YK, Polat U, Biegon A (2010) Intracranial electrode implantation produces regional neuroinflammation and memory deficits in rats. *Experimental Neurology*, *222*(1), 42–50.

Hobbie RK, Roth BJ (2015) *Intermediate Physics for Medicine and Biology*, 5th Ed., Springer, New York.

Hodgkin AL, Huxley AF (1939) Action potentials recorded from inside a nerve fibre. *Nature*, *144*(3651), 710–711.

Hodgkin AL, Katz B (1949) The effect of sodium ions on the electrical activity of giant axon of the squid. *Physiol J*, *108*(1), 37–77.

Hodgkin AL, Huxley AF (1952) A quantitative description of membrane current and its application to conduction and excitation in nerve. *Physiol J*, *117*(4), 500-544.

Jeong H, Deng J, Bonmassar G (2021) Planar figure-8 coils for ultra-focal and directional micromagnetic brain stimulation. *J Vac Sci Technol B*, *39*, 063202.

Khalifa A, Zaeimbashi M, Zhou TX, Abrishami SM, Sun N, Park S, Sumarac T, Qu J, Zohar I, Yacoby A, Cash S, Sun NX (2021) The development of microfabricated solenoids with magnetic cores for micromagnetic neural stimulation. *Microsyst Nanoeng*, *7*, 91.

Koch G, Bonni S, Pellicciari MC, Casula EP, Mancini M, Esposito R, Ponzo V, Picazio S, Di Lorenzo F, Serra L, Motta C, Maiella M, Marra C, Cercignani M, Martorana A, Caltagirone C, Bozzali M (2018) Transcranial magnetic stimulation of the precuneus enhances memory and neural activity in prodromal Alzheimer's disease. *NeuroImage*, *169*, 302–311.

Lee SW, Fried SI (2015) Suppression of subthalamic nucleus activity by micromagnetic stimulation. *IEEE Trans Neural Syst Rehabil Eng*, *23*, 116–127.

Lee SW, Fallegger F, Casse BDF, Fried SI (2016) Implantable microcoils for intracortical magnetic stimulation. *Science Advances, 2*, e1600889.

Lee, SW, Thyagarajan K, Fried, SI (2019) Micro-coil design influences the spatial extent of responses to intracortical magnetic stimulation. *IEEE Transactions on Biomedical Engineering*, *66*(6), 1680–1694.

Lee KJ, Park B, Jang J-W, Kim S (2023) Magnetic stimulation of the sciatic nerve using an implantable high-inductance coil with low-intensity current. *J Neural Eng*, *20*, 036035.

Lefaucheur J-P, Aleman A, Baeken C, Benninger DH, Brunelin J, Di Lazzaro V, Filipović SR, Grefkes C, Hasan A, Hummel FC, Jääskeläinen SK, Langguth B, Leocani L, Londero A, Nardone R, Nguyen J-P, Nyffeler T, Oliveira-Maia AJ, Oliviero A, Padberg F, Palm U, Paulus W, Poulet E, Quartarone A, Rachid F, Rektorová I, Rossi S, Sahlsten H, Schecklmann M, Szekely D, Ziemann U (2020) Evidence-based guidelines on the therapeutic use of repetitive transcranial magnetic stimulation (rTMS): An update (2014–2018). *Clinical Neurophysiology*, *131*, 474–528.

Liu X, Whalen AJ, Ryu SB, Lee SW, Fried SI, Kim K, Cai C, Lauritzen M, Bertram N, Chang B, et al. (2023) MEMS micro-coils for magnetic neurostimulation. *Biosens Bioelectron*, *227*, 115143.

Maccabee PJ, Amassian VE, Eberle L, Cracco RQ (1993) Magnetic coil stimulation of straight and bent amphibian and mammalian peripheral nerve in vitro: Locus of excitation. *J Physiol*, *460*, 201–219.

Minusa S, Muramatsu S, Osanai H, Tateno T (2019) A multichannel magnetic stimulation system using submillimeter-sized coils: System development and experimental application to rodent brain in vivo. *J Neural Eng*, *16*, 066014.

Nagarajan SS, Durand DM, Warman EN (1993) Effects of induced electric fields on finite neuronal structures: a simulation study. *IEEE Trans Biomed Eng*, *40*, 1175–1188.

Nilsson J, Panizza M, Roth BJ, Basser PJ, Cohen LG, Caruso G, Hallett M (1992). Determining the site of stimulation during magnetic stimulation of a peripheral nerve. *Electroencephalography and clinical neurophysiology*, *85*(4), 253–264.

Nitz WR, Brinker G, Diehl D, Frese G (2005) Specific absorption rate as a poor indicator of magnetic resonance-related implant heating. *Invest Radiol*, *40*(12), 773-776.

Park HJ, Bonmassar G, Kaltenbach JA, Machado AG, Manzoor NF, Gale JT (2013) Activation of the central nervous system induced by micro-magnetic stimulation. *Nat Commun*, *4*, 2463.

Park HJ, Kang H, Jo J, Chung E, Kim S (2018) Planar coil-based contact-mode magnetic stimulation: synaptic responses in hippocampal slices and thermal considerations. *Scientific Reports*, *8*, 13423.

Peckham PH, Knutson JS. (2005) Functional electrical stimulation for neuromuscular applications. *Annu Rev Biomed Eng*, *7*, 327-360.

Perlmutter JS, Mink JW (2006) Deep brain stimulation. *Annu Rev Neurosci*, *29*, 229-257.

Press WH, Flannery BP, Teukolsky SA, Vetterling WT (1992) *Numerical Recipes in FORTRAN 77*. Cambridge University Press, Cambridge, UK.

Raman IM, Ferster DL (2021) *The Annotated Hodgkin and Huxley: A Reader's Guide*. Princeton University Press.

Rattay F (1989) Analysis of models for extracellular fiber stimulation. *IEEE Trans Biomed Eng*, *36*(7), 676-82.

Ridding MC, Rothwell JC (2007) Is there a future for therapeutic use of transcranial magnetic stimulation? *Nat Rev Neurosci*, *8*, 559–567.

Rizvi S, Khan AM (2019) Use of transcranial magnetic stimulation for depression. *Cureus*, *11*, e4736.

Roth BJ, Basser PJ (1990) A model of the stimulation of a nerve fiber by electromagnetic induction. *IEEE Trans Biomed Eng, 37*, 588–597.

Roth BJ, Cohen LG, Hallett M (1991) The electric field induced during magnetic stimulation. *Electroenceph Clin Neurophysiol* Supplement, 43, 268-278.

Roth BJ (1994) Mechanisms for electrical stimulation of excitable tissue. *Crit Rev Biomed Eng,* 22, 253-305.

Saha R, Benally OJ, Faramarzi S, Bloom R, Wu K, *Tonini* D, Shiao M, Keirstead SA, Low WC, Netoff TI, Wang J-P (2024) Planar microcoil arrays for in vitro cellular-level micromagnetic activation of neurons. *J Vac Sci Technol B*, *42*, 033001.

Saha R, Van Helden D, Hopper MS, Low WC, Netoff TI, Osborn J, Wang J-P (2024) Impact of anesthesia on micromagnetic stimulation (μMS) of the vagus nerve. *Biomed Phys Eng Express*, *10*, 035028.

Sugai S, Higuchi H, Nishikawa J, Satoh K, Murakami S, Tateno T (2020) Numerical Analysis of Microcoil-Induced Electric Fields and Evaluation of *In vivo* Magnetic Stimulation of the Mouse Brain. *IEEJ Transactions on Electrical and Electronic Engineering*, *15*(11), 1672–1680.

Syrek P, Bărbulescu R (2017) Parametric curves to trace the TMS coils windings : In Proceedings of the 10th International Symposium on Advanced Topics in Electrical Engineering, Bucharest, Romania, 23–25 March 2017; 386–391.

Syrek P (2019) Uncertainty problem as illustrated by magnetotherapy. *ACES J*, *34*, 1445–1452.

Thielscher A, Kammer T (2004). Electric field properties of two commercial figure-8 coils in TMS: calculation of focality and efficiency. *Clinical neurophysiology : Official journal of the International Federation of Clinical Neurophysiology*, *115*(7), 1697–1708.

Tian L, Liu Q, Song L, Jin Z, Dong L, Zheng Y (2023) Design and optimization of resonance-based wireless power transmission for millimeter-sized planar square inductors micro-magnetic stimulation. *IEEE Trans Instrum Meas*, *72*, 4009010.

Tranchina D, Nicholson C (1986) A model for the polarization of neurons by extrinsically applied electric fields. *Biophys J, 50*, 1139–1156.

Wagner T, Valero-Cabre A, Pascual-Leone A (2007) Noninvasive human brain stimulation. *Annu Rev Biomed Eng*, *9*, 527–565.

Wu J, Wikswo JP (1997) Effects on bath resistance on action potentials in the squid giant axon: Myocardial implications. *Biophys J, 73*, 2347-2358.

Wyszkowska J, Jankowska M, Gas P (2019) Electromagnetic fields and neurodegenerative diseases. *Przegląd Elektrotechniczny*, *95*, 129-133.

Ye H, Barrett L (2021) Somatic inhibition by microscopic magnetic stimulation. *Sci Rep*, *11*, 13591.

Ye H, Hall V, Hendee J (2023) Improving focality and consistency in micromagnetic stimulation. *Front Comput Neurosci*, *17*, 1105505.

Yesavage JA, Fairchild JK, Mi Z, Biswas K, Davis-Karim A, Phibbs CS, Forman SD, Thase M, Williams LM, Etkin A, O'Hara R, Georgette G, Beale T, Huang GD, Noda A, George MS, (2018) VA Cooperative Studies Program Study Team. Effect of repetitive transcranial magnetic stimulation on treatment-resistant major depression in US veterans: A randomized clinical trial. *JAMA Psychiatry*, *75*(9), 884–893.

Yoshikawa T, Higuchi H, Furukawa R, Tateno T (2022) Temporal and spatial profiles of evoked activity induced by magnetic stimulation using millimeter-sized coils in the mouse auditory cortex in vivo. *Brain Research*, *1796*, 148092.

Zeng F-G, Rebscher S, Harrison W, et al. (2008) Cochlear implants: System design, integration, and evaluation. *IEEE Reviews in Biomedical Engineering*, *1*, 115–142.